CRADA FINAL REPORT

CRADA Number ORNL02-0648

CRADA FINAL REPORT

CRADA Number ORNL02-0648

Alloy Design and Development of Cast Cr-W-V Ferritic Steels for Improved High-Temperature Strength for Power Generation Applications

R. L. Klueh
P. J. Maziasz
J. M. Vitek
N. D. Evans
N. Hashimoto

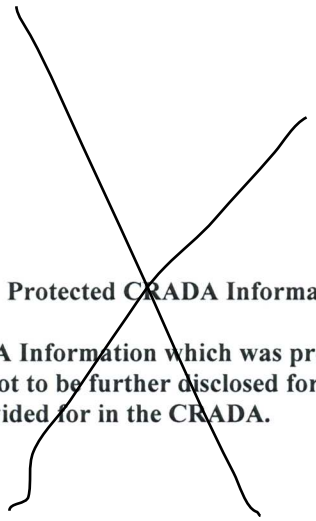

ABSTRACT

Economic and environmental concerns demand that the power-generation industry seek increased efficiency for gas turbines. Higher efficiency requires higher operating temperatures, with the objective temperature for the hottest sections of new systems ≈593°C, and increasing to ≈650°C. Because of their good thermal properties, Cr-Mo-V cast ferritic steels are currently used for components such as rotors, casings, pipes, etc, but new steels are required for the new operating conditions.

The Oak Ridge National Laboratory (ORNL) has developed new wrought Cr-W-V steels with 3-9% Cr, 2-3% W, 0.25%V (compositions are in wt. %), and minor amounts of additional elements. These steels have the strength and toughness required for turbine applications. Since cast alloys are expected to behave differently from wrought material, work was pursued to develop new cast steels based on the ORNL wrought compositions.

Nine casting test blocks with 3, 9, and 11% Cr were obtained. Eight were Cr-W- V-Ta-type steels based on the ORNL wrought steels; the ninth was COST CB2, a 9Cr-Mo-Co-V-Nb cast steel, which was the most promising cast steel developed in a European alloy-development program. The COST CB2 was used as a control to which the new compositions were compared, and this also provided a comparison between Cr-W-V- Ta and Cr-Mo-V-Nb compositions.

Heat treatment studies were carried out on the nine castings to determine normalizing-and-tempering treatments. Microstructures were characterized by both optical and transmission electron microscopy (TEM). Tensile, impact, and creep tests were conducted. Test results on the first nine cast steel compositions indicated that properties of the 9Cr-Mo-Co-V-Nb composition of COST CB2 were better than those of the 3Cr-, 9Cr-, and 11Cr-W-V-Ta steels.

Analysis of the results of this first iteration using computational thermodynamics raised the question of the effectiveness in cast steels of the Cr-W-V-Ta combination versus the Cr-Mo-V-Nb combination in COST CB2. To explore this question, nine more casting test blocks, four 3Cr steels and five 11Cr steels were purchased, and microstructure and mechanical properties studies similar to those described above for the first iteration of test blocks were conducted.

Experimental results from the second iteration indicated that 11 Cr steels with excellent properties are possible. The 11Cr-1.5Mo-V-Nb steels were superior to 11Cr-2W-V-Ta steels, and it appears the former class of steels can be developed to have tensile and creep properties exceeding those of COST CB2. The W-Nb combination in an 11Cr-2W-V-Nb steel had tensile and short-time creep properties at 650°C better than the 11Cr-1.5Mo-V-Nb steels, although long-time low-stress properties may not be as good because of Laves phase formation. Based on the results, the next step in the development of improved casting steels involves acquisition of 11Cr-1.5Mo-V-Nb-N-B-C and 11Cr-2W-V-Nb-N-B-C steels on which long-term creep-rupture tests (>10,000 h) be conducted. For better oxidation and corrosion resistance, development of 11Cr steels, as opposed to a 9Cr steels, such as COST CB2, are important for future turbine designs that envision operating temperatures of 650°C.

PROJECT OBJECTIVE

The objective of this project was to design and develop new cast elevated-temperature ferritic/martensitic steels for gas-turbine applications with mechanical properties as good as or better than the commercially available cast steels now used for that application. To that end, the cast steels were patterned after Cr-W- V-Ta-type wrought steels developed at ORNL work. The ultimate goal is improved critical component material for use in higher efficiency steam turbine and gas turbine technology for electric power generation. The new steels must be capable of higher operating temperatures than the commercial steels now being used.

BENEFITS TO DOE'S MISSION

Over the last decade, high-temperature steel research and development for future power-generation systems has been neglected in the U.S., while industry-government consortiums in Europe and Japan have pursued aggressive materials-development programs for advanced steam and gas conditions. For the U.S. power-generation industry to stay competitive, a program to develop advanced ferritic/martensitic steels (and other high-temperature materials) is required.

This project sought to combine the scientific expertise and research facilities in elevated-temperature materials of a DOE laboratory with the technical expertise on existing commercial materials and manufacturing approaches of GE Power Systems of General Electric Company, a world leader in the development and manufacture of power-generating equipment. Although the proposed work cannot hope to make up the lead currently held by other countries in this field, the type of strong science-based approach using modeling and experimental studies with a strong emphasis on microstructural understanding can form the basis to close the large gap that presently exists, thus advancing the competitive position of the U.S. power-generation industry. A long-term project such as the one begun with this work could, if followed through, once again put DOE in the forefront of the development of advanced steels for elevated-temperature service, as was the case when modified 9Cr-1Mo steel was developed at ORNL in the 1970s. That steel is presently used in power plants throughout the world, and it is being used by researchers in Europe and Japan as the basis for comparison of new steels being developed there.

TECHNICAL DISCUSSION

The experimental phase of the work began with the purchase by GE Power Systems of nine casting test blocks of different heats of 3-11% Cr steels. Heat treatment studies on material from each heat were conducted to determine optimum heat treatment conditions; evaluation of the steels involved hardness measurements and optical metallography examination. Once a heat treatment was determined, the blocks were normalized and tempered, specimens for tensile and creep studies were obtained, and tests were conducted. Transmission electron microscopy examination was conducted on each of the heats. Based on these tests, a second heat treatment was conducted on several heats, and more tensile and creep tests were conducted.

After evaluation of the first batch of test blocks, a second batch of nine more test blocks were purchased by ORNL, and tests similar to those on the first nine heats were conducted.

In the following sections, details on the tests and evaluation of the casting test blocks will be presented and discussed.

Experimental—Part I

Composition and Heat Treatment

Nine casting test blocks of different composition (Table 1) were obtained through GE Power Systems, who purchased the steels from Voestalpine Giesserei, Linz GMBH, Linz, Austria. The test block size is shown in Fig. 1 before the riser (Normalspeiser) was removed. After the riser was removed, the casting test block (bottom portion on the drawing) consisted of a polyhedron with rectangular faces. It was ≈140 mm (5.5 in) high, with the base (the surface created by removal of the riser) 230 x 115 mm (≈9.1 x 4.5 in) and the top surface (parallel to the base) 184 x 70 mm (≈7.2 x 2.8 in).

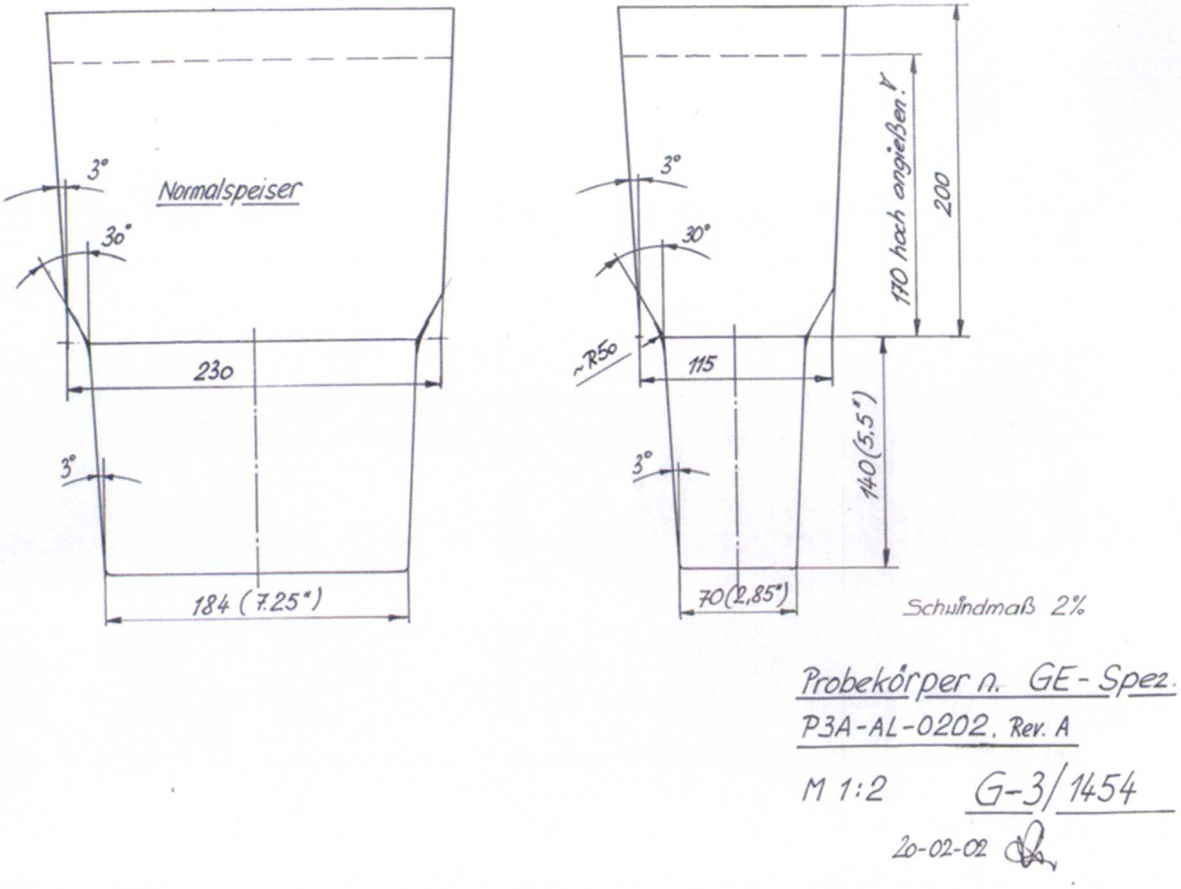

Figure 1. Drawing of the casting test block (Probenkorper) with riser (Normalspeiser).

Eight of the compositions in Table 1 were those requested by ORNL based on the high-strength wrought steels developed at ORNL; the ninth was COST CB2 (CB2) that was introduced into the project as a control. This 9Cr steel was developed in Europe in the wide-

Table 1. Chemical Composition of Steel Casts*

Element	No. 1	No. 2	No. 3	No. 18	No. 21	No. 29	No. 31	No. 36	No. 45
C	0.11	0.10	0.10	0.17	0.10	0.10	0.16	0.14	0.12
Mn	0.53	0.52	0.49	0.50	0.50	0.52	0.51	0.51	0.82
P	0.013	0.012	0.013	0.013	0.012	0.013	0.013	0.013	0.012
S	0.003	0.003	0.004	0.010	0.008	0.009	0.007	0.009	0.008
Si	0.25	0.25	0.26	0.23	0.23	0.24	0.23	0.24	0.17
Ni	0.02	0.02	0.03	0.48	0.03	0.02	0.50	0.49	0.20
Cr	2.99	2.98	2.99	10.85	3.35	8.80	10.76	10.75	9.21
Mo	0.01	0.01	0.48	0.26	0.01	0.01	0.01	0.01	1.50
V	0.24	0.24	0.24	0.25	0.25	0.25	0.25	0.23	0.21
Nb	0.002	0.002	0.002	0.002	0.001	0.001	0.001	0.001	0.063
Ti	0.004	0.004	0.004	0.002	0.005	0.001	0.002	0.001	0.002
Co	0.010	0.010	0.009	0.010	0.010	0.010	0.012	0.012	0.80
Cu	0.03	0.03	0.03	0.03	0.03	0.03	0.03	0.03	0.04
Al	0.015	0.015	0.018	0.023	0.025	0.020	0.019	0.024	0.020
B	0.001	0.001	0.001	<0.001	0.004	<0.001	<0.001	0.005	0.008
Ta	0.01	0.09	0.01	<0.01	0.10	0.09	0.09	0.09	<0.01
W	3.04	3.04	2.02	1.05	2.91	2.04	2.05	2.05	<0.01
As	0.007	0.011	0.008	0.005	0.008	0.011	0.008	0.008	0.011
Sn	0.008	0.008	0.006	0.005	0.007	0.007	0.006	0.007	0.002
N	0.007	0.008	0.009	0.031	0.018	0.027	0.034	0.033	0.028
O	0.004	0.004	0.003	0.005	0.003	0.005	0.007	0.004	0.004

Steel Designations:

No. 1: 3Cr-3WV
No. 2: 3Cr-3WVTa
No. 3: 3Cr-2WMoV
No. 21: 3Cr-3WVTaB
No. 29: 9Cr-2WVTa
No. 18: 11Cr-1WMoV
No. 31: 11Cr-2WVTa
No. 36: 11Cr-2WVTaB
No. 45: COST CB2—9Cr-1.5MoCoVNb

ranging experimental COST program to develop steels for the next generation of power plants. The COST CB2 composition was the most promising steel developed for cast applications in that extensive steel research and development program.

To determine normalizing-and-tempering conditions, pieces of the test blocks were heat treated. Normalization involved three austenitization treatments followed by air cooling on three pieces of blocks; austenitization was 1 h at 1050, 1100, and 1175°C. After normalization, the blocks were sectioned, and the hardness across the block was determined (Figs. 2-4). Because of uneven cuts, it was impossible to determine Rockwell hardness, and a portable hardness tester was used. Figures 5-7 show the effect of the tempering on Rockwell hardness. The curves were obtained by tempering normalized blocks for 1 h at 400, 500, 600, 700, 750, and 800°C.

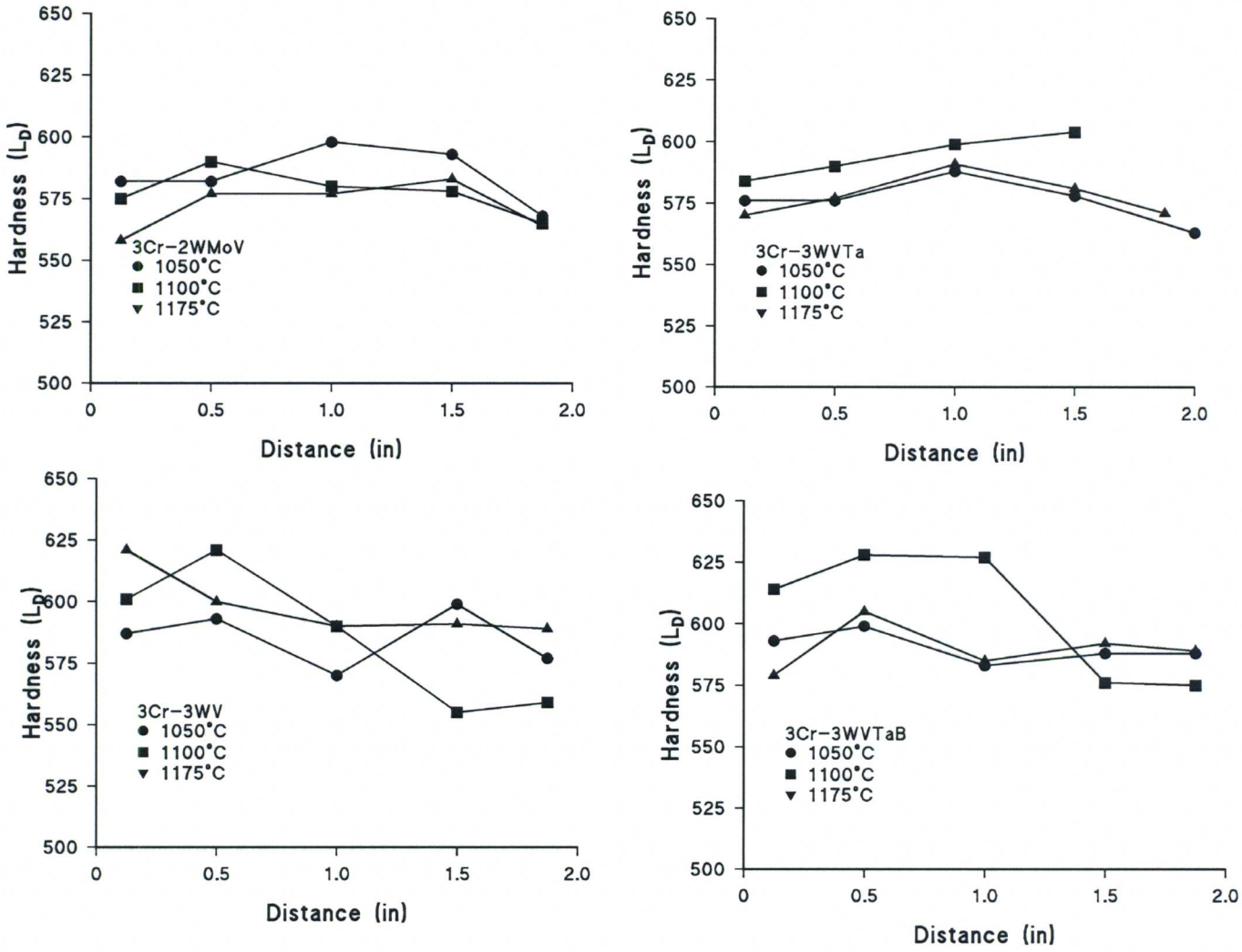

Figure 2. Hardness profile across normalized 3% Cr steels for three austenitizing conditions.

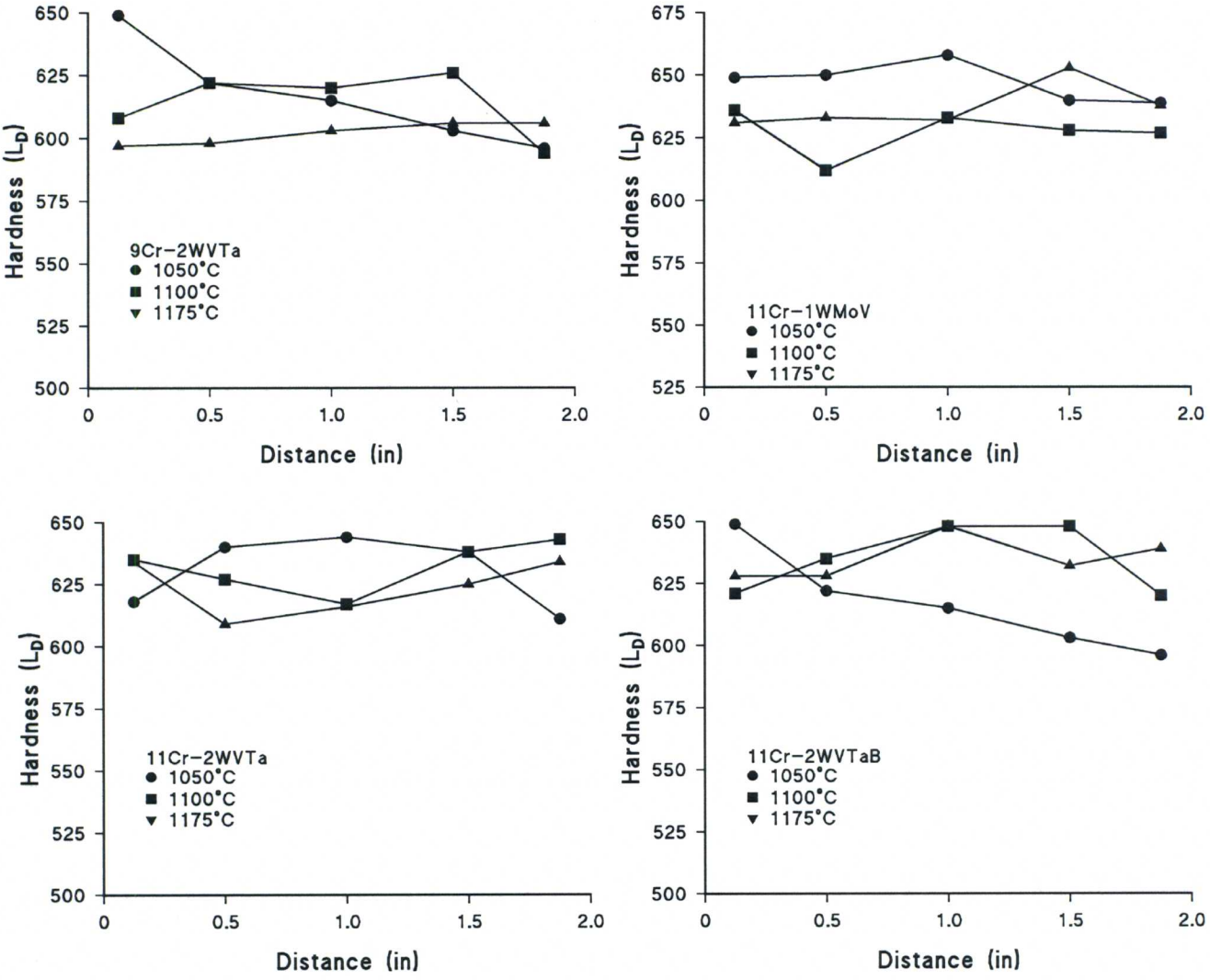

Figure 3. Hardness profile across normalized 9% and 11% Cr steels for three austenitizing conditions.

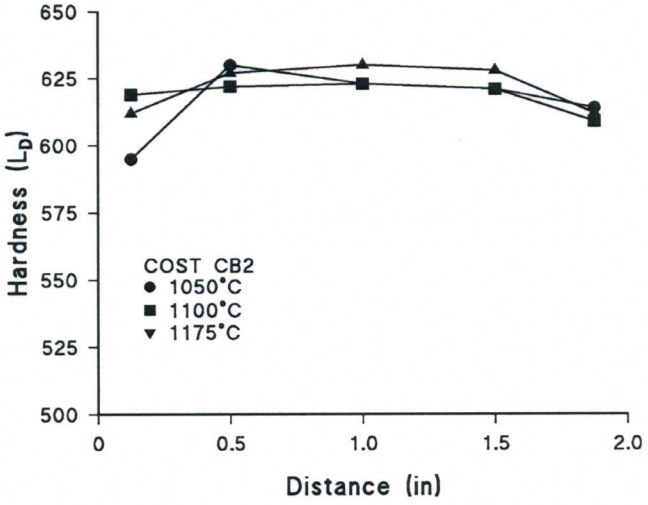

Figure 4. Hardness profile across normalized COST CB2 steel for three austenitizing conditions.

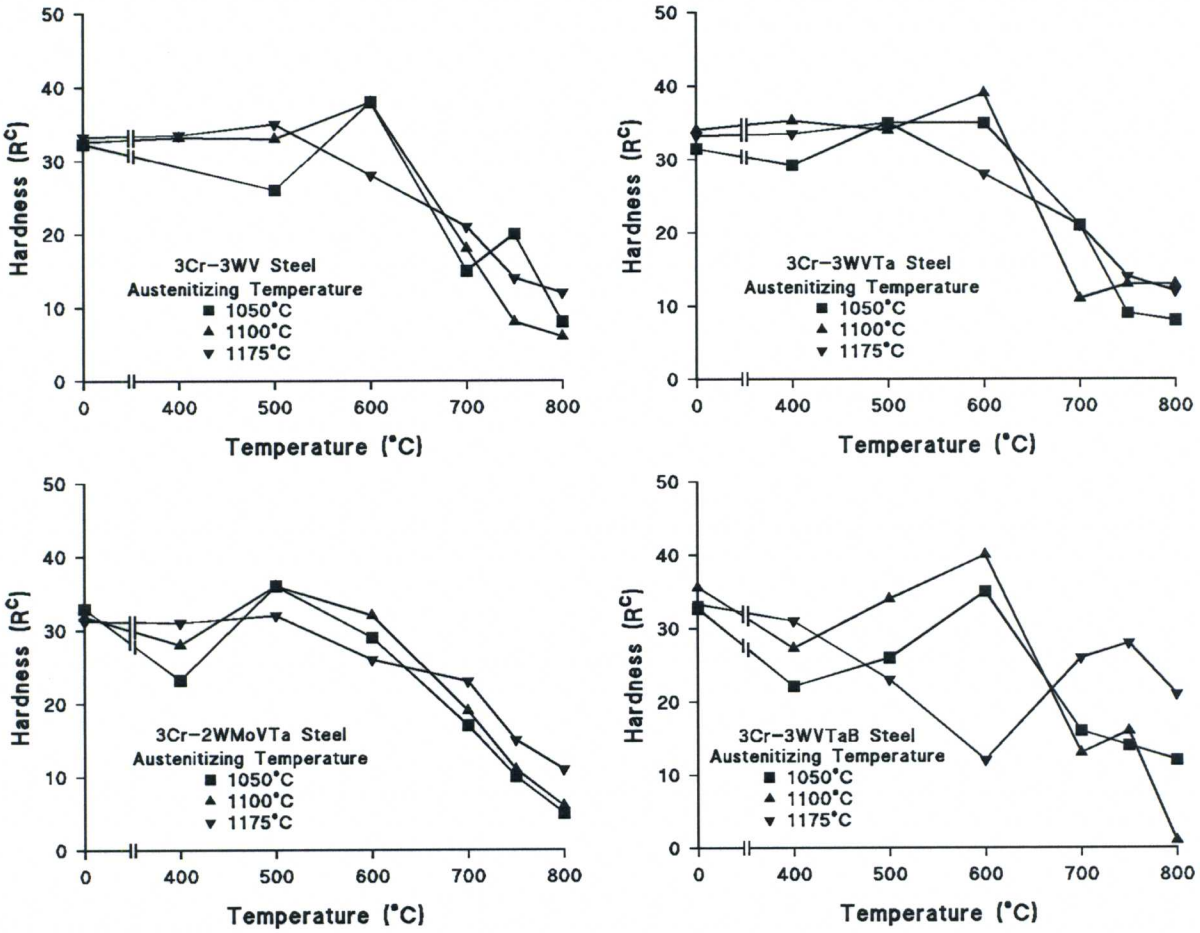

Figure 5. Tempering curves for 3% Cr steels normalized with three austenitizing conditions.

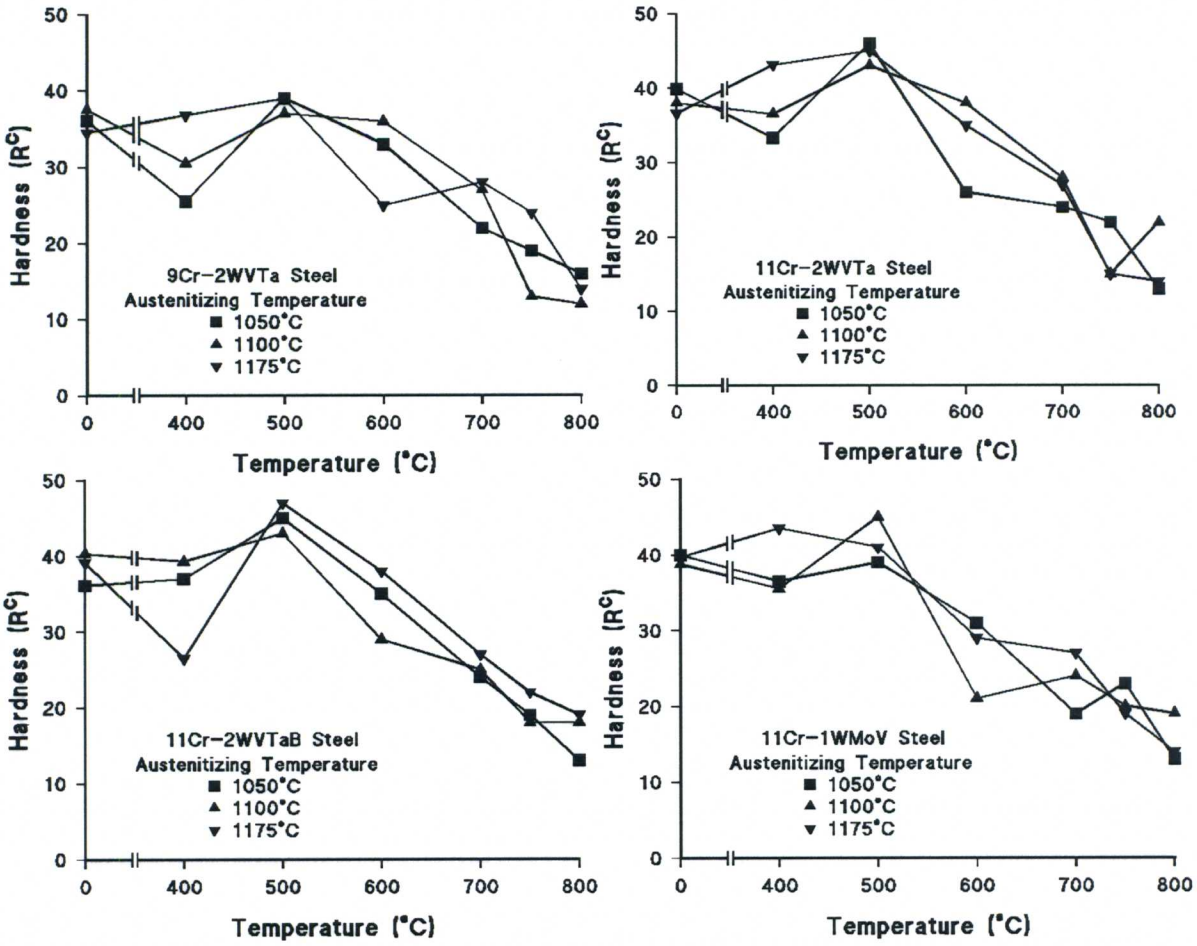

Figure 6. Tempering curves for 9% and 11% Cr steels normalized with three austenitizing conditions.

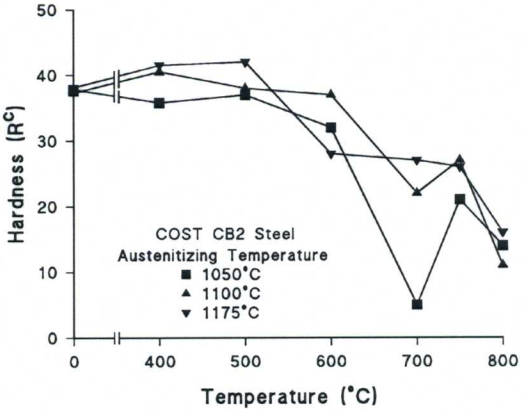

Figure 7. Tempering curves for COST CB2 steel normalized with three austenitizing conditions.

Metallography

Vickers hardness was determined from polished-and-etched specimens for the normalized steels (Table 2). Optical microstructures were obtained after normalization: austenitization of 1 h at 1050 (Fig. 8-10), 1100 (Fig. 11-13), and 1175°C (Fig. 14-16) followed by an air cool. When the steels were examined as-polished, there were indications of porosity that was also often visible after etching (Figs. 8-16). Some porosity may be from a phase removed during polishing. Delta-ferrite was also observed.

Table 2. Vickers Hardness of Normalized Steels

Steel	Average Hardness (HV)		
	1050°C/1h	1100°C/1h	1175°C/1h
3Cr-3WV	371	342	352
3Cr-3WVTa	351	340	354
3Cr-3WMoVTa	360	347	346
3Cr-3WVTaB	366	357	360
9Cr-2WVTa	401	394	387
11Cr-1WMoV	475	461	456
11Cr-2WVTa	450	436	459
11Cr-2WVTaB	433	439	440
COST CB2	398	398	412

Figures 17-19 and 20-22 show microstructures normalized by austenitizing at 1100°C and tempering 1 h at 700°C and 750°C, respectively. These microstructures are at higher magnification than Figs. 8-16, thus bringing out the acicular structure and the δ-ferrite. The 3Cr steels were 100% bainite, and the 9 and 11Cr steels were primarily martensite, but all contained δ-ferrite. The δ-ferrite amounts were estimated as follows: ≈14% for 9Cr-2WVTa, ≤1, 7, and 3% for 11Cr-1WMoV, 11Cr-2WVTa, and 11Cr-2WVTaB, respectively, and ≤1% for COST CB2.

Table 3 gives Vickers microhardness for normalized (1100°C/1h/AC)-and-tempered (700°C/1h and 750°C/1h) steels. Because of the low hardness of the 3Cr steels after the 750°C temper, a 700°C temper was chosen for the 3Cr steels. The 9 and 11Cr steels had relatively similar hardnesses after the 750°C temper, which was chosen for tempering the high-chromium steels. A 750°C temper is the temper arrived at for COST CB2 in the development program.

Table 3. Vickers Hardness of Normalized (1100°C/1h/AC)-and Tempered Steels

Steel	Average Hardness (HV)	
	Tempered 1h 700°C	Tempered 1h 750°C
3Cr-3WV	252	240
3Cr-3WVTa	274	249
3Cr-3WMoVTa	240	234
3Cr-3WVTaB	296	247
9Cr-2WVTa	240	266
11Cr-1WMoV	289	278
11Cr-2WVTa	286	268
11Cr-2WVTaB	287	276
COST CB2	287	284

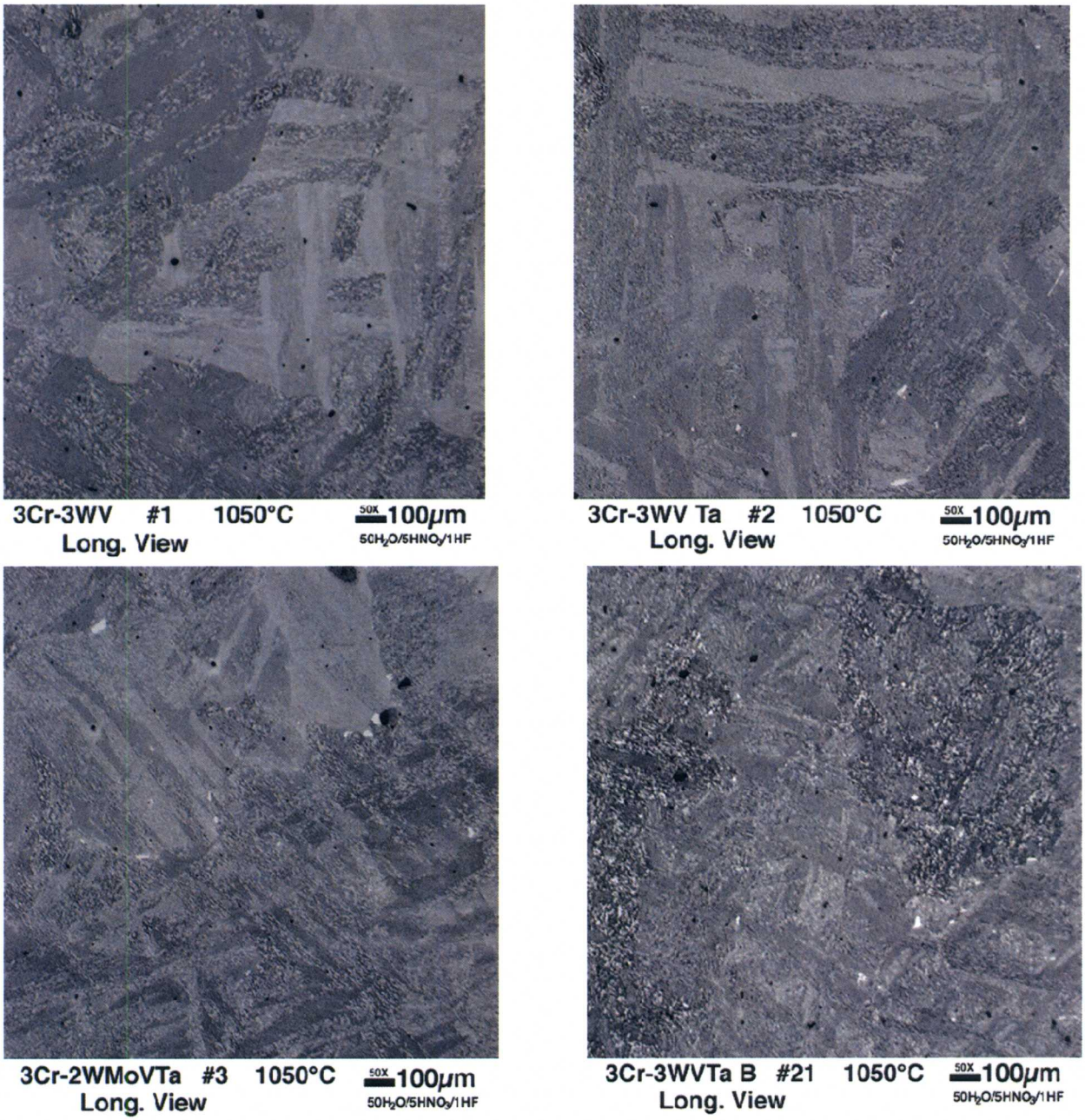

Figure 8. Optical microstructures of 3Cr steel casting test blocks austenitized 1 h at 1050°C. See photos for designations.

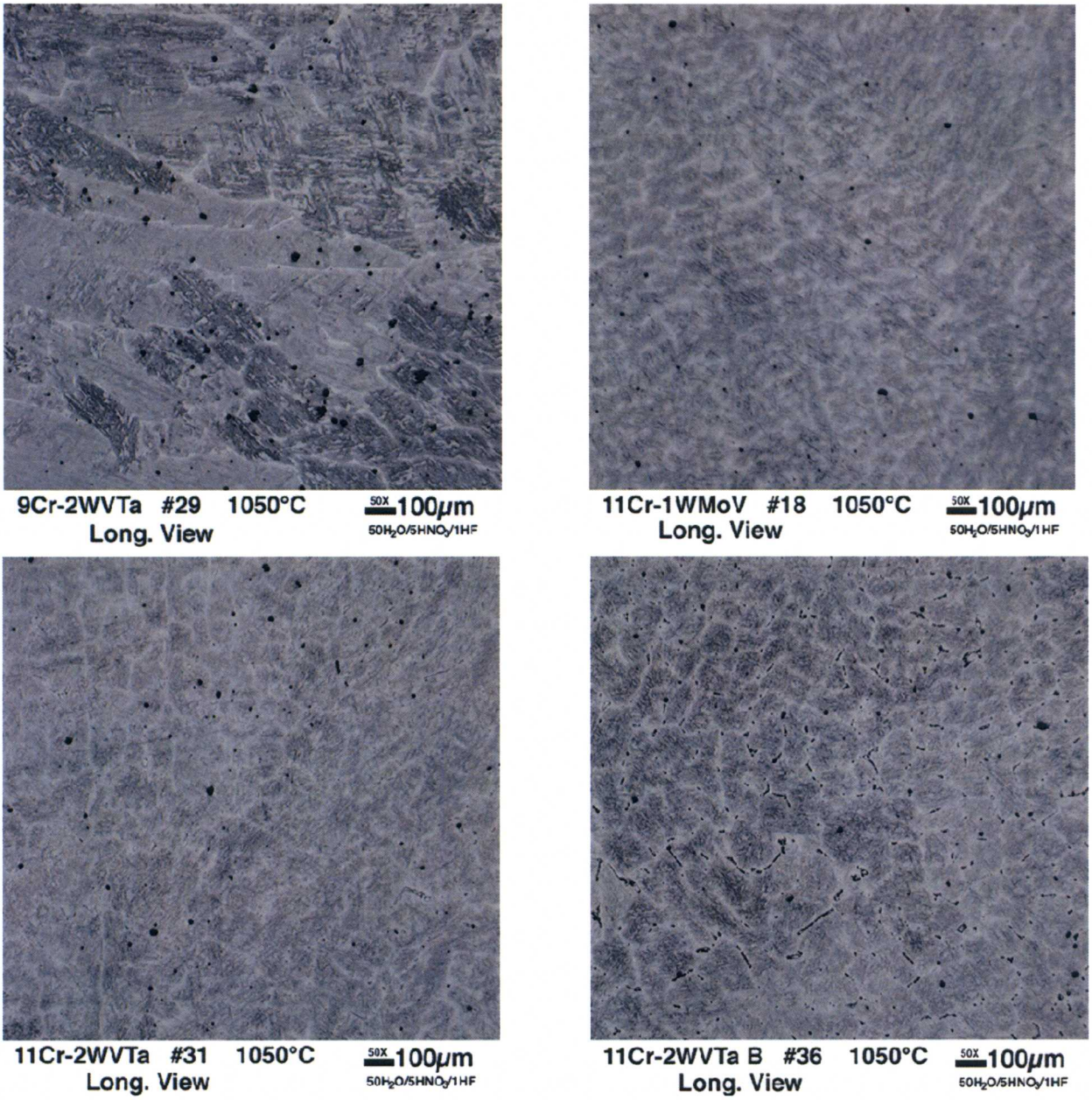

Figure 9. Optical microstructures of 9Cr and 11Cr steel casting test blocks austenitized 1 h at 1050°C. See photos for designations.

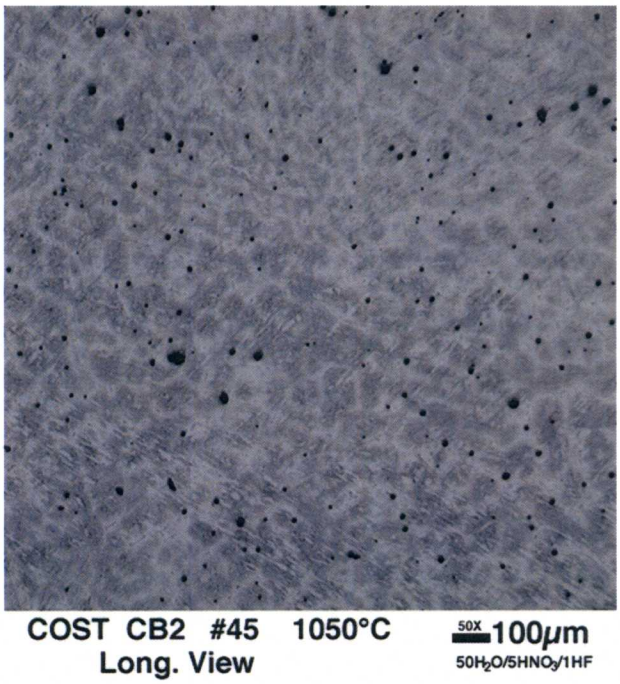

Figure 10. Optical microstructure of COST CB2 casting test block austenitized 1 h at 1050°C.

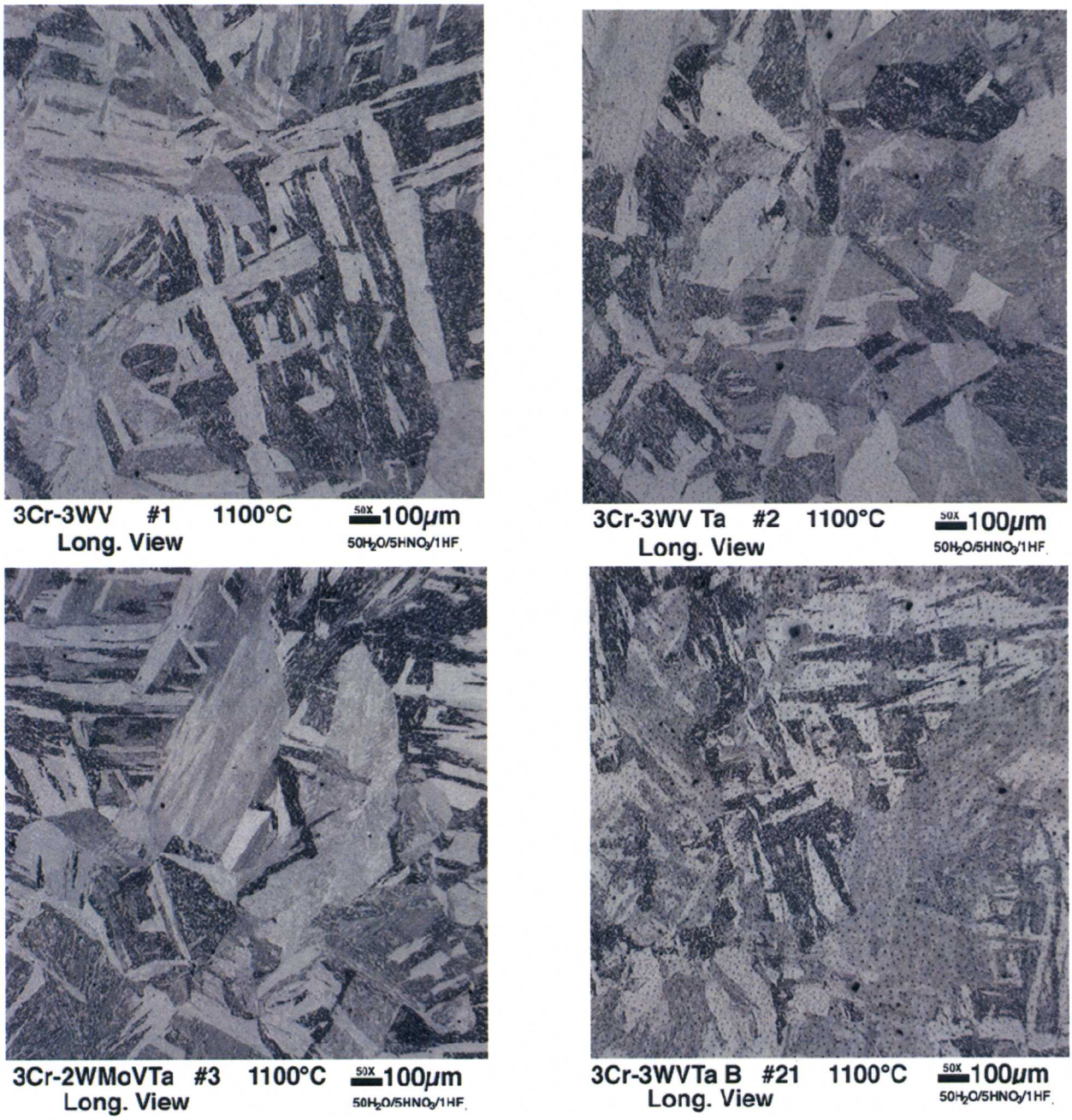

Figure 11. Optical microstructures of 3Cr steel casting test blocks austenitized 1 h at 1050°C. See photos for designations.

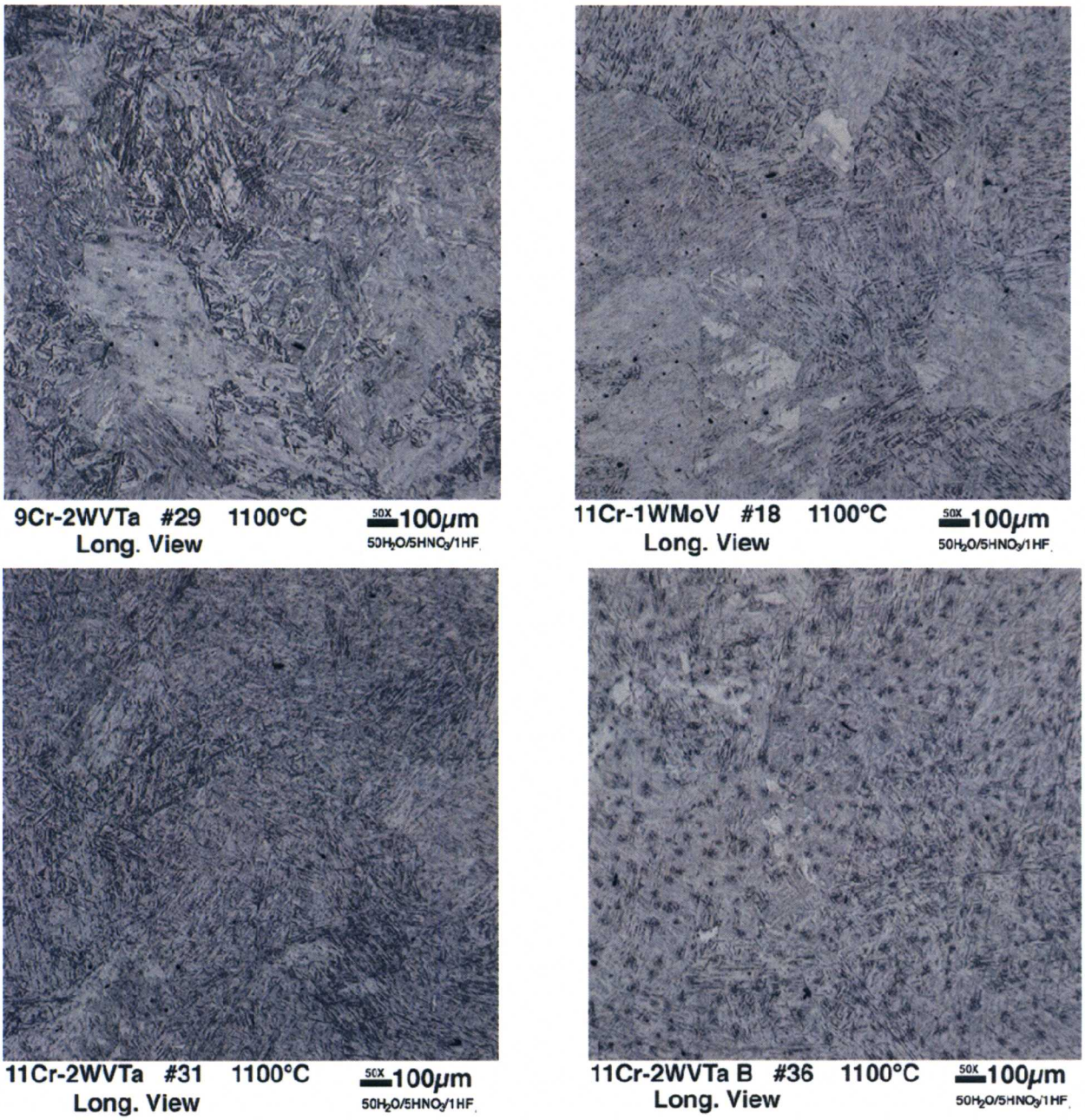

Figure 12. Optical microstructures of 9Cr and 11Cr steel casting test blocks austenitized 1 h at 1100°C. See photos for designations.

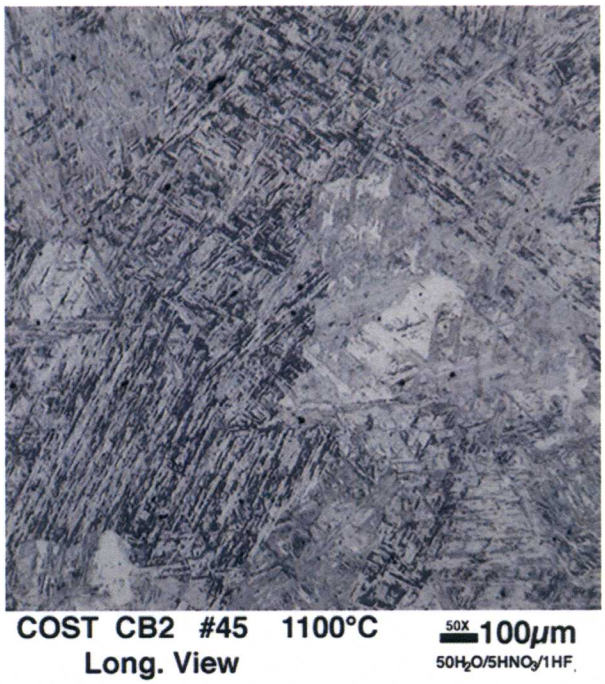

Figure 13. Optical microstructure of COST CB2 casting test block austenitized 1 h at 1150°C.

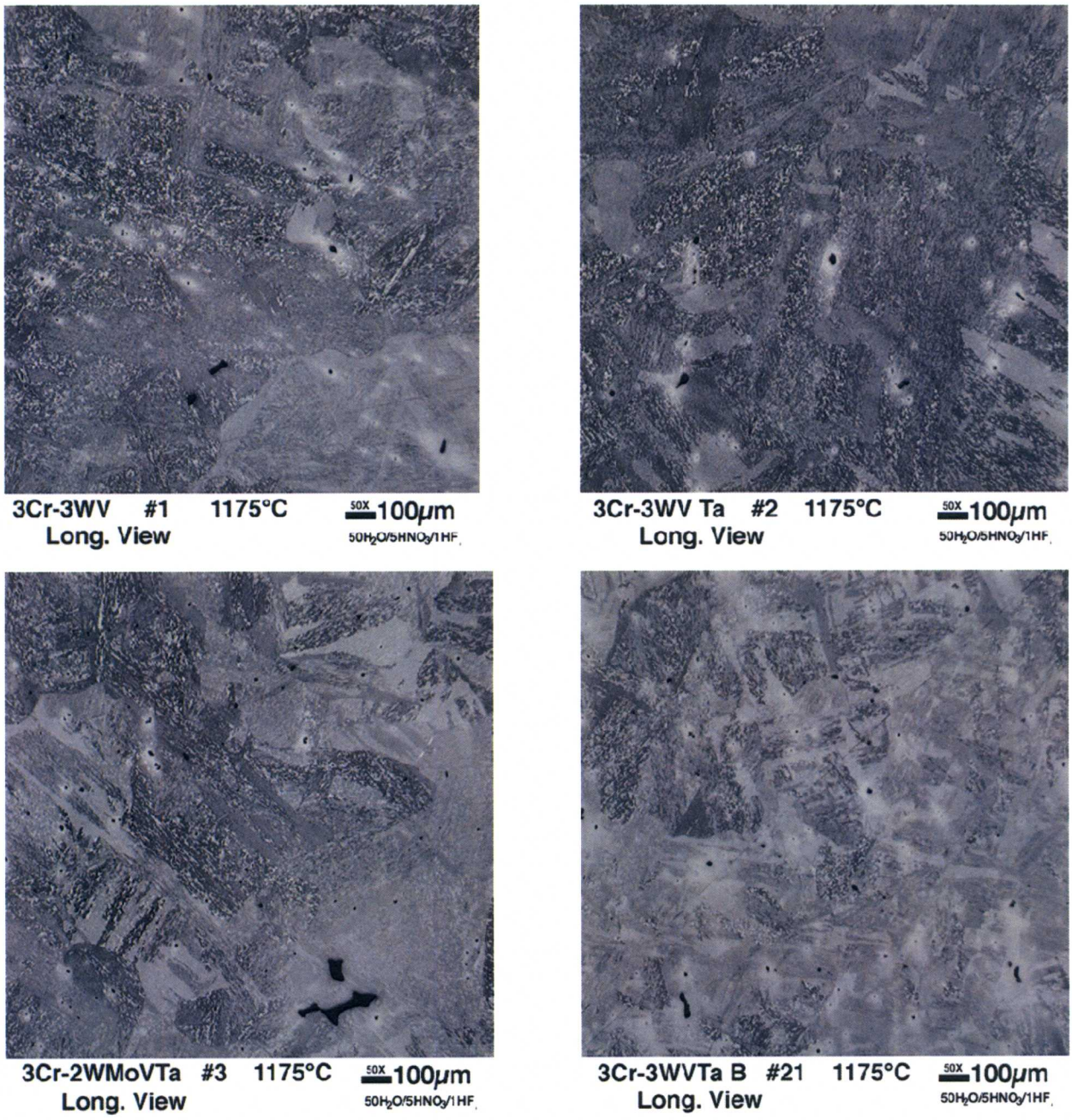

Figure 14. Optical microstructures of 3Cr steel casting test blocks austenitized 1 h at 1175°C. See photos for designations.

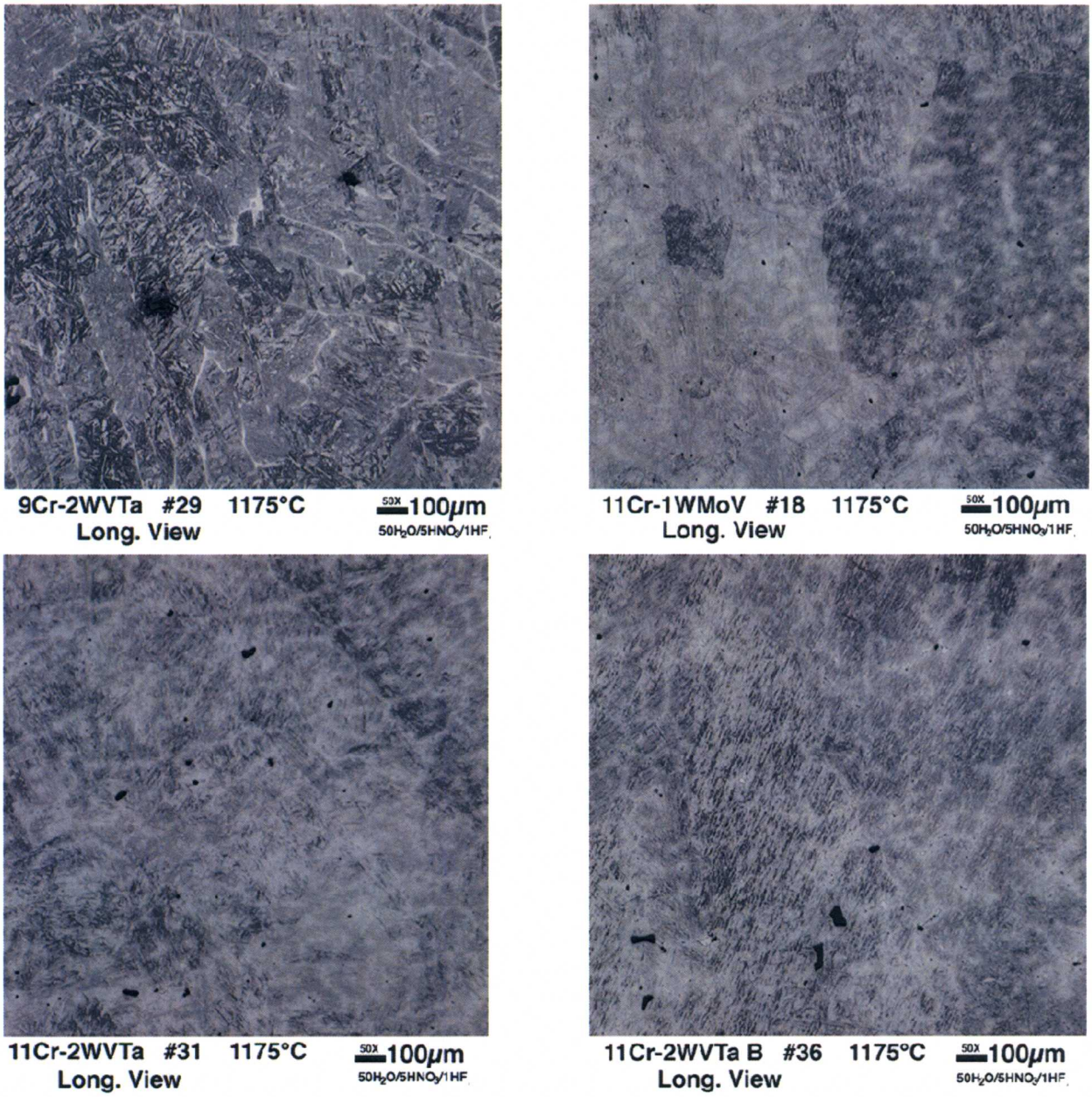

Figure 15. Optical microstructures of 9Cr and 11Cr steel casting test blocks austenitized 1 h at 1175°C. See photos for designations.

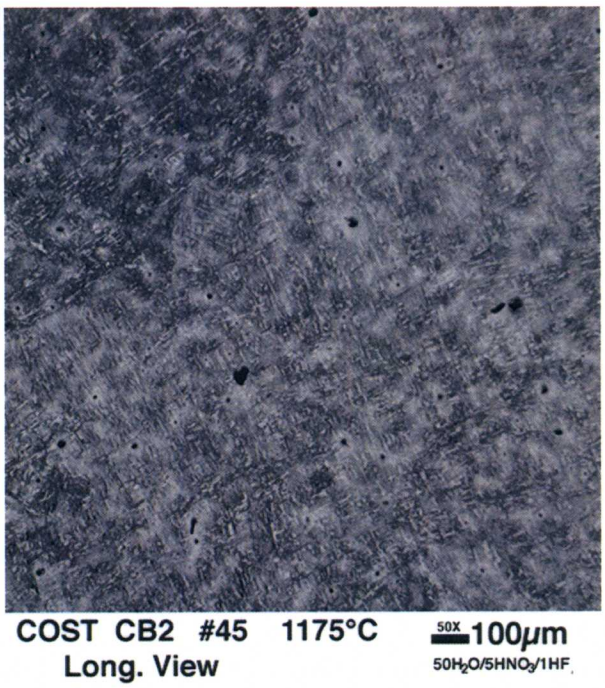

Figure 16. Optical microstructure of COST CB2 casting test blocks austenitized 1 h at 1175°C.

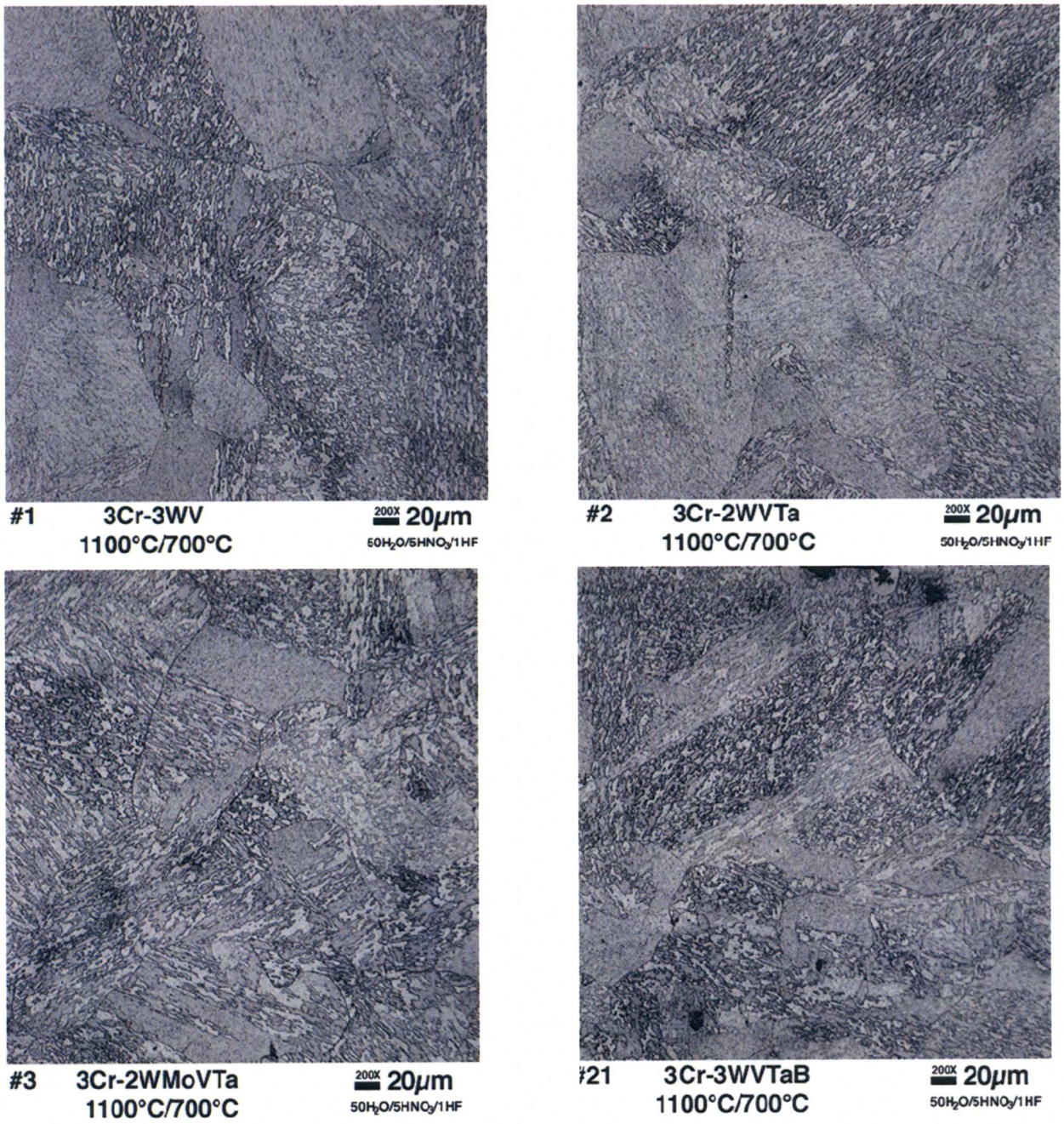

Figure 17. Optical microstructures of normalized-and-tempered 3Cr steel casting test blocks: austenitized 1 h at 1100°C, air cooled; tempered 1 h at 700°C. See photos for designations.

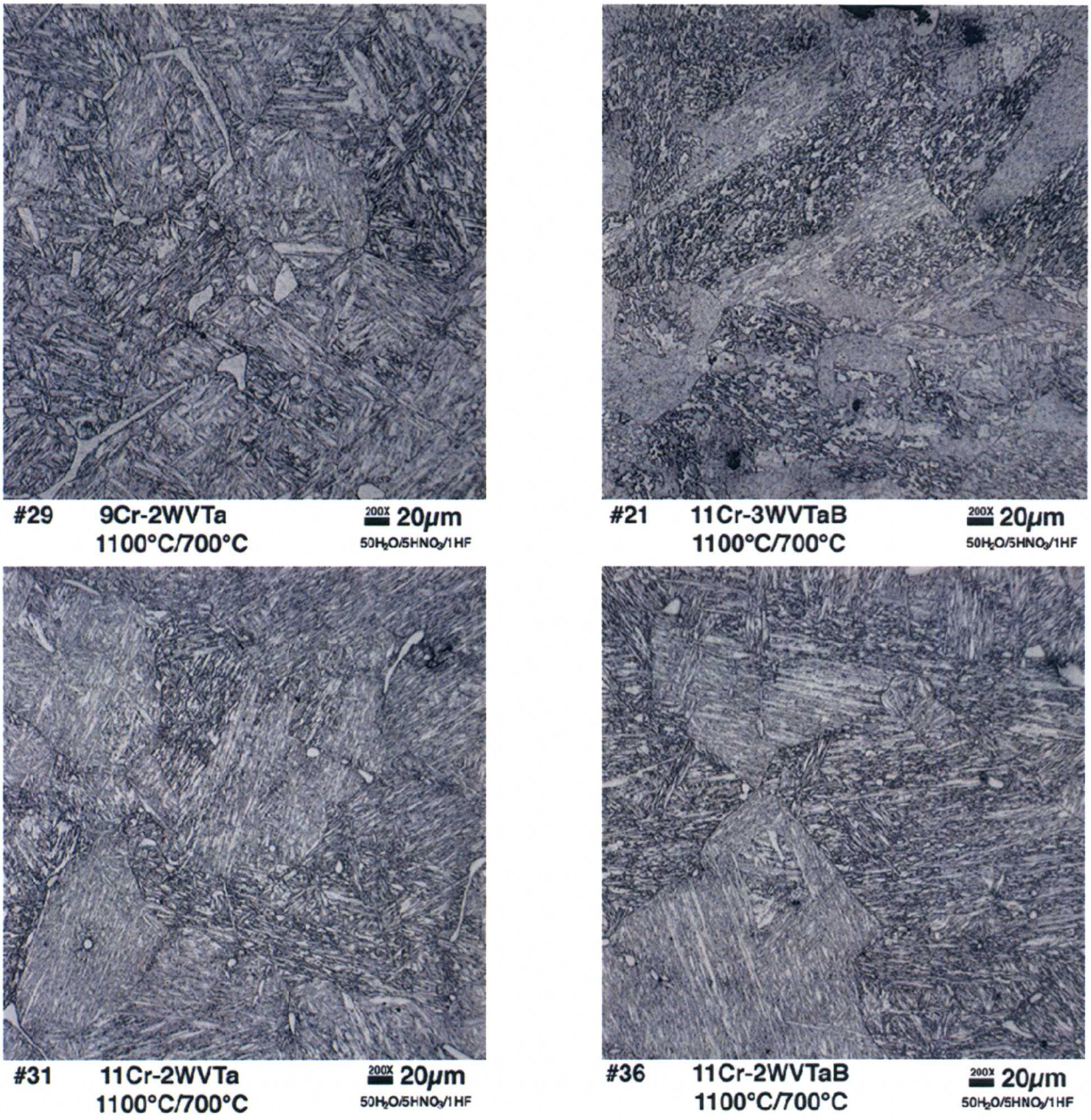

Figure 18. Optical microstructures of normalized-and-tempered 9 and 11Cr steel casting test blocks: austenitized 1 h at 1100°C, air cooled; tempered 1 h at 700°C. See photos for designations.

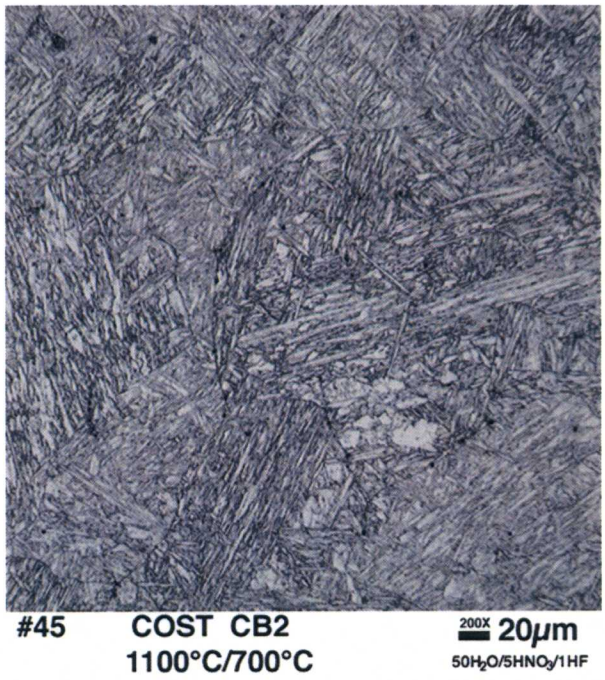

Figure 19. Optical microstructure of normalized-and-tempered COST CB2 steel casting test block: austenitized 1 h at 1100°C, air cooled; tempered 1 h at 700°C.

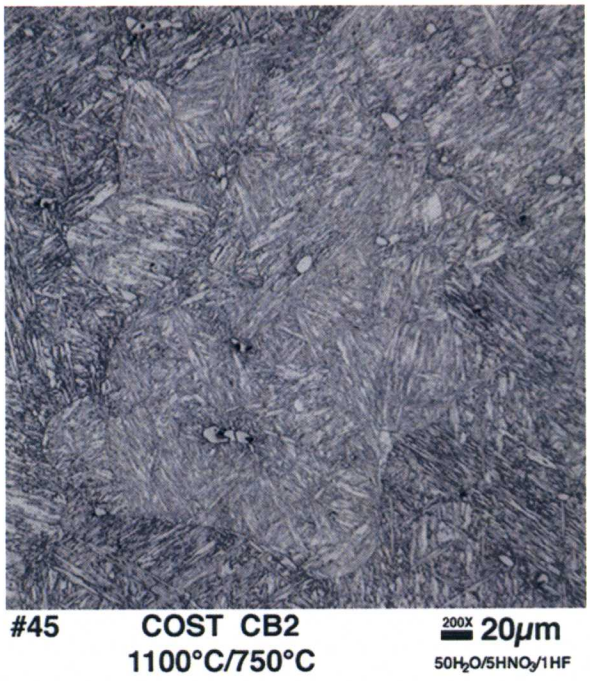

Figure 20. Optical microstructure of normalized-and-tempered COST CB2 steel casting test block: austenitized 1 h at 1100°C, air cooled; tempered 1 h at 750°C.

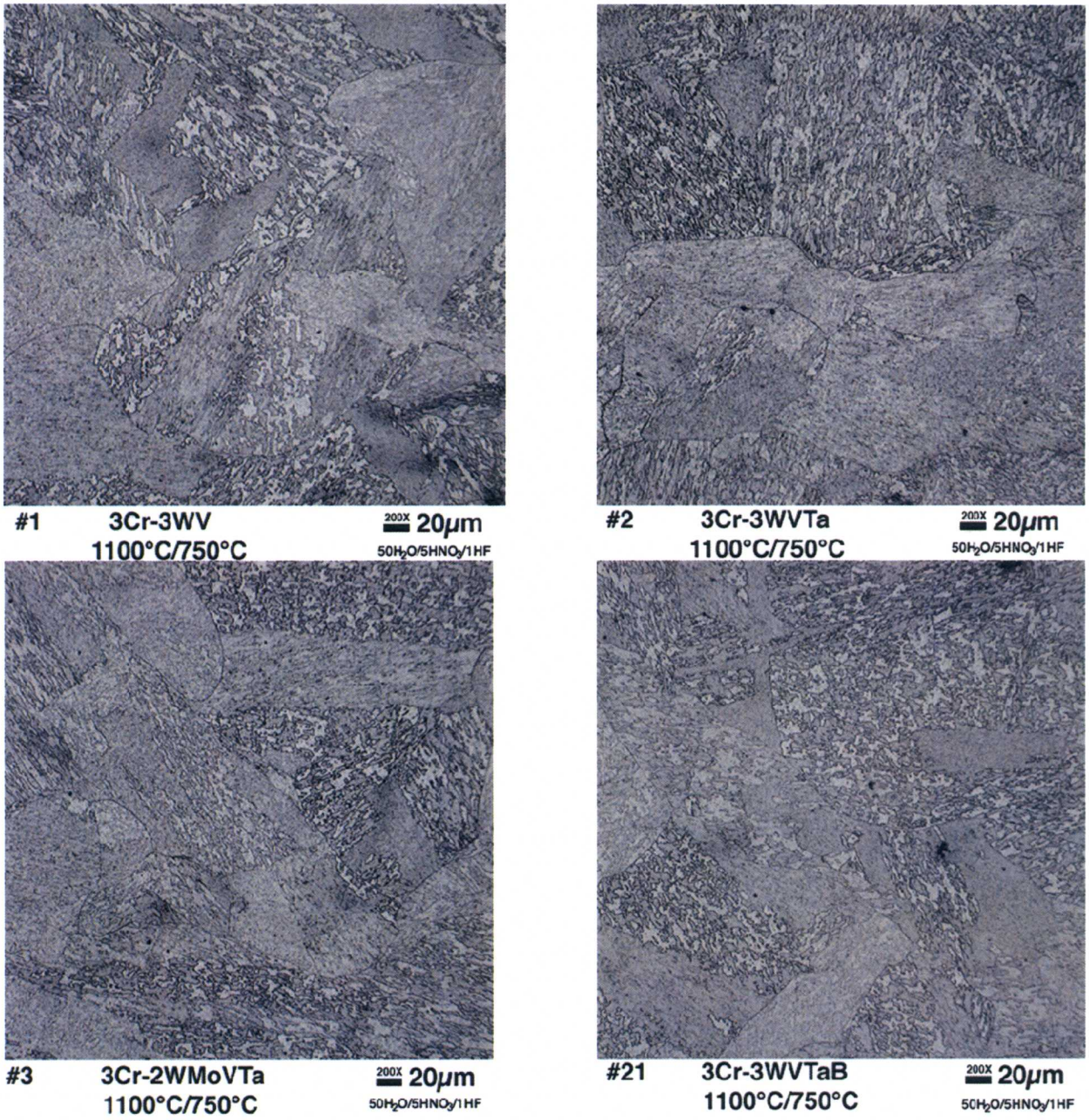

Figure 21. Optical microstructures of normalized-and-tempered 3Cr steel casting test blocks: austenitized 1 h at 1100°C, air cooled; tempered 1 h at 700°C. See photos for designations.

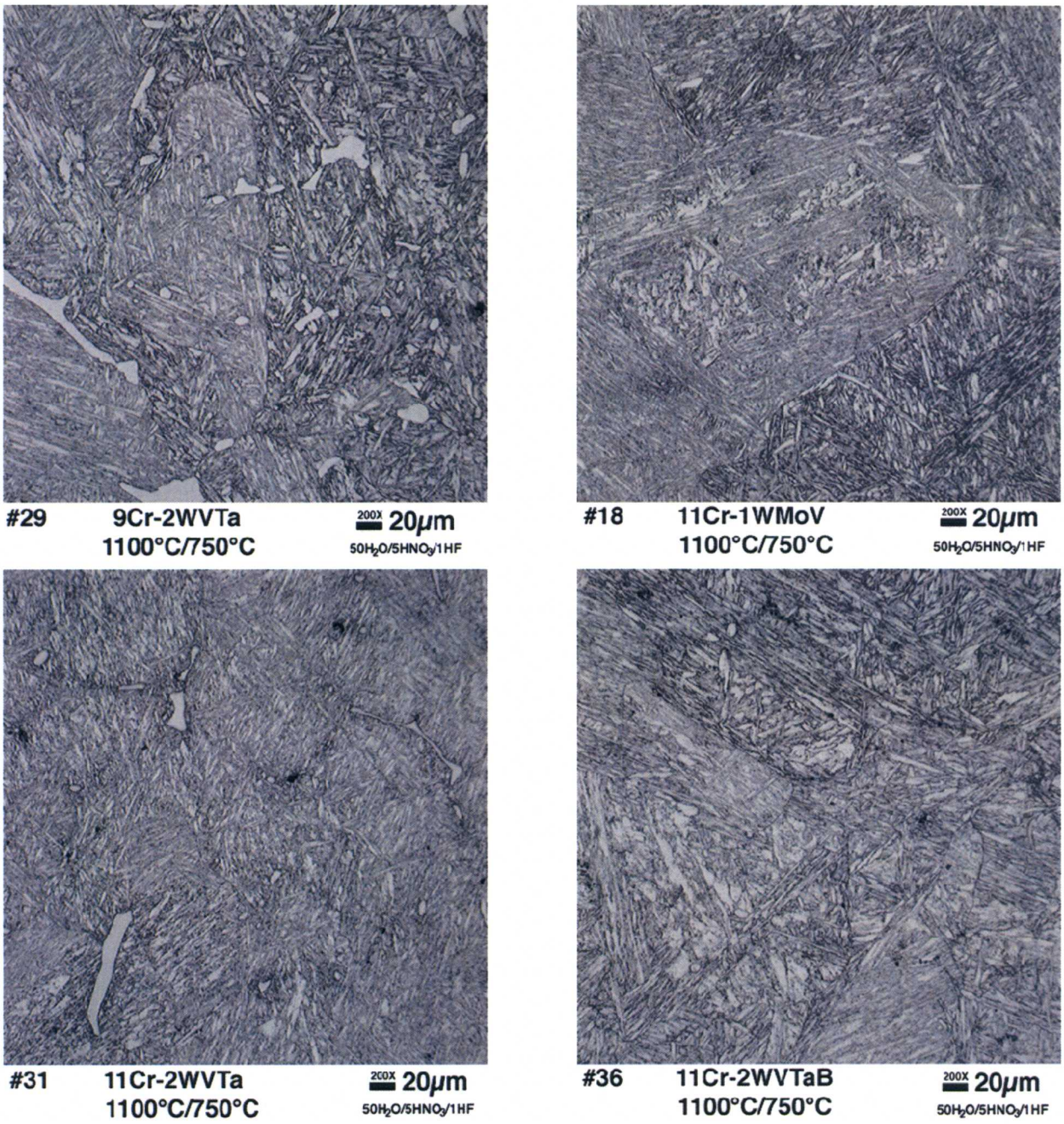

Figure 22. Optical microstructures of normalized-and-tempered 9 and 11Cr steel casting test blocks: austenitized 1 h at 1100°C, air cooled; tempered 1 h at 700°C. See photos for designations.

Transmission Electron Microscopy—Foil Specimens

Transmission electron microscopy (TEM) specimens were thinned from each of the cast steels in the normalized-and-tempered conditions used for the mechanical properties tests: 1100°C/1h/AC plus 1h at 700°C and 1h at 750°C temper for the 3Cr and high-chromium steels, respectively.

3Cr Steels

The TEM microstructures for the four 3Cr steels showed them to be characterized by a high number density of precipitates (Figs. 23-26). Optical microscopy indicated that the normalized-and-tempered microstructures were essentially 100% bainite (Fig. 17), and the TEM observations are in agreement with that conclusion in that the matrix of the steels has a relatively high dislocation density, even in the tempered condition.

In previous work on wrought 3Cr-3WV and 3Cr-3WVTa steels, we concluded the type of bainite developed during continuous cooling from the austenitization temperature differed from classical upper and lower bainite developed during an isothermal transformation [1]. Two types of bainite formed during continuous air cooling (normalization) following austenitization: granular bainite and carbide-free acicular bainite.

Detailed interpretation of microstructures will not be discussed. However, based on previous observations of these non-classical bainites [1], the 3Cr-3WV (Fig. 23), 3Cr-3WVTa (Fig. 24), and 3Cr-2WMoV (Fig. 25) have the characteristics of tempered granular bainite. On the other hand, the 3Cr-3WVTaB microstructure (Fig. 26) is characteristic of tempered carbide-free acicular bainite, the desired microstructure based on earlier work on wrought steels [1].

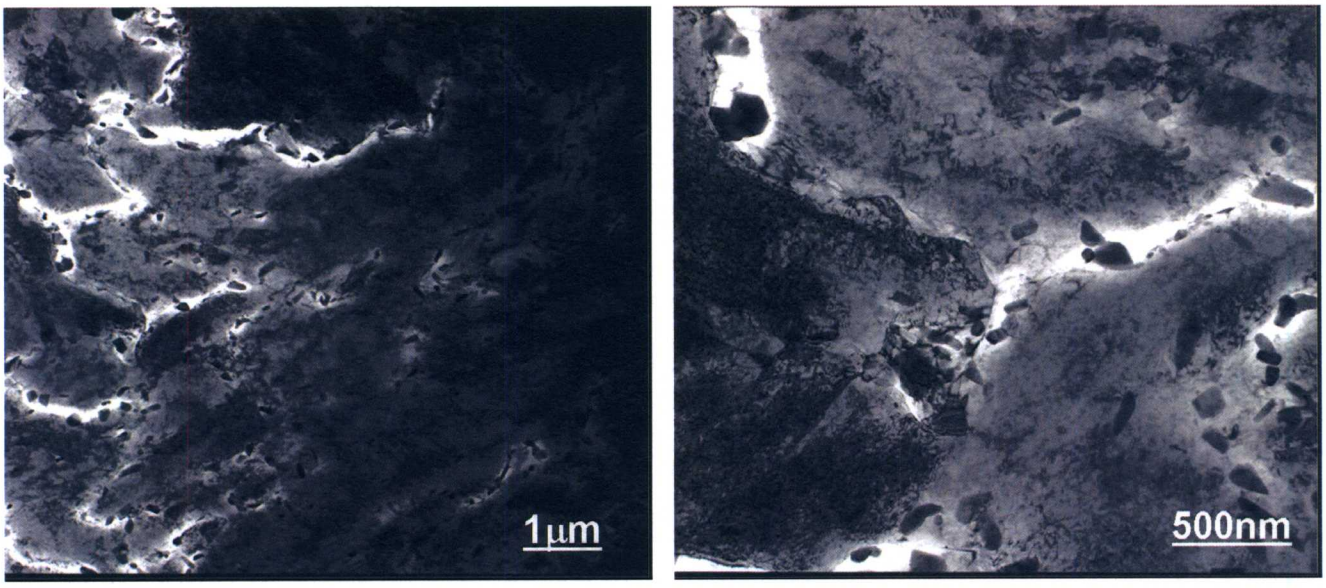

Figure 23. TEM photomicrograph of 3Cr-3WV steel.

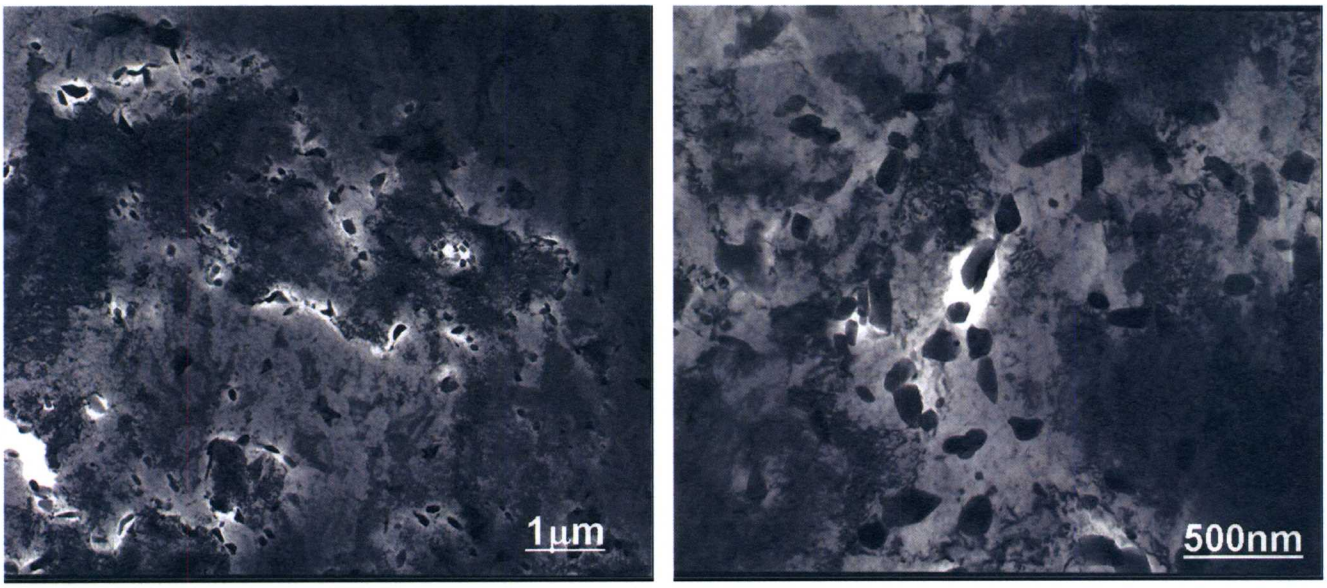

Figure 24. TEM photomicrograph of 3Cr-3WVTa steel.

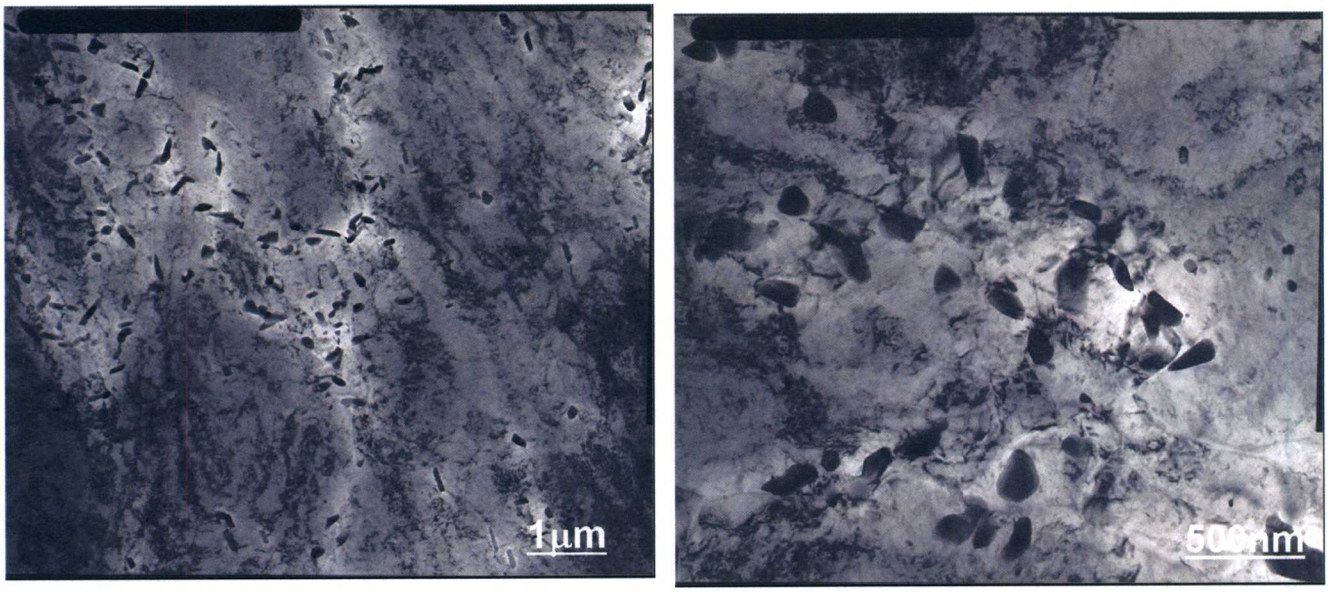

Figure 25. TEM photomicrograph of 3Cr-2WMoV steel.

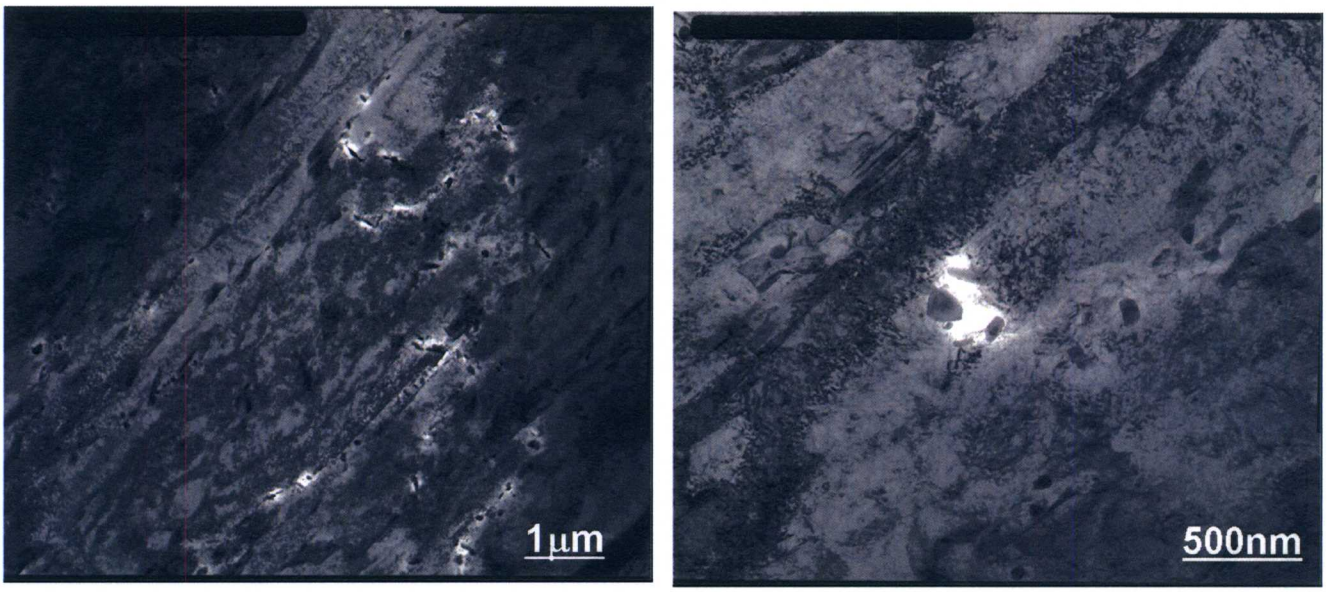

Figure 26. TEM photomicrograph of 3Cr-3WVTaB steel.

High-Chromium Steels

Transmission electron microscopy examination of the 9Cr-2WVTa (Fig. 27), 11Cr-1WMoV (Fig. 28), 11Cr-2WVTa (Fig. 29), and 11Cr-2WVTaB (Fig. 30) revealed differences in the steels, but in general they displayed the typical tempered martensite microstructures for these types of steel. One difference was that tempering the 11Cr-1WMoV steel appeared to cause considerably more recovery than in the other three steels. Although there were still indications

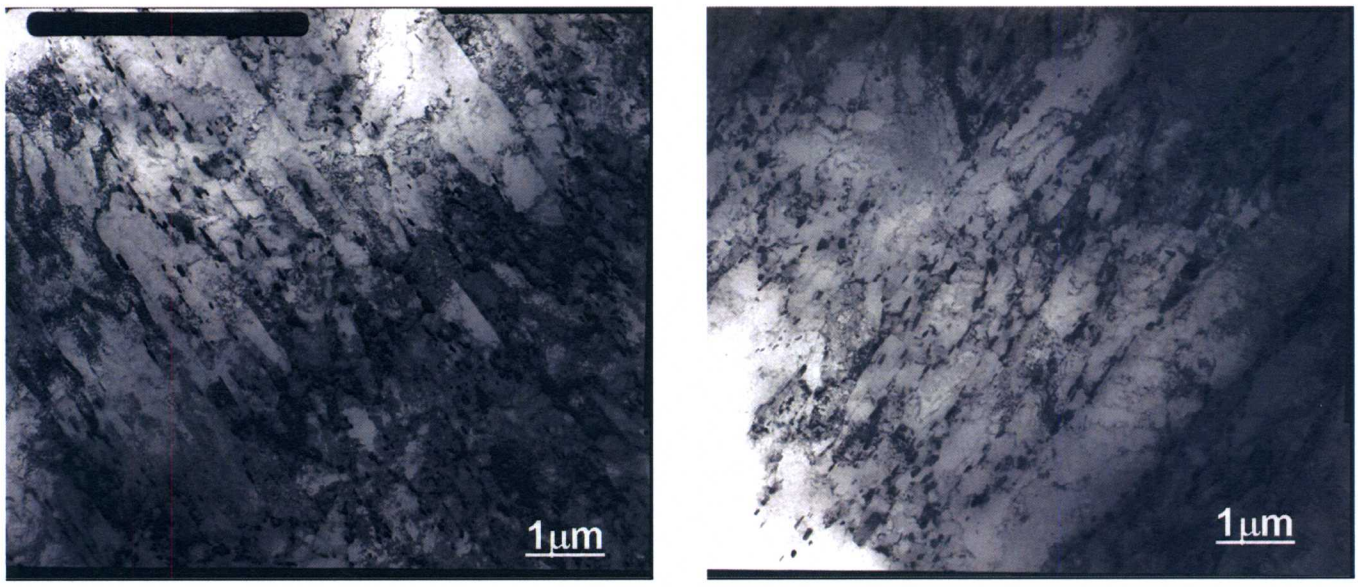

Figure 27. TEM photomicrograph of 9Cr-2WVTa steel.

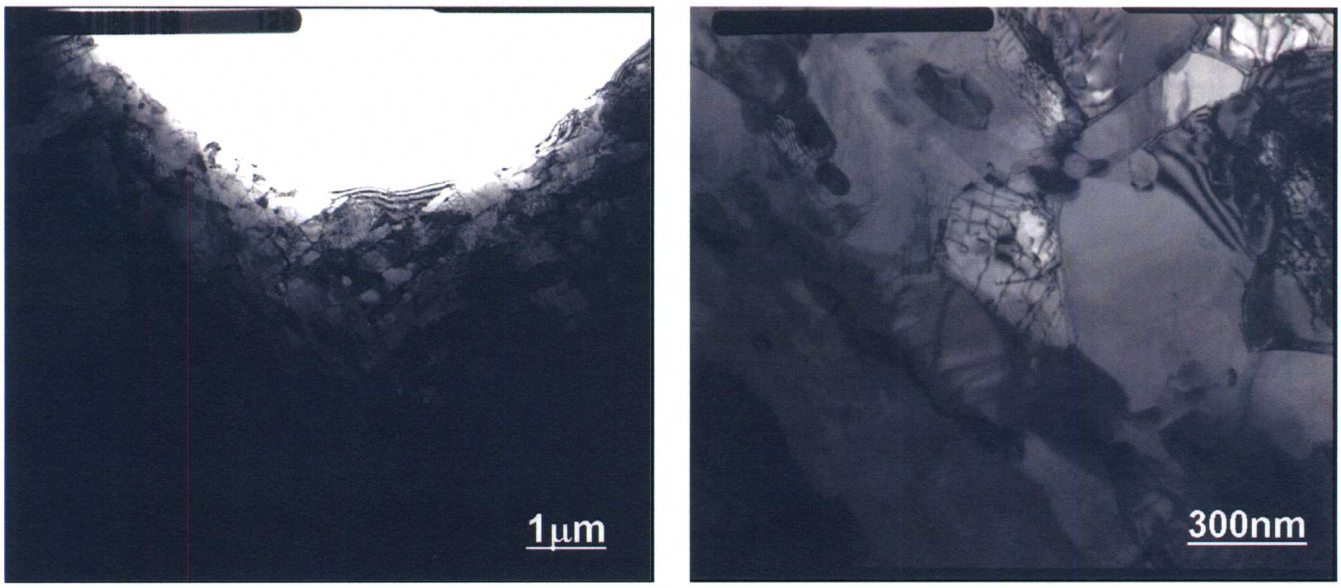

Figure 28. TEM photomicrograph of 11Cr-1WMoV steel.

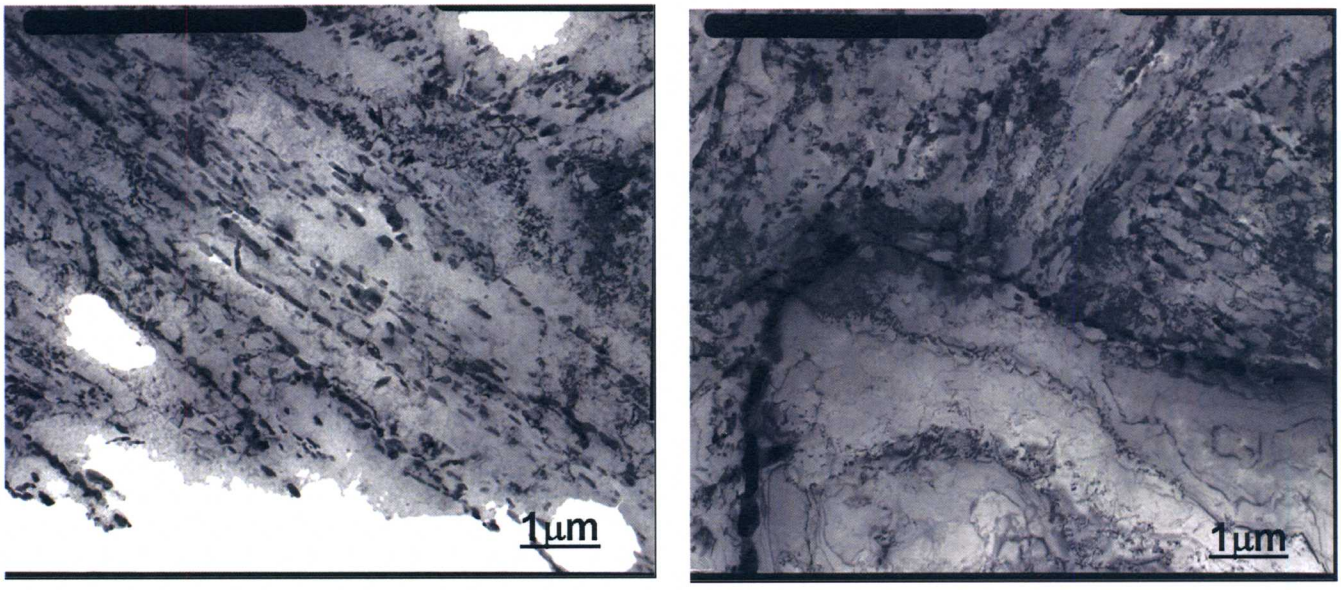

Figure 29. TEM photomicrograph of 11Cr-2WVTa steel.

of laths in this steel, there appeared to have been considerable subgrain growth; the steel also appeared to have considerably less precipitate than the other four steels, which had a high number density of various precipitate sizes. This may be an effect of molybdenum diffusion rate versus tungsten diffusion rate, as discussed later. Figs. 29 and 30 contain images of δ-ferrite and show an almost continuous film of precipitate on the δ-ferrite/tempered martensite boundary.

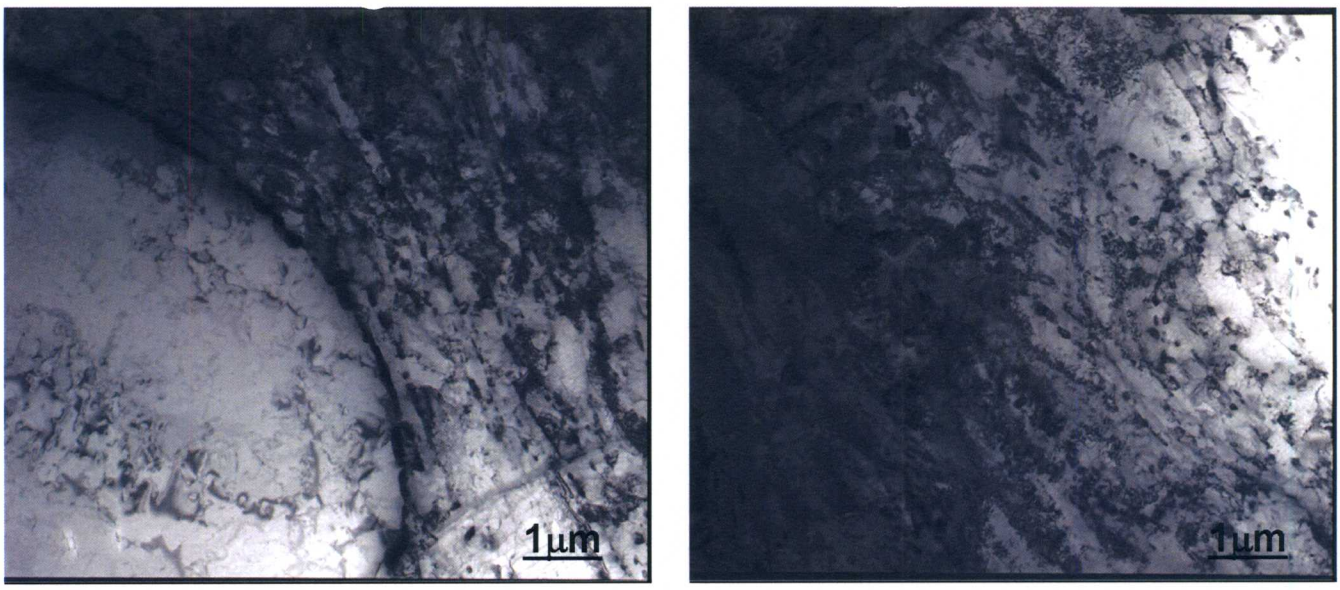

Figure 30. TEM photomicrograph of 11Cr-2WVTaB steel.

Although optical microscopy of COST CB2 indicated this steel to be almost 100% martensite after normalization, TEM showed a somewhat different microstructure for this steel (Fig. 31) compared to that of the other high-chromium steels (Figs. 28-30). The lath structure in the tempered martensite of COST CB2 is not as obvious as it is for the other three steels, where the lath structures are defined by the precipitates formed on lath boundaries. It appears this steel may contain a high number density of finer precipitates that obscure the boundaries.

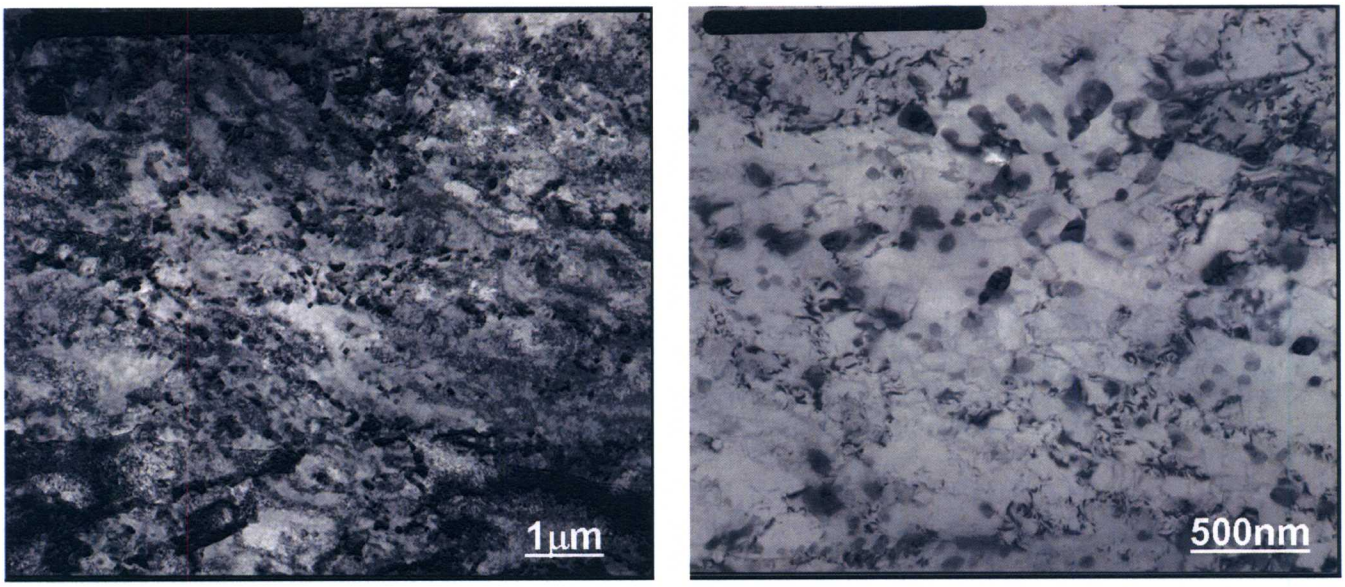

Figure 31. TEM photomicrograph of COST CB2 steel.

Transmission Electron Microscopy—Extraction Replicas

3Cr Steels

Extraction replicas of the four 3% Cr steels were examined, and energy dispersive x-ray spectroscopy data were obtained to identify the precipitates, as shown in Figs. 32-35 for 3Cr-3WV, 3Cr-3WVTa, 3Cr-2WMoVTa, and 3Cr-3WVTaB steels, respectively.

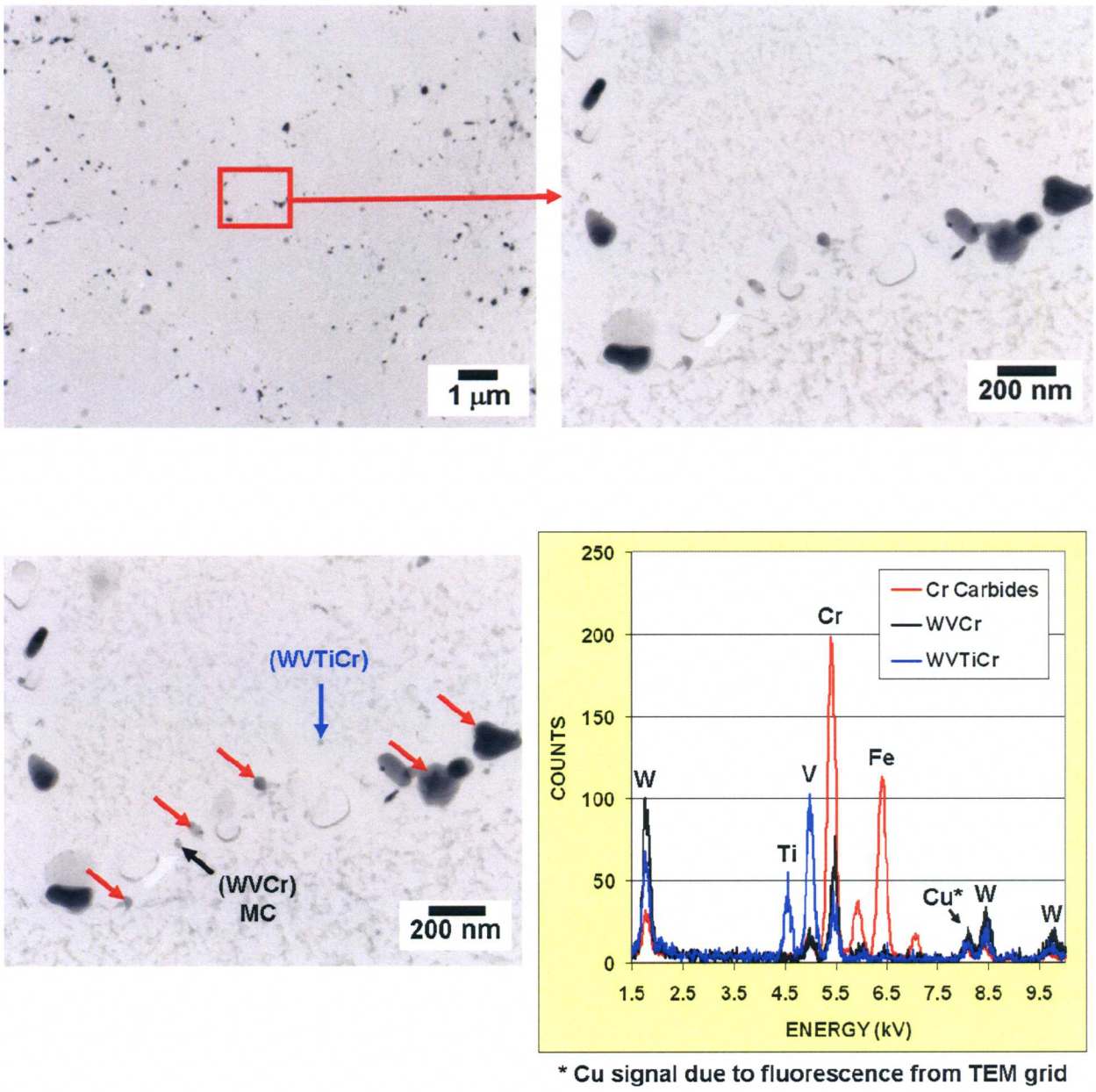

Figure 32. Extraction replica images (above) and energy dispersive x-ray spectroscopy spectra (below) for normalized-and-tempered 3Cr-3WV steel casting.

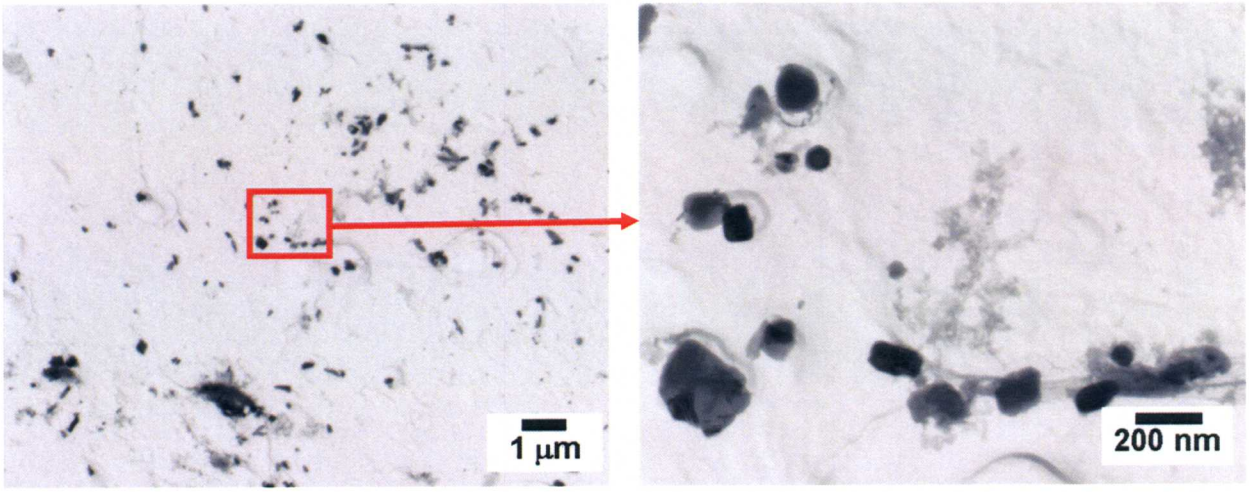

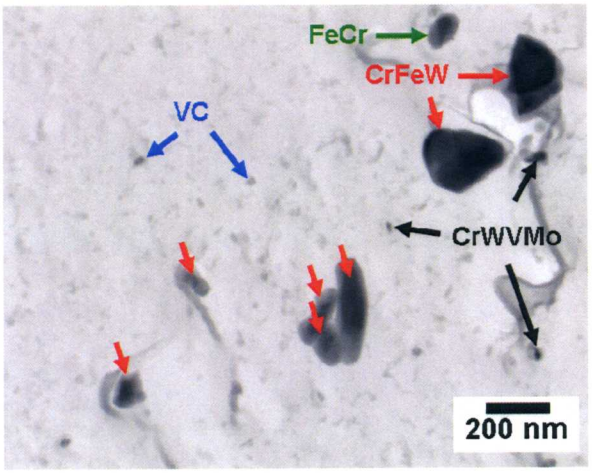

TEM Extraction Replica

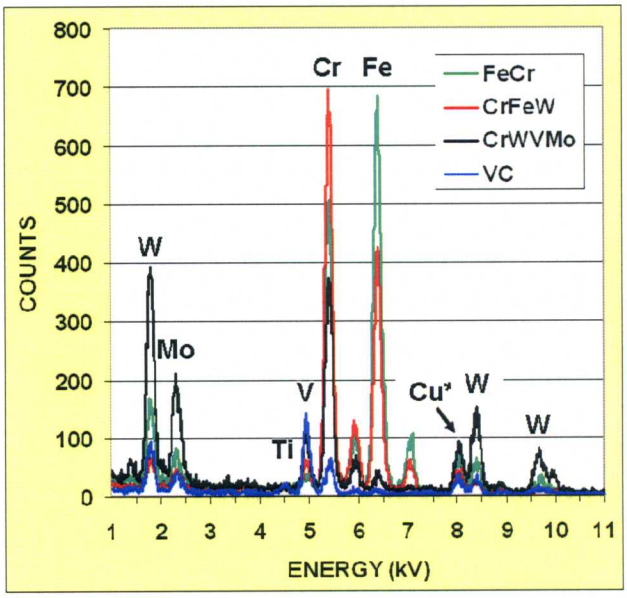

* Cu signal due to fluorescence from TEM grid

Figure 33. Extraction replica images (above) and energy dispersive x-ray spectroscopy spectra (below) for normalized-and-tempered 3Cr-3WVTa steel casting.

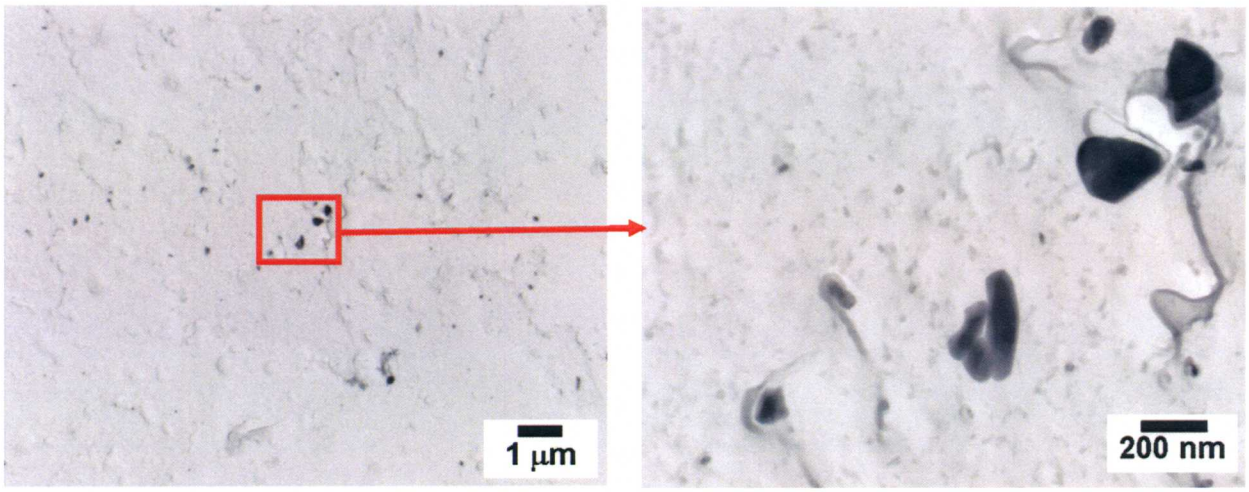

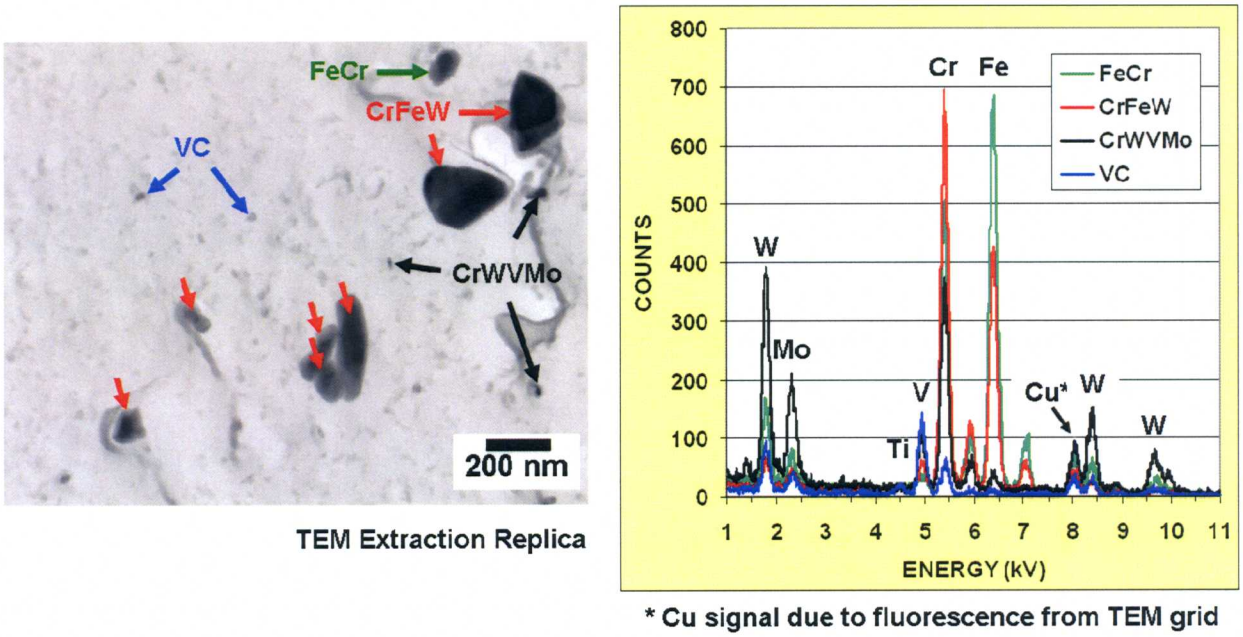

Figure 34. Extraction replica images (above) and energy dispersive x-ray spectroscopy spectra (below) for normalized-and-tempered 3Cr-2WMoVTa steel casting.

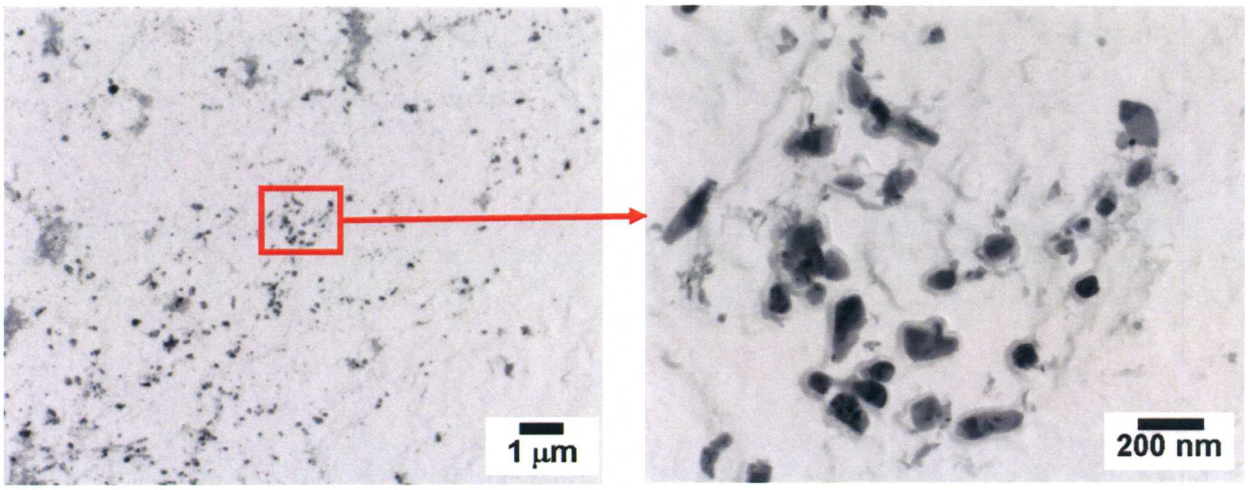

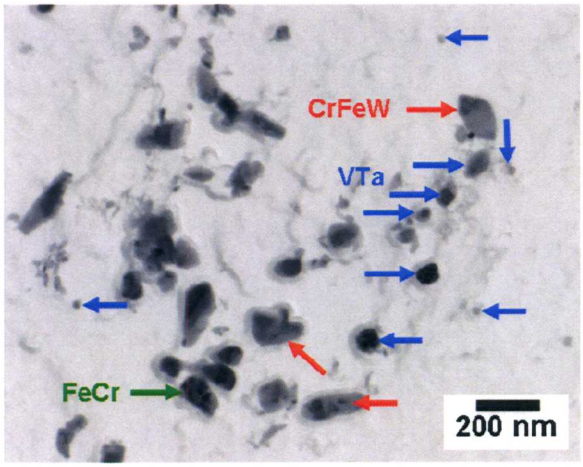

TEM Extraction Replica

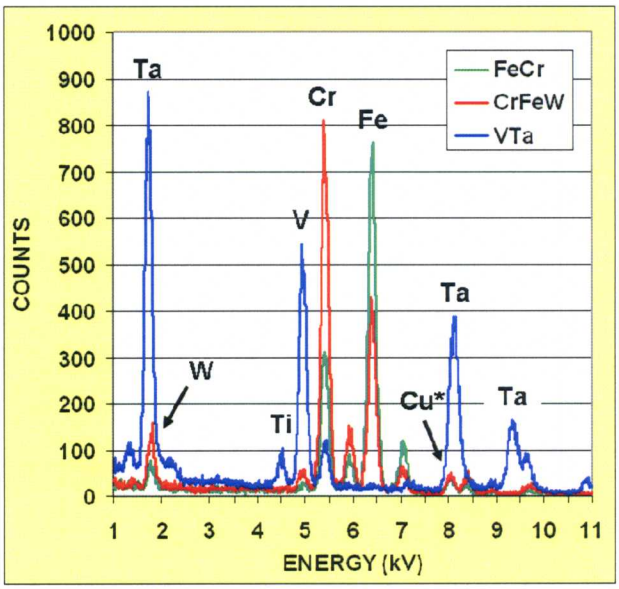

*** Cu signal due to fluorescence from TEM grid**

Figure 35. Extraction replica images (above) and energy dispersive x-ray spectroscopy spectra (below) for normalized-and-tempered 3Cr-3WVTaB steel casting.

High-Chromium Steels

Extraction replicas were examined and energy dispersive x-ray spectroscopy data were obtained to identify the precipitates for COST CB2 (Fig. 36), 9Cr-2WVTa (Fig. 37), 11Cr-1WMoV (Fig. 38), 11Cr-2WVTa (Fig. 39), and 11Cr-2WVTaB (Figs. 40 and 41) steels, and for 11Cr-2WVTaB, electron-diffraction of precipitates on the replicas was used to show that the chromium-rich precipitate was $M_{23}C_6$ and the vanadium-rich precipitate was MX.

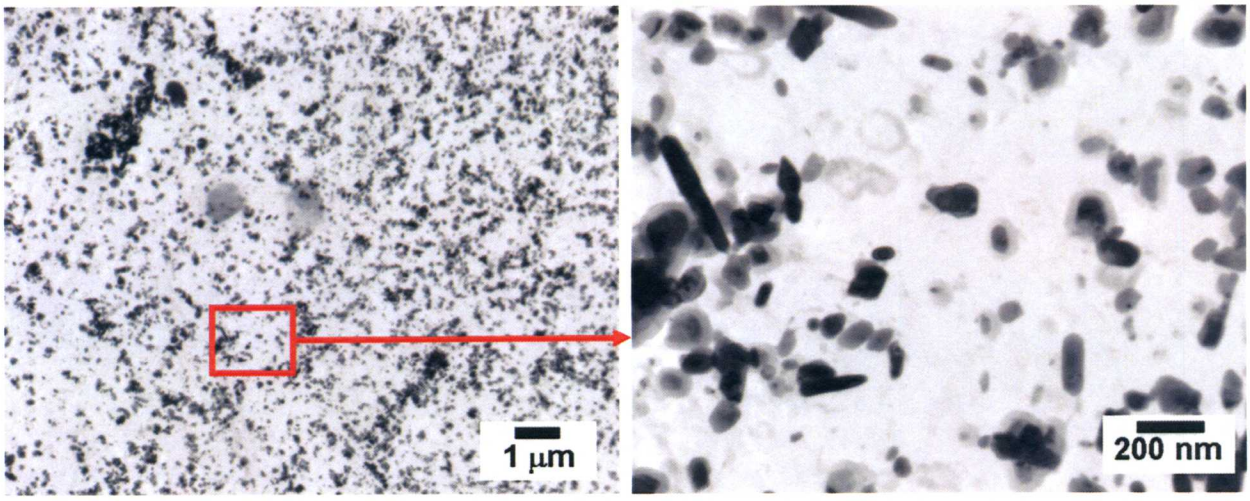

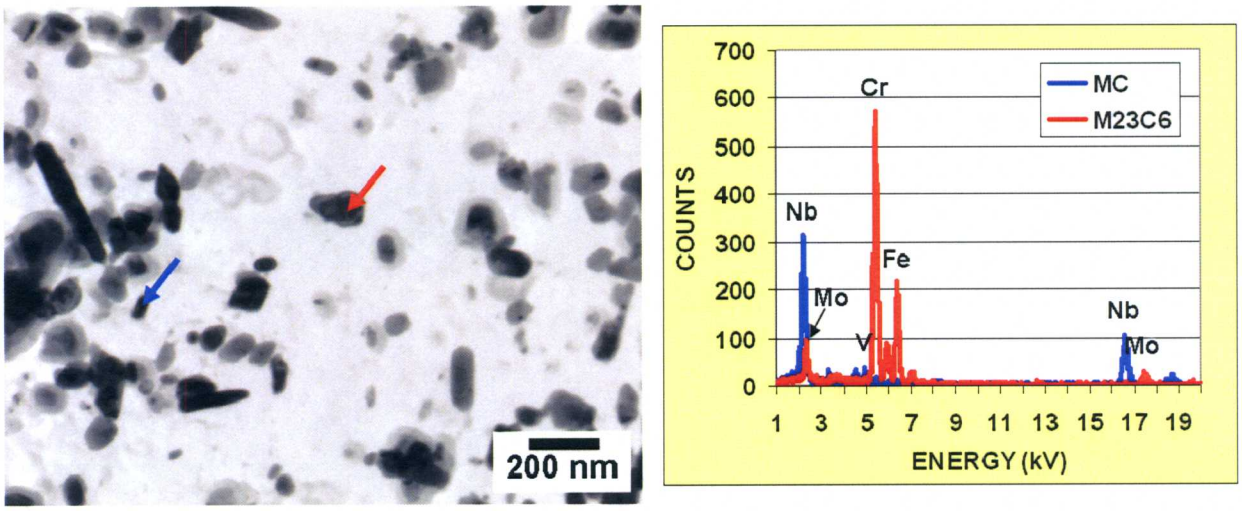

Figure 36. Extraction replica images (above) and energy dispersive x-ray spectroscopy spectra (below) for normalized-and-tempered COST CB2 steel casting.

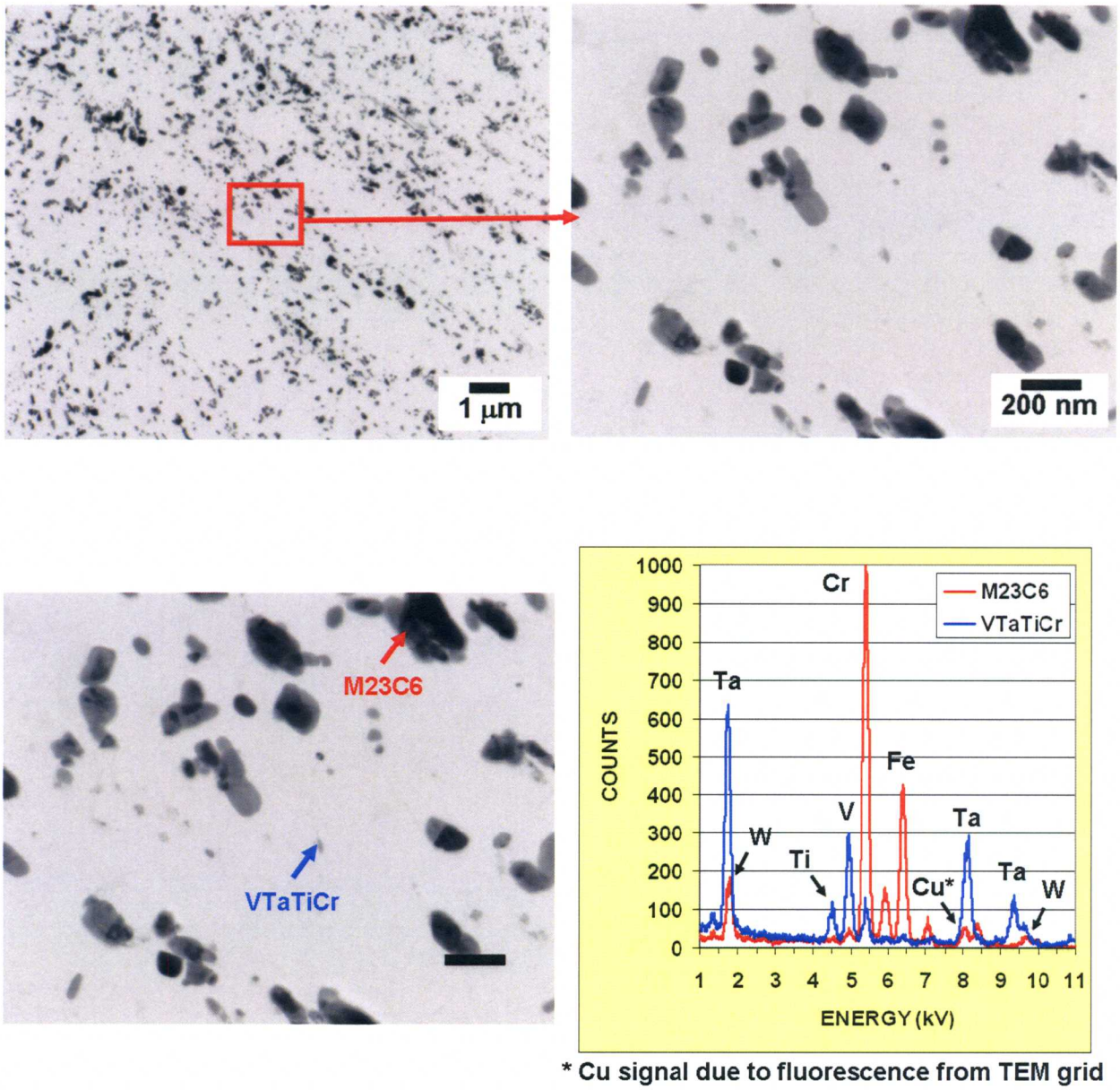

Figure 37. Extraction replica images (above) and energy dispersive x-ray spectroscopy spectra (below) for normalized-and-tempered 9Cr-2WVTa steel casting.

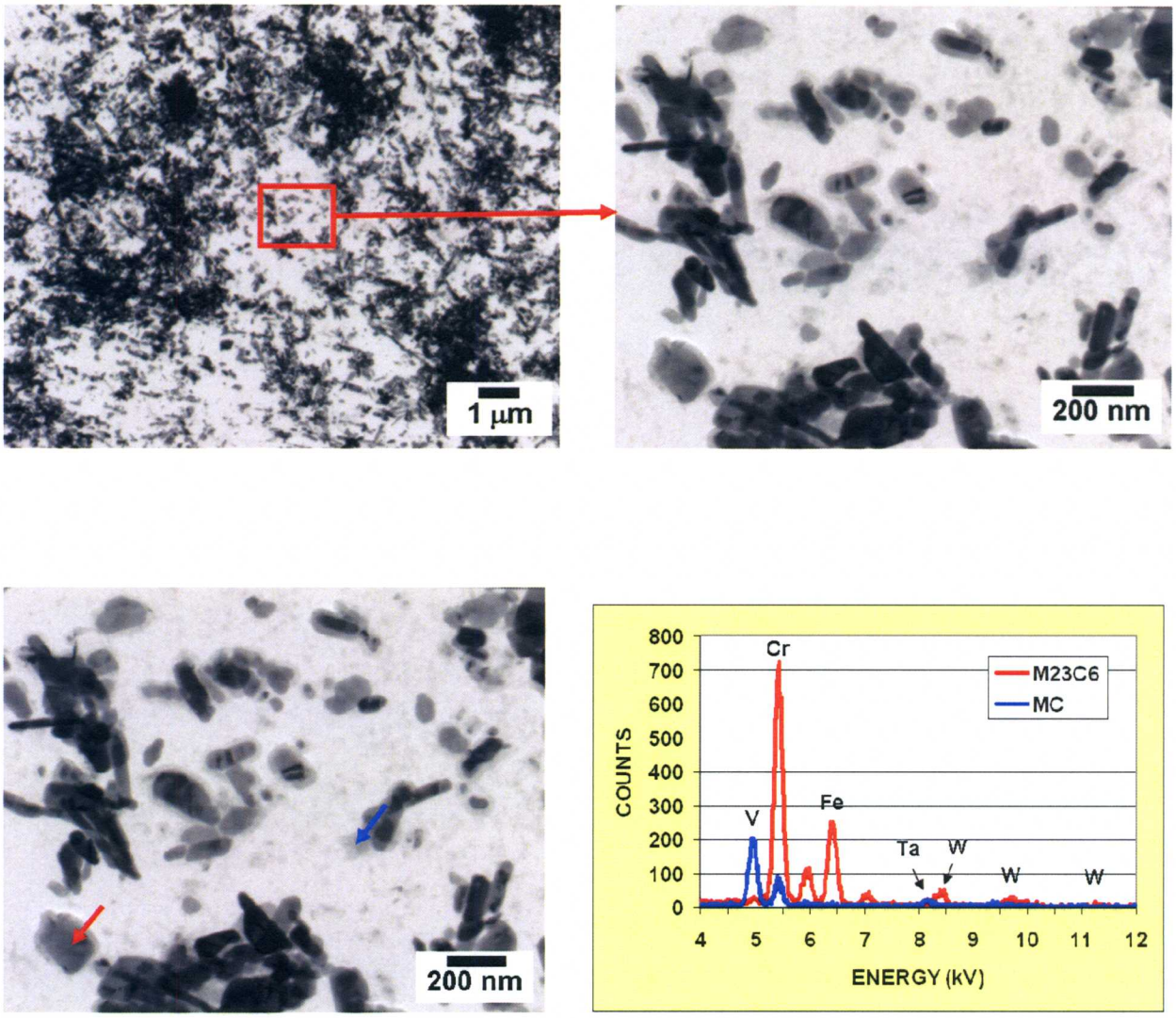

Figure 38. Extraction replica images (above) and energy dispersive x-ray spectroscopy spectra (below) for normalized-and-tempered 11Cr-2WVTa steel casting.

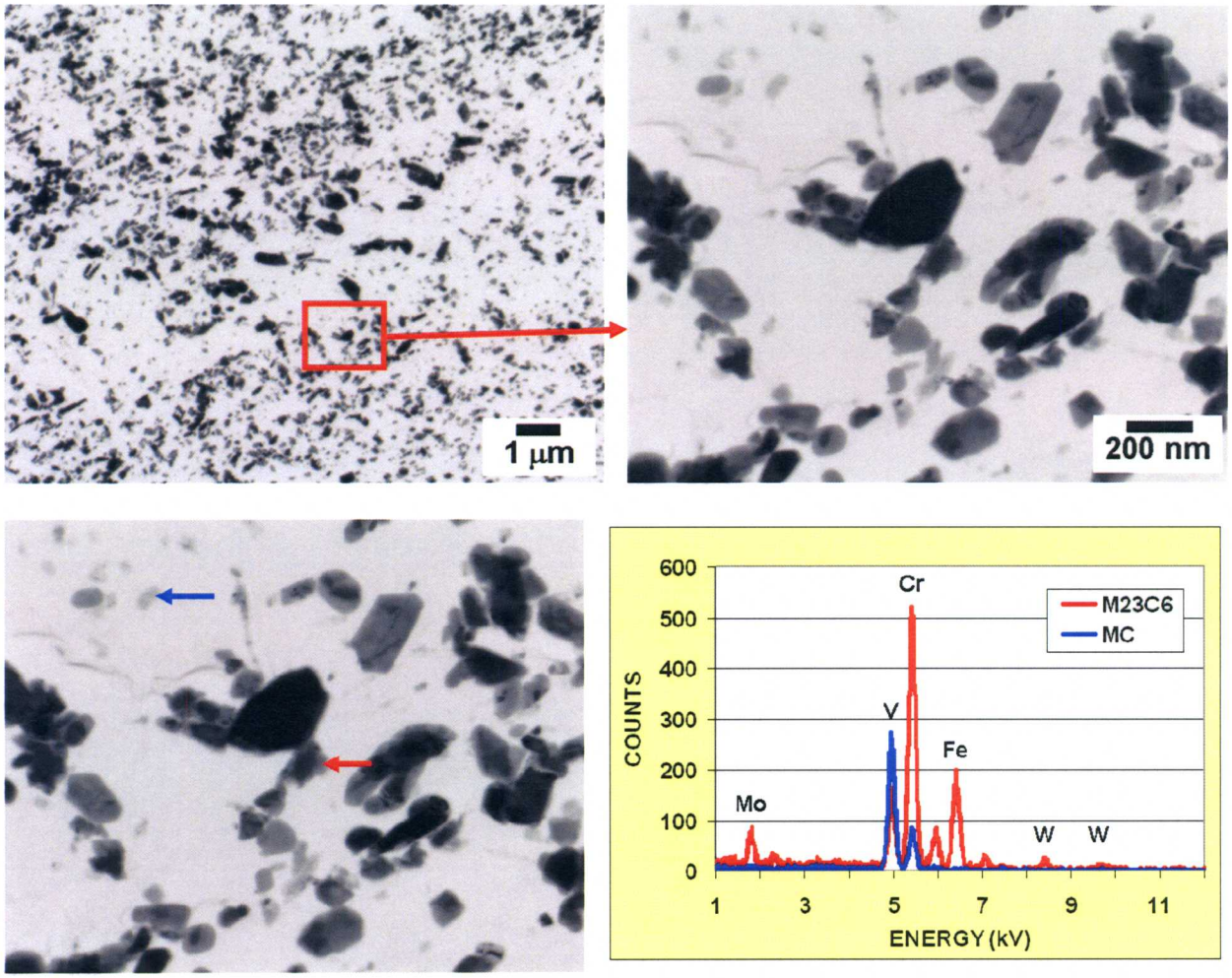

Figure 39. Extraction replica images (above) and energy dispersive x-ray spectroscopy spectra (below) for normalized-and-tempered 11Cr-1W0.5MoV steel casting.

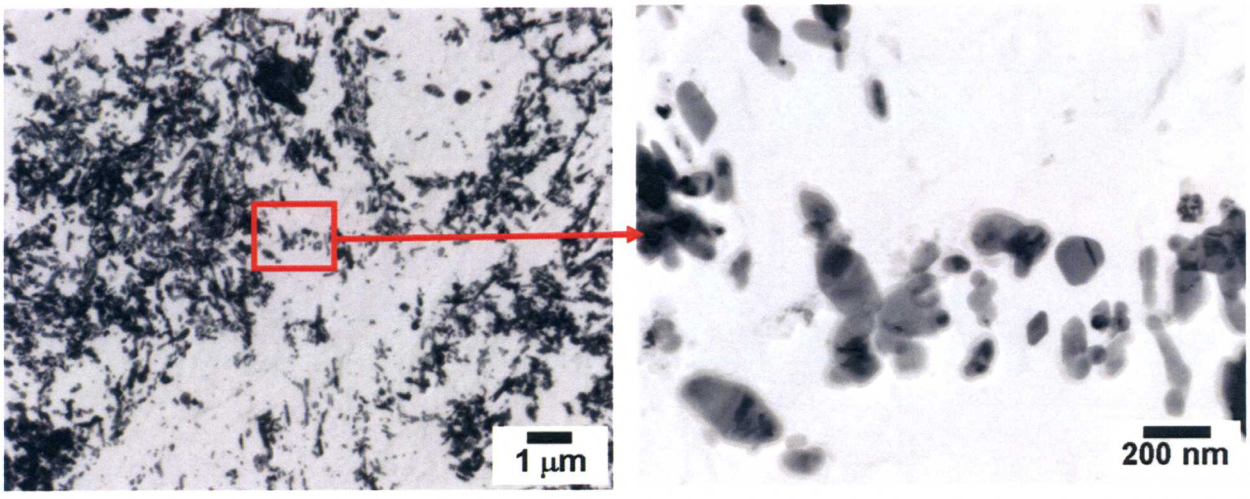

Figure 40. Extraction replica images for normalized-and-tempered 11Cr-2WVTaB steel casting.

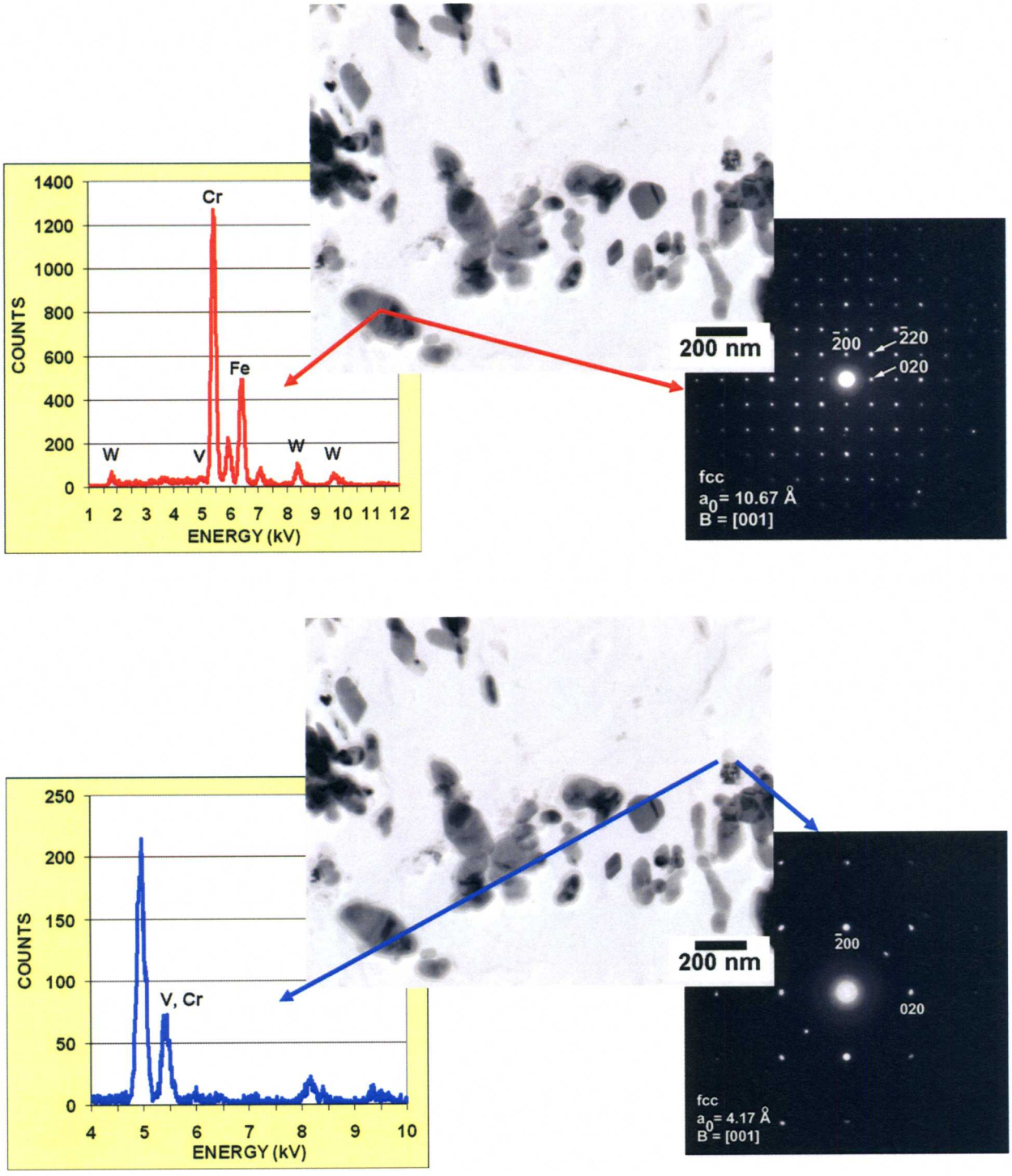

Figure 41. Extraction replica images, energy dispersive x-ray spectroscopy spectra, and an electron diffraction image for normalized-and-tempered 11Cr-2WVTaB steel casting for Cr-rich (above) and V-rich (below) precipitates.

Precipitate Extraction

Precipitates from the steels were extracted electrochemically and collected on a filter, and the mass of the specimen was measured with an accuracy of ±0.1mg before and after extraction. The amounts extracted are given in Table 4.

Table 4. Amount of Precipitate in Steels

Steel	Extracted Precipitate (wt. %)
3Cr-3WV	1.18
3Cr-3WVTa	1.30
3Cr-2W-0.5MoV	1.40
3Cr-3WVTaB	3.33
9Cr-2WVTa	1.49
11Cr-1WMoV	3.07
11Cr-2WVTa	3.10
11Cr-2WVTaB	2.82
9Cr-1.5MoCoVNb	3.13

Mechanical Properties

After the heat-treatment studies, the remainder of the respective test blocks were heat treated. An objective stated by GE was to test all steels at similar strength levels. Based on hardness measurements, a 700°C temper was chosen for 3Cr steels and 750°C temper for the 9 and 11Cr steels. These were the conditions of the test blocks from which tensile, creep, and Charpy specimens were obtained.

Tensile and creep test specimens were machined from the test blocks and tested by Metcut Research Inc., Cincinnati, OH. Charpy specimens were machined and tested at the Saint Louis Testing Laboratories, Inc., Saint Louis, MO.

Tensile Properties

Tensile tests were conducted at room temperature, 400, 500, and 600°C (Table 5). As seen in Fig. 42, three of the 3Cr steels are stronger than COST CB2.

The 1100°C austenitization treatment and the 750°C tempering treatment were the same as those GE used for COST CB2. Although the hardnesses of the high-chromium steels after the 1100°C austenitization and 750°C temper gave comparable hardnesses for the different steels, it is obvious that it did not produce comparable strengths. The tensile properties of the 9Cr-2WVTa steel approached those of COST CB2 (Fig. 43). However, all of the 11Cr steels were weaker than COST CB2 (Fig. 44), although the 11Cr-2WVTa steel had tensile properties that approached those of COST CB2.

Table 5. Tensile Properties of Normalized-and-Tempered Cast Test Blocks

Steel	Cast	Temp C	YS (ksi)	YS (MPa)	UTS (ksi)	UTS (MPa)	Elgn (%)	RA (%)
3Cr-3WV	1	21	136.0	937.0	153.0	1054.2	15	39
3Cr-3WV	1	400	118.0	813.0	136.0	937.0	14	48
3Cr-3WV	1	500	107.0	737.2	121.0	833.7	16	63
3Cr-3WV	1	600	88.0	606.3	101.0	695.9	9	24
3Cr-3WV	1	650	74.5	513.3	87.5	602.9	6.5	17
3Cr-3WVTa	2	21	132.0	909.5	147.0	1012.8	17	51
3Cr-3WVTa	2	400	112.0	771.7	127.0	875.0	12	47
3Cr-3WVTa	2	500	101.0	695.9	113.0	778.6	18	62
3Cr-3WVTa	2	600	83.0	571.9	94.0	647.7	13	30
3Cr-3WVTa	2	650	69.5	478.9	80.0	551.2	11	30
3Cr-3WMoVTa	3	21	111.0	764.8	124.0	854.4	20	64
3Cr-3WMoVTa	3	400	94.0	647.7	106.0	730.3	17	63
3Cr-3WMoVTa	3	500	85.5	589.1	94.5	651.1	20	71
3Cr-3WMoVTa	3	600	70.0	482.3	78.0	537.4	22	74
3Cr-3WMoVTa	3	650	55.5	382.4	65.0	447.9	25	61
3Cr-3WVTaB	21	21	144.0	992.2	162.0	1116.2	12	47
3Cr-3WVTaB	21	400	120.0	826.8	142.0	978.4	14	52
3Cr-3WVTaB	21	500	112.0	771.7	128.0	881.9	17	57
3Cr-3WVTaB	21	600	89.5	616.7	105.0	723.5	11	30
3Cr-3WVTaB	21	650	76.5	527.1	89.5	616.7	7.5	26
11Cr-1WMoV	18	21	83.5	575.3	110.0	757.9	16	42
11Cr-1WMoV	18	400	68.0	468.5	85.5	589.1	14	47
11Cr-1WMoV	18	500	59.0	406.5	70.5	485.7	23	64
11Cr-1WMoV	18	600	40.9	281.8	49.7	342.4	35	86
11Cr-1WMoV	18	650	27.5	189.5	37.5	258.4	39	91
11Cr-2WVTa	31	21	108.0	744.1	129.0	888.8	15	49
11Cr-2WVTa	31	400	89.5	616.7	103.0	709.7	14	49
11Cr-2WVTa	31	500	79.0	544.3	89.0	613.2	20	62
11Cr-2WVTa	31	600	56.0	385.8	65.5	451.3	32	82
11Cr-2WVTa	31	650	43.0	296.3	52.5	361.7	33	84
11Cr-2WVTaB	36	21	93.5	644.2	116.0	799.2	15	47
11Cr-2WVTaB	36	400	77.0	530.5	92.0	633.9	14	48
11Cr-2WVTaB	36	500	67.5	465.1	77.5	534.0	18	60
11Cr-2WVTaB	36	600	48.3	332.8	57.0	392.7	38	82
11Cr-2WVTaB	36	650	35.5	244.6	44.9	309.4	27	81
9Cr-2WVTa	29	21	104.0	716.6	122.0	840.6	16	45
9Cr-2WVTa	29	400	86.5	596.0	96.5	664.9	13	48
9Cr-2WVTa	29	500	74.5	513.3	83.0	571.9	17	64
9Cr-2WVTa	29	600	57.5	396.2	65.0	447.9	26	80
9Cr-2WVTa	29	650	41.8	288.0	50.0	344.5	28	84
COST CB2	45	21	111.0	764.8	130.0	895.7	13	47
COST CB2	45	400	94.0	647.7	106.0	730.3	14	53
COST CB2	45	500	85.0	585.7	95.5	658.0	19	56
COST CB2	45	600	65.0	447.9	73.0	503.0	22	72
COST CB2	45	650	51.0	351.4	61.0	420.3	21	79

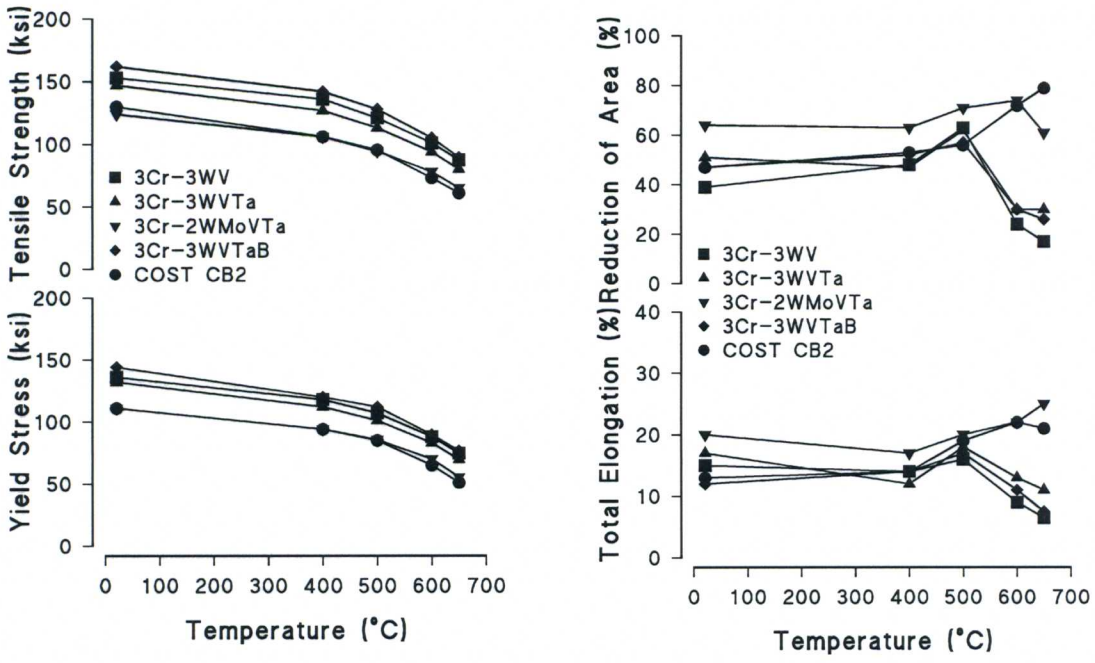

Figure. 42. Tensile properties of 3Cr steels compared to COST CB2 steel.

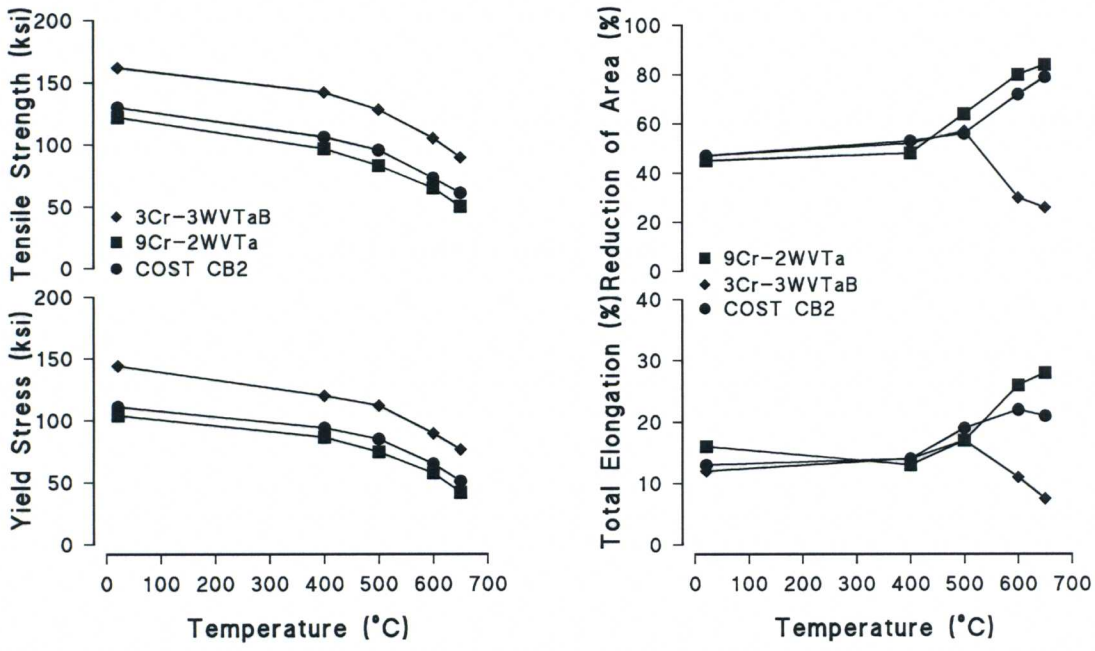

Figure 43. Tensile properties of 9Cr-2WVTa compared to COST CB2 and strongest 3Cr steel.

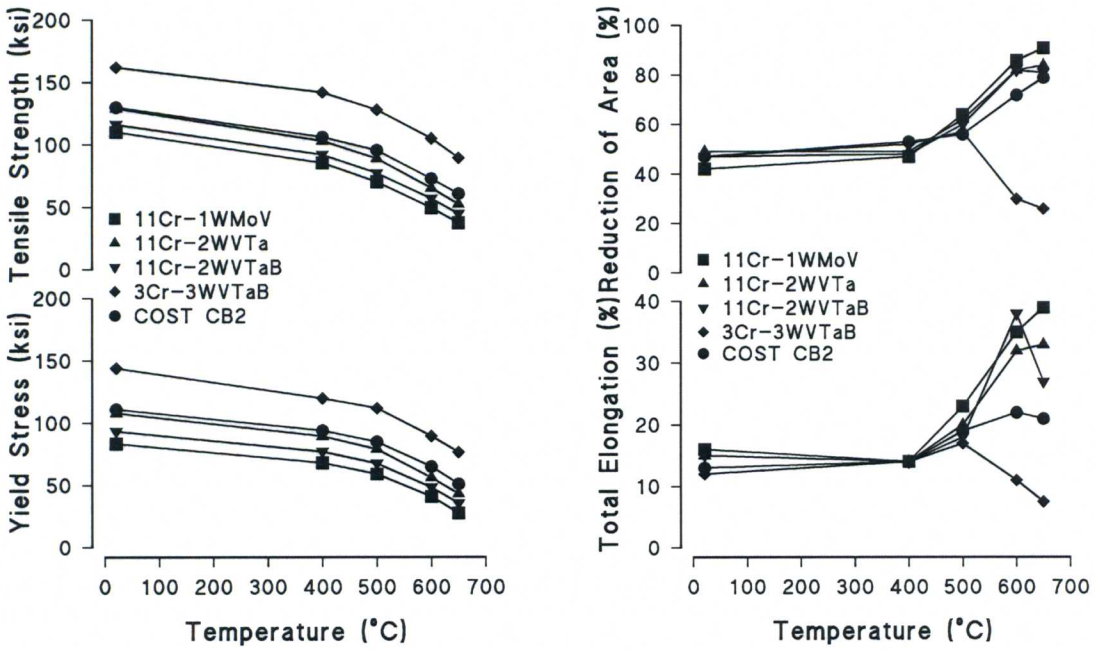

Fig. 44. Tensile properties of 11Cr steels compared to COST CB2 steel and strongest 3Cr steel.

Impact Properties

Charpy impact data are plotted in Fig. 45, and they generally reflect the strengths; that is, the weakest materials have the best impact properties. An encouraging observation is that the 9Cr-2WVTa and 11Cr-2WVTa steels, which had strengths approaching the CB2 strength, also had impact properties comparable to those of COST CB2.

Creep-Rupture Properties

Creep-rupture tests were conducted at 600 and 650°C (Table 6), and creep-rupture curves based on the limited tests were plotted (Fig. 46). In all cases, results indicated that COST CB2 has better creep-rupture strength than all the other steels. Certainly COST CB2 is much stronger than the 3Cr steels. A similar conclusion might follow for the 9 and 11 Cr steels, but there may be more promise there. As a result of the observations of inferior properties relative to COST CB2, the tests for the data points in Fig. 46 shown with arrows were discontinued prior to rupture.

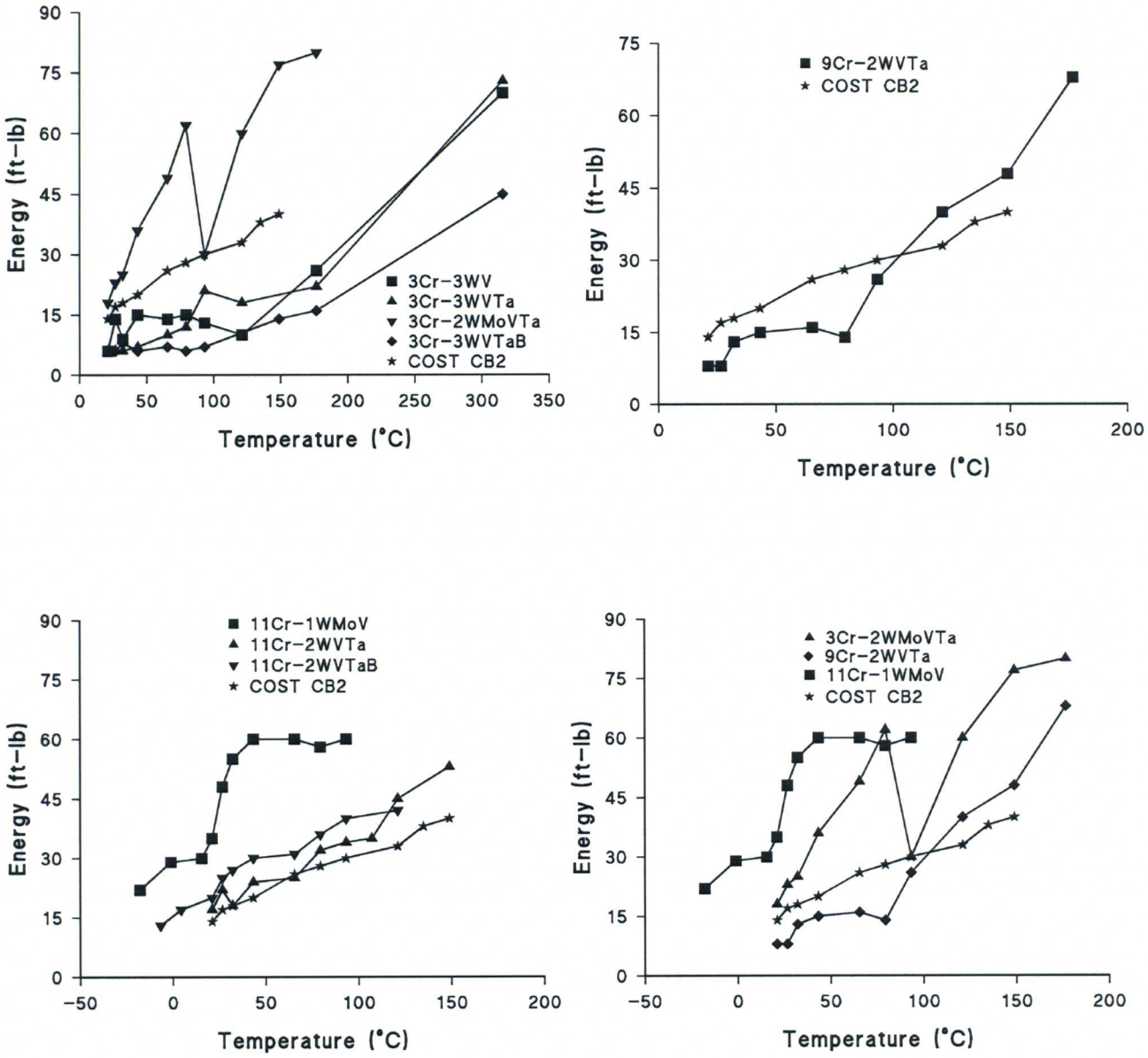

Figure 45. Charpy curves for the 3Cr (upper left), 9Cr (upper right), 11 Cr (lower left) compared to COST CB2 and the best 3Cr, 9Cr, and 11Cr compared to COST CB2 (lower right).

Table 6. Creep-Rupture Properties

Steel	Cast	Spec No	Temp °C	Stress Ksi	Time-0.5% h	Time-1% h	Rup time h	Elon %	RA %
3Cr-3WV	1	1-CR-1	650	20	23.5	42.7	100.6	28.2	57.0
3Cr-3WV	1	1-CR-2	600	40			70.1	1.7	0.4
3Cr-3WV	1	1-CR-3	650	10	98	207	1822.6	12.1	19.8
3Cr-3WV	1	1-CR-4	600	25	235	392	655.8	12.2	28.0
3Cr-3WVTa	2	2-CR-1	650	20	97.8	161	252.9	10.8	31.0
3Cr-3WVTa	2	2-CR-2	600	40			134.4	1.7	2.0
3Cr-3WVTa	2	2-CR-3	600	25	906	1468	1692.7	5.6	7.4
3Cr-3WVTa	2	2-CR-4	650	10	267	529	2475.1[a]		
3Cr-3WMoVTa	3	3-CR-1	650	20	27.6	47.5	100.9	25.5	53.0
3Cr-3WMoVTa	3	3-CR-2	600	40	38.9	71.8	106.4	8.9	16.0
3Cr-3WMoVTa	3	3-CR-3	650	10	110	217	1592.9	[b]	36.5
3Cr-3WMoVTa	3	3-CR-4	600	25	230	370	637	14.2	33.0
3Cr-3WVTaB	21	21-CR-1	600	40			103.9	1.2	2.0
3Cr-3WVTaB	21	21-CR-2	650	20	82.2	123	162.1	5.2	8.0
3Cr-3WVTaB	21	21-CR-3	600	25	583	944	945.9	2.5	4.5
3Cr-3WVTaB	21	21-CR-4	650	10	204	413	3292	12.4	14.9
11Cr-1WMoV	18	18-CR-1	600	35	0.08	0.2	2.4	27.8	78.0
11Cr-1WMoV	18	18-CR-2	650	20	0.32	1.4	23.3	34.6	87.0
11Cr-1WMoV	18	18-CR-3	600	20	22.3	135	1555.4	14.7	34.0
11Cr-1WMoV	18	18-CR-4	650	30	0.01	0.03	0.4	33.4	85.0
11Cr-2WVTa	31	31-CR-1	600	40	0.23	0.8	8.5	22.4	79.0
11Cr-2WVTa	31	31-CR-2	650	20	18.1	49	241.8	22.9	76.0
11Cr-2WVTa	31	31-CR-3	600	25	299	1463	3463.4		
11Cr-2WVTa	31	31-CR-4	650	10	823		3476.4		
11Cr-2WVTaB	36	36-CR-1	600	35	0.57	2.37	29.5	20.4	68.5
11Cr-2WVTaB	36	36-CR-2	650	15	195	825	3648.9[a]		
11Cr-2WVTaB	36	36-CR-3	600	25	119	1021	2447.3[a]		
11Cr-2WVTaB	36	36-CR-4	650	20	21	82	379.3	15.1	57.0
9Cr-2WVTa	29	29-CR-1	600	40	0.7	2.7	14.7	21.5	75.0
9Cr-2WVTa	29	29-CR-2	650	20	45.5	90.8	197.5	22.7	81.0
9Cr-2WVTa	29	29-CR-3	600	25	309	1097	3143.2	18.6	69.2
9Cr-2WVTa	29	29-CR-4	650	10	977		3428.9[a]		
COST CB2	45	45-CR-1	650	30	17.3	34	50.6	13.0	52.9
COST CB2	45	45-CR-2	650	20	553	1231	1831.3	8.9	29.9
COST CB2	45	45-CR-3	600	45	9.2	33.1	97.4	16.2	63.8
COST CB2	45	45-CR-4	600	30	1382		4145.5[a]		

[a] Test discontinued before rupture; [b] Specimen drilled out of grips.

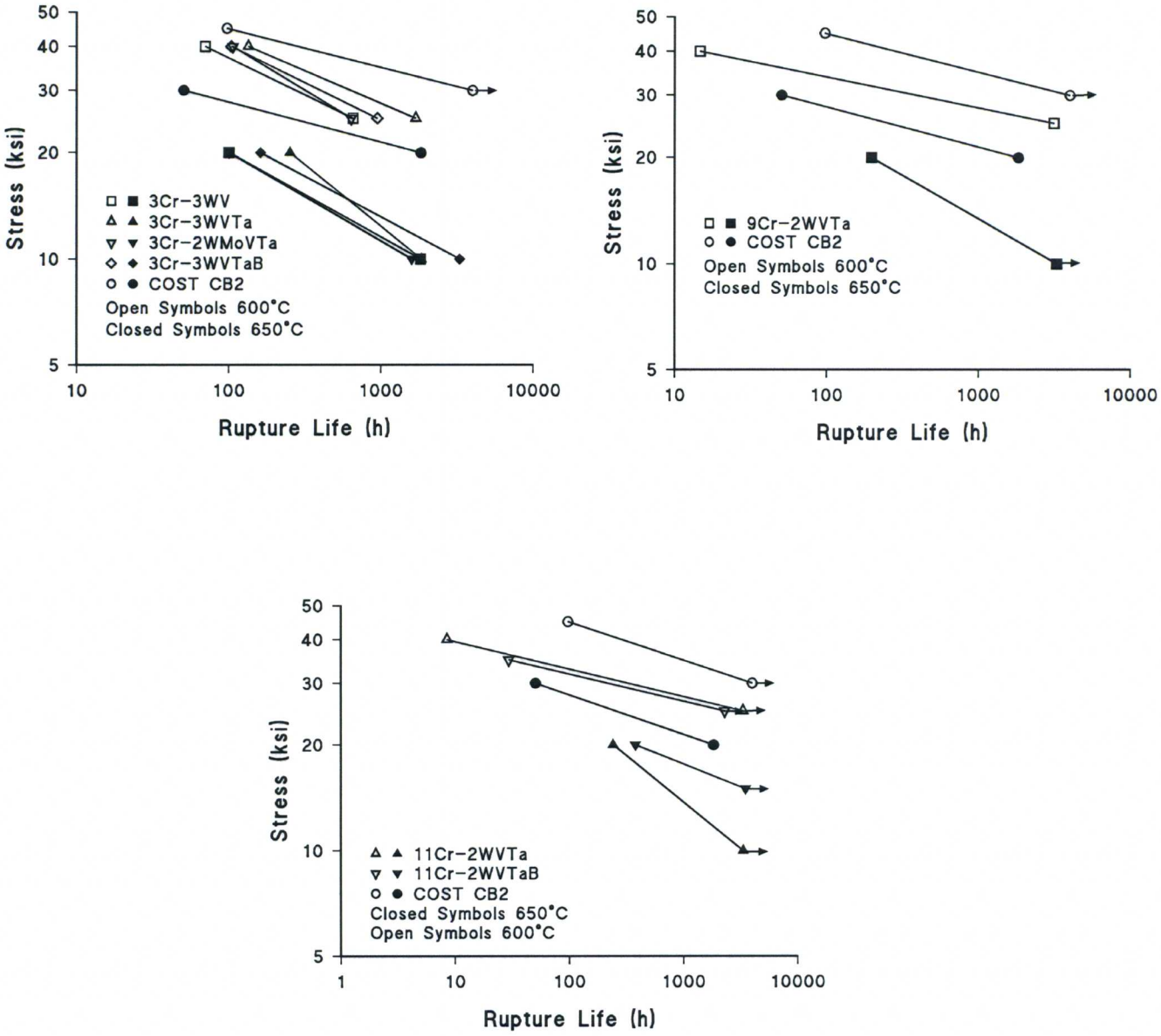

Figure. 46. Creep rupture curves at 600 and 650°C for 3Cr (upper left), 9Cr (upper right), 11Cr (lower center) steels compared with the COST CB2.

Experimental—Part II

Heat Treatment Number 2—High-Chromium Steels

In the above presentation of the tensile and creep properties of ORNL compositions and the COST CB2 composition, none of the ORNL steels had properties equivalent to the COST CB2. One difference in microstructure of the ORNL high-chromium (9 and 11Cr) steels and the COST CB2 was the higher amount of δ-ferrite in the former. A possible cause of this difference may be segregation during solidification of the casting and the subsequent homogenization, or lack thereof, during the austenitization treatment. The difference may be due to the diffusion of tungsten (in the ORNL steels) vs. molybdenum (in COST CB2). The diffusion coefficient for tungsten in austenite at 1280°C (where data were available) is about an order-of-magnitude less than for molybdenum [2]. It is assumed there would be a similar or greater difference at 1100°C, thus providing a reason for a longer time or higher temperature required to eliminate δ-ferrite from tungsten-containing steels. This conclusion is bolstered by the observation that the 11Cr-1WMoV steel contained essentially no δ-ferrite after 1 h at 1100°C.

To explore the elimination of δ-ferrite in the high-chromium steels, austenitizing times longer than 1 h at 1100 and 1175°C were examined on the strongest ORNL steels—9Cr-2WVTa, 11Cr-2WVTa, and 11Cr-2WVTaB (11Cr-1WMoV was not examined because it was considerably weaker than the other three steels). Microhardness measurements (Table 7) and microstructural examination indicated that a longer austenitization time at 1100°C reduced the amount of δ-ferrite present and increased the hardness over that for 1 h at 1100°C. There was also an increase in hardness with time after the1175°C treatment. However, there was considerable δ-ferrite remaining in the microstructure of the 9Cr-2WVTa steel after 5 h at 1175°C, with a lesser amount in the 11Cr-2WVTa steel. None could be detected in the 11Cr-2WVTaB steel after 5 h at 1175°C, which was also reflected in the hardness for this steel.

A 5 h austenitization at 1100°C was chosen for these three steels, and they were tempered 1 h at 750°C.

Table 7. Vickers Hardness of Selected Steels After Additional Austenitization Treatments

Steel	Vickers Hardness (HV)					
	1100°C/1h	1100°C/3h	1100°C/5h	1175°C/1h	1175°C/3h	1175°C/5h
9Cr-2WVTa	394	431	445	387	411	420
11Cr-2WVTa	436	514	507	459	493	471
11Cr-2WVTaB	439	501	507	440	492	517

Mechanical Properties II—High-Chromium Steels

Tensile Studies

After normalization with a 5 h at 1100°C austenitization, a 1 h at 750°C temper was applied to the 9Cr-2WVTa, 11Cr-2WVTa, and 11Cr-2WVTaB steel test blocks. Tensile specimens were then machined and tested at 21, 600, and 650°C and compared with the COST CB2. The new heat treatment caused an increase in yield stress and ultimate tensile strength of both the 9Cr (Fig 47) and 11 Cr (Fig. 48) steels. However, the strengths were still inferior to that of COST CB2.

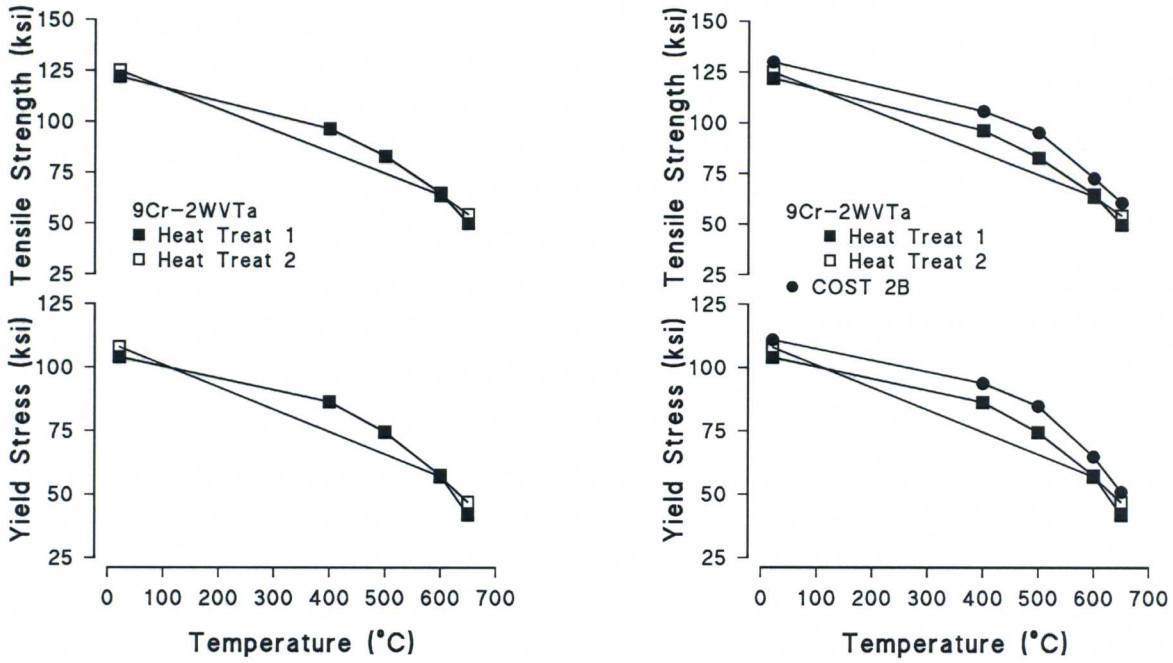

Figure 47. Yield stress and ultimate tensile strength of 9Cr-2WVTa steel (left) after two heat treatments and (right) compared with the COST CB2 steel.

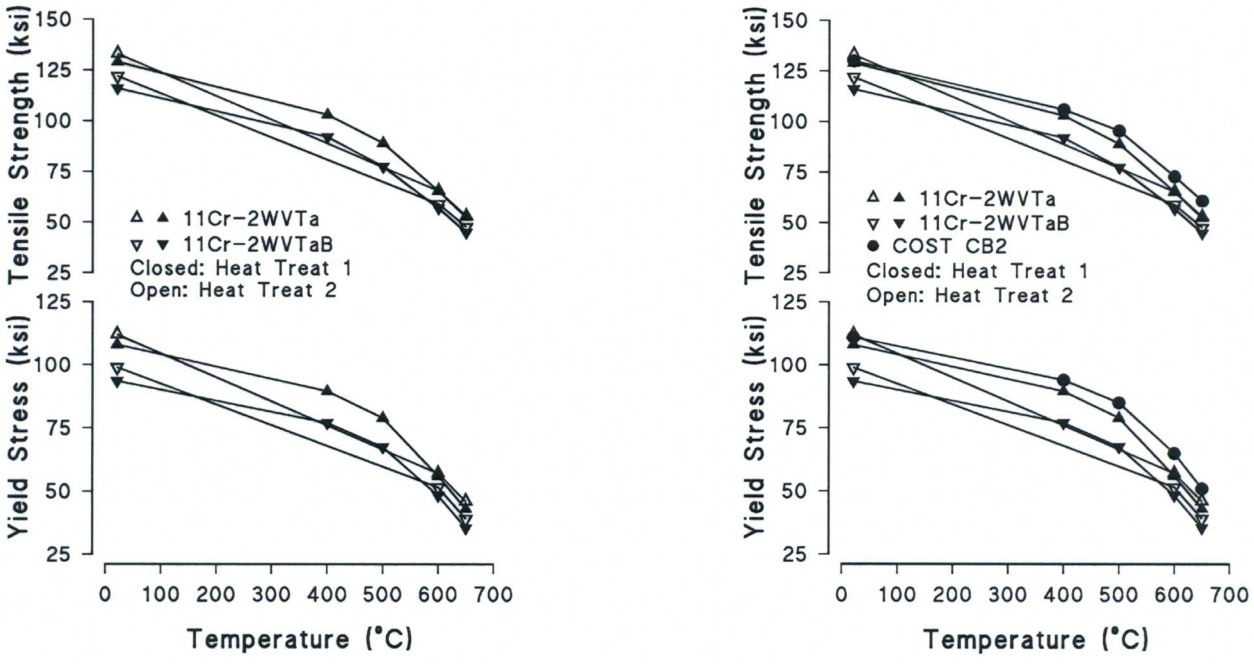

Figure 48. Yield stress and ultimate tensile strength of 11Cr-2WVTa and 11Cr-2WVTaB steels (left) after two heat treatments and (right) compared with the COST CB2 steel.

Creep Studies

Although the tensile results did not look promising relative to COST CB2, creep specimens were machined from each of the steels given the 5 h at 1100°C austenitization treatment. Specimens were put into test at 30 ksi at 600°C and 20 ksi at 650°C. The 5 h at 1100°C treatment produced longer rupture times than 1 h at 1100°C (Table 8). However, the 650°C tests ruptured in relatively short times compared to COST CB2, and because of the relatively short rupture times at 650°C, the tests at 600°C were evaluated in terms of 0.5% creep strain. When the time to 0.5% creep strain was compared to that of COST CB2 and found to be substantially lower, the 30 ksi tests at 600°C were discontinued.

Table 8. Creep Properties of Steels After Second Heat Treatment

Steel	Time 0.5% Creep/600°C/30 ksi (hr)	Time Rupture/650°C/20 ksi (hr)	
		1100°C/1h	1100°C/5h
9Cr-2WVTa	252	197.5	342.0
11Cr-2WVTa	255	241.8	324.4
11Cr-2WVTaB	196	379.3	399.1
COST CB2	1382	1831.3	

Analysis of Results—High-Chromium Steels

Comparison of ORNL Steels and COST CB2

When compositions of the two 9Cr steels, 9Cr-2WVTa and COST CB2, are compared, the major differences are that COST CB2 contains Mo, Nb, Co, and B, which are not in 9Cr-2WVTa. The 9Cr-2WVTa contains W and Ta, which are not in COST CB2. The 9Cr-2WVTa wrought steel was developed for fusion applications and patterned after modified 9Cr-1Mo under the assumption that W and Ta would behave like Mo and Nb in modified 9Cr-1Mo if substituted on an atom-for-atom basis. This assumption was based on the respective elements W and Mo and Ta and Nb being in the same column of the periodic table of elements and having similar alloying characteristics in steels. It was also based on the observations that some Cr-WVTa wrought steels have improved properties over Cr-MoVNb steels [3-5]. In addition there are differences in compositions: the W-Mo relationship between the 9Cr-2WVTa and COST CB2 is not atom-for-atom as there is ≈50 at % more molybdenum in COST CB2 than tungsten in 9Cr-2WVTa. There is also 0.02% more C, 0.8% Co, and 0.008% B in the COST CB2.

In the 3Cr steels an atom-for-atom substitution of Mo for W was made, but the Mo-containing steel (3Cr-2W-0.5MoVTa) turned out to be the weakest 3Cr steel. Similarly, the 11Cr1WMoV was also the weakest of the 11Cr steels, but there was also the difference that this steel did not contain tantalum, so the comparison is not direct, as it is for the 3Cr steels.

Boron-containing steels were examined for the 3Cr and 11Cr steels. The 3Cr-3WVTaB steel had a higher yield stress than 3Cr-3WVTa at room temperature, but the difference decreased with increasing test temperature. There was still a difference at 600°C, but the difference disappeared for the 650°C tests. The 3Cr-3WVTa had a slight advantage over the 3Cr-3WVTaB in creep strength at 600 and 650°C. In tensile tests of the 11Cr steels, the 11Cr-

2WVTa steel was slightly stronger than 11Cr-2WVTaB, but there was relatively little difference in creep.

Computational Thermodynamics Analysis: High-Chromium Steels

To explore the origin of the difference between COST CB2 and 9Cr-2WVTa, 11Cr-2WVTa, and 11Cr-2WVTaB steels—the strongest high-chromium steels—equilibrium phases for the different compositions were calculated with the computational thermodynamics program JMatPro using the iron database. Such calculations determine which phases are to be expected to form. No information is obtained concerning the size and distribution of the precipitates, which can play an important role in the strength of a steel.

Although the primary assumption in the development of reduced-activation steels was that the replacement molybdenum and niobium by tungsten and tantalum, respectively, should take place without a major change in the phases formed, the results from JMatPro indicate otherwise (Figs. 49 and 50). What is more important, it appears that mechanical properties can be affected by the change in composition—at least in the cast condition—as evidenced by the better properties of the COST CB2 (Figs. 47 and 48).

Calculated phases for 9Cr-2WVTa (calculation was for Fe-9Cr-2W-0.25V-0.1Ta-0.25Si-0.5Mn-0.1C-0.028N) (Fig. 49) and COST CB2 (calculation was for Fe-9Cr-1.5Mo-0.25V-0.063Nb-0.008Si-0.82Mn-0.8Co-0.2Ni-0.12C-0.028N) (Fig. 50) indicate there are differences in the precipitate phases. Major differences involve Ta- and V-rich MX-type precipitates in 9Cr-2WVTa compared with V- and Nb-rich MX in COST CB2. JMatPro labels MX phases in 9Cr-2WVTa as M(C,N) and TiN (essentially MN) and in COST CB2 just M(C,N). The amounts of these phases stable in the two steels during austenitization at 1100°C, during tempering at 750°C, and during service or creep at 600°C is not too different (Table 9). The calculated combination of TiN and M(C,N) in 9Cr-2WVTa is slightly larger than the M(C,N) in COST CB2 at all three temperatures.

Table 9. Amounts of MX Precipitate in 9Cr-2WVTa and COST CB2 Steels (wt. %)

Precipitate	**9Cr-2WVTa**			**COST CB2**		
	1100°C	**750°C**	**600°C**	**1100°C**	**750°C**	**600°C**
M(C,N)	0.08	0.10	0.10	0.06	0.20	0.19
TiN (MN)	0.01	0.17	0.16			

The compositions of the M(C,N) in the two steels are different. In 9Cr-2WVTa, it is basically MX (Fig. 51), while in the COST CB2 it is MN, where M is a combination of V and Nb (Fig. 52). "TiN" is how JMatPro identifies nitrogen-rich MX, and according to JMatPro, it is essentially VN with some Cr and Ta (Fig. 51). The amount of tantalum in TiN decreases and the amount of vanadium increases with decreasing temperature from 1100°C down to 600°C. On the other hand, in M(C,N) in COST CB2, there is also a large decrease in the niobium and increase in vanadium with decreasing temperature from 1100°C down to ≈900°C, but between the tempering temperature (750°C) and the service temperature (600°C), the relative amounts of niobium and vanadium are relatively constant (Fig. 52). According to the calculations, below 800°C essentially all the nitrogen is in the TiN of 9Cr-2WVTa and M(C,N) of COST CB2. Essentially all carbon in the COST CB2 is in $M_{23}C_6$, whereas the M(C,N) of the 9Cr-2WVTa is essentially TaC (Fig. 52), although this still leaves almost 95% of the carbon in the $M_{23}C_6$.

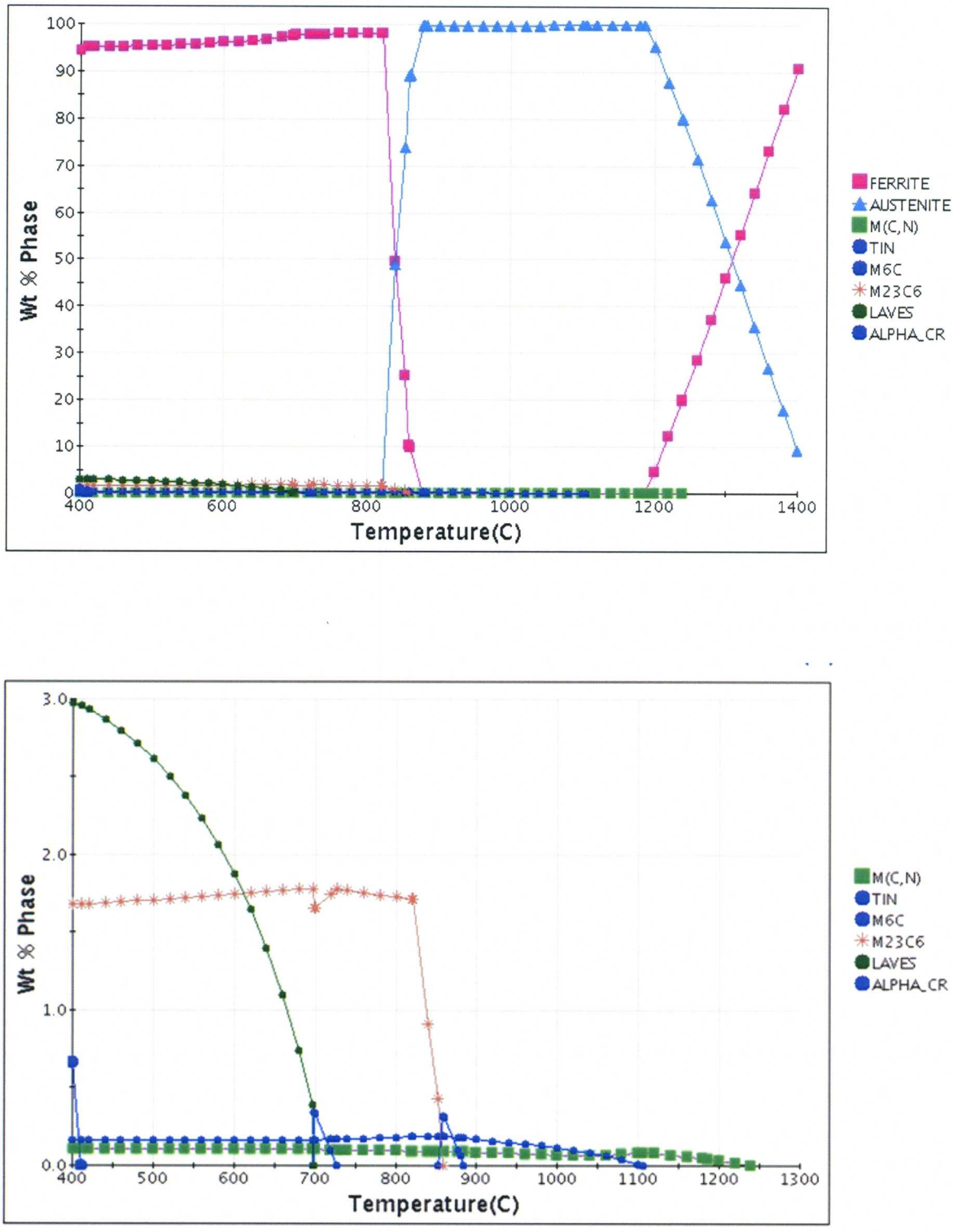

Figure 49. Calculated phases for 9Cr-2WVTa steel over the range 400-1400°C: (a) all phases and (b) precipitate phases.

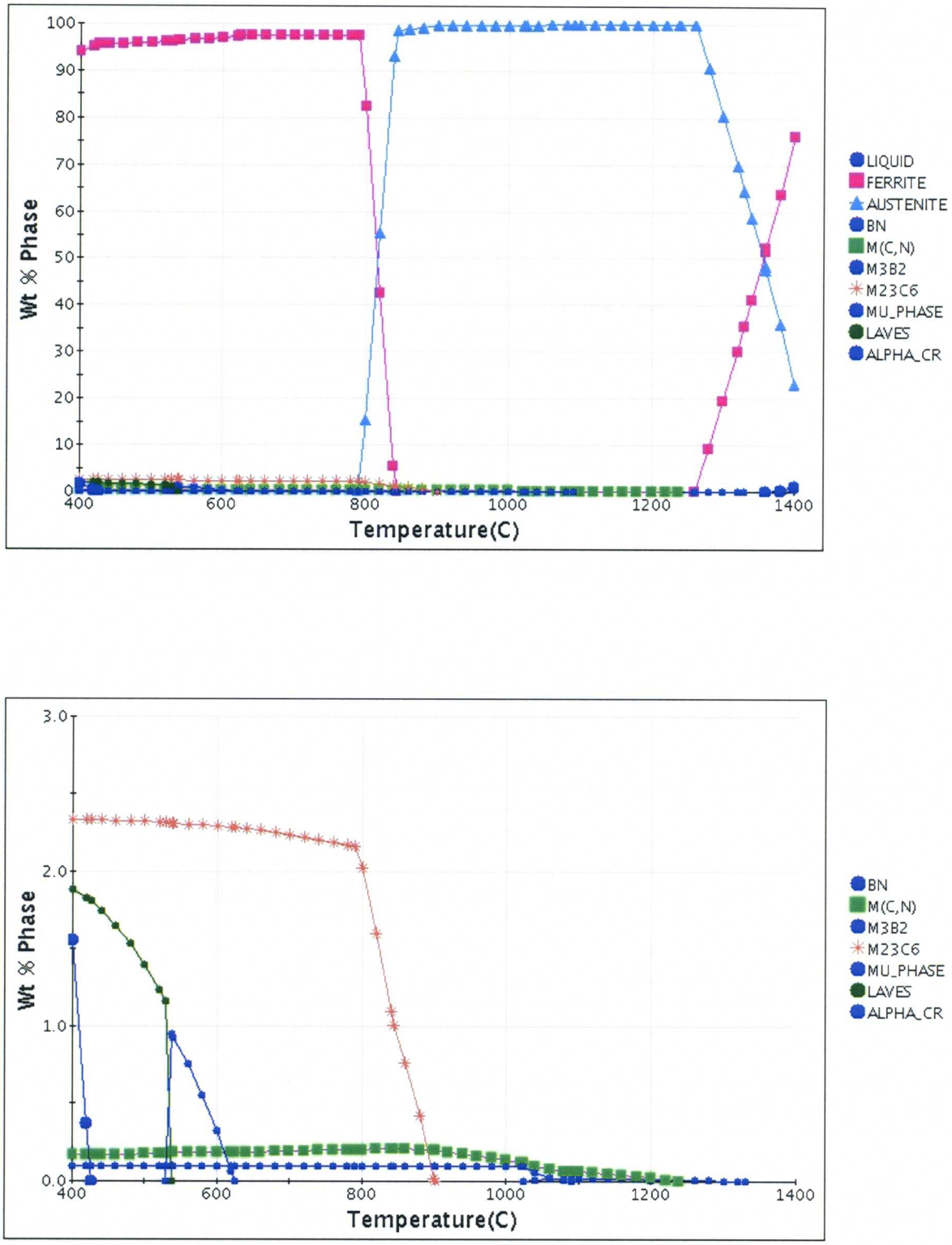

Figure 50. Calculated phases for COST CB2 steel over the range 400-1400°C: (a) all phases and (b) precipitate phases.

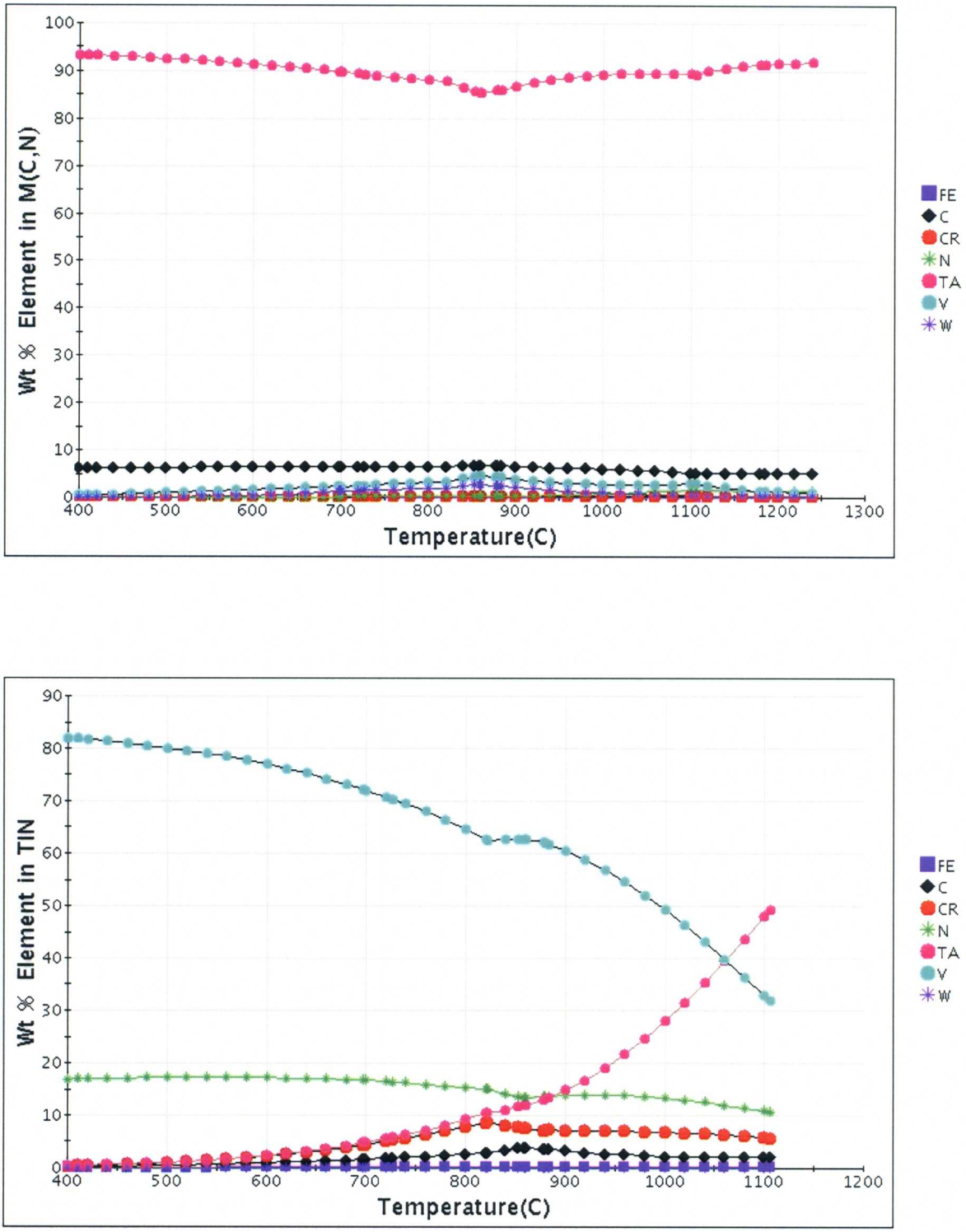

Figure 51. Calculated elemental compositions for (a) M(C,N) and (b) TiN precipitates in 9Cr-2WVTa steel over the range 400-1400°C.

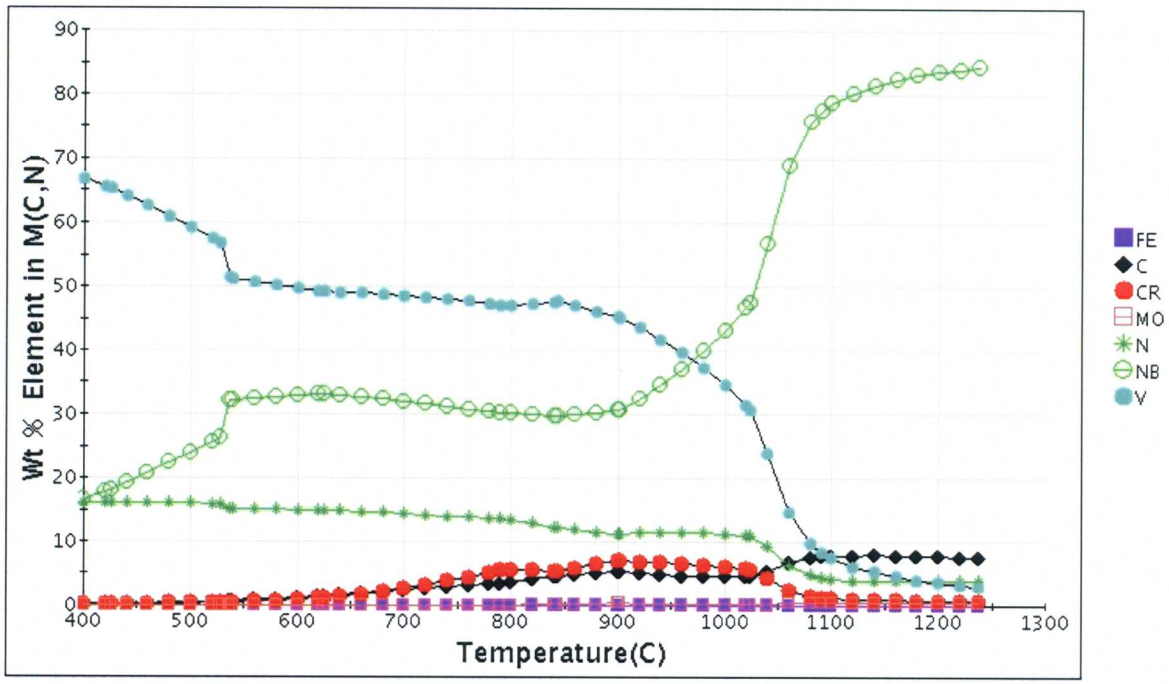

Figure 52. Calculated elemental compositions for M(C,N) precipitates in COST CB2 steel over the range 400-1400°C.

Figures 53 and 54 show the disposition of the V and Ta for the 9Cr-2WVTa and the V and Nb for the COST CB2, respectively. Note that considerable niobium goes from M(C,N) to Laves phase below ≈500°C. According to the calculation, Ta is not important to the Laves phase of the 9Cr-2WVTa steel.

Disposition of the tungsten (Fig. 55) in the 9Cr-2WVTa and the molybdenum (Fig. 56) in COST CB2 is quite complicated over the temperature range considered. However, at 600°C about 59% of the tungsten in the 9Cr-2WVTa is in the Laves phase, 8% in $M_{23}C_6$, with the remaining ≈33% in the ferrite. Only about 10% of the molybdenum is in Laves phase at 600°C, while 30% is in the $M_{23}C_6$, with the remaining ≈60% in the ferrite.

The other two elements of interest are the cobalt and boron in the COST CB2. Cobalt is essentially all in solid solution, either in the austenite or ferrite. Below 1000°C, boron is calculated to be ≈100% in about 0.1% of the compound M_3B_2 (Fig. 50) with about 0.005% of the boron in $M_{23}C_6$. Above about 1020°C, ≈0.02% BN is calculated to be present. It is interesting to note that the addition of 0.008% B lowers the melting point to below 1400°C, while without boron (separate calculations not shown), the melting point is greater than 1400°C.

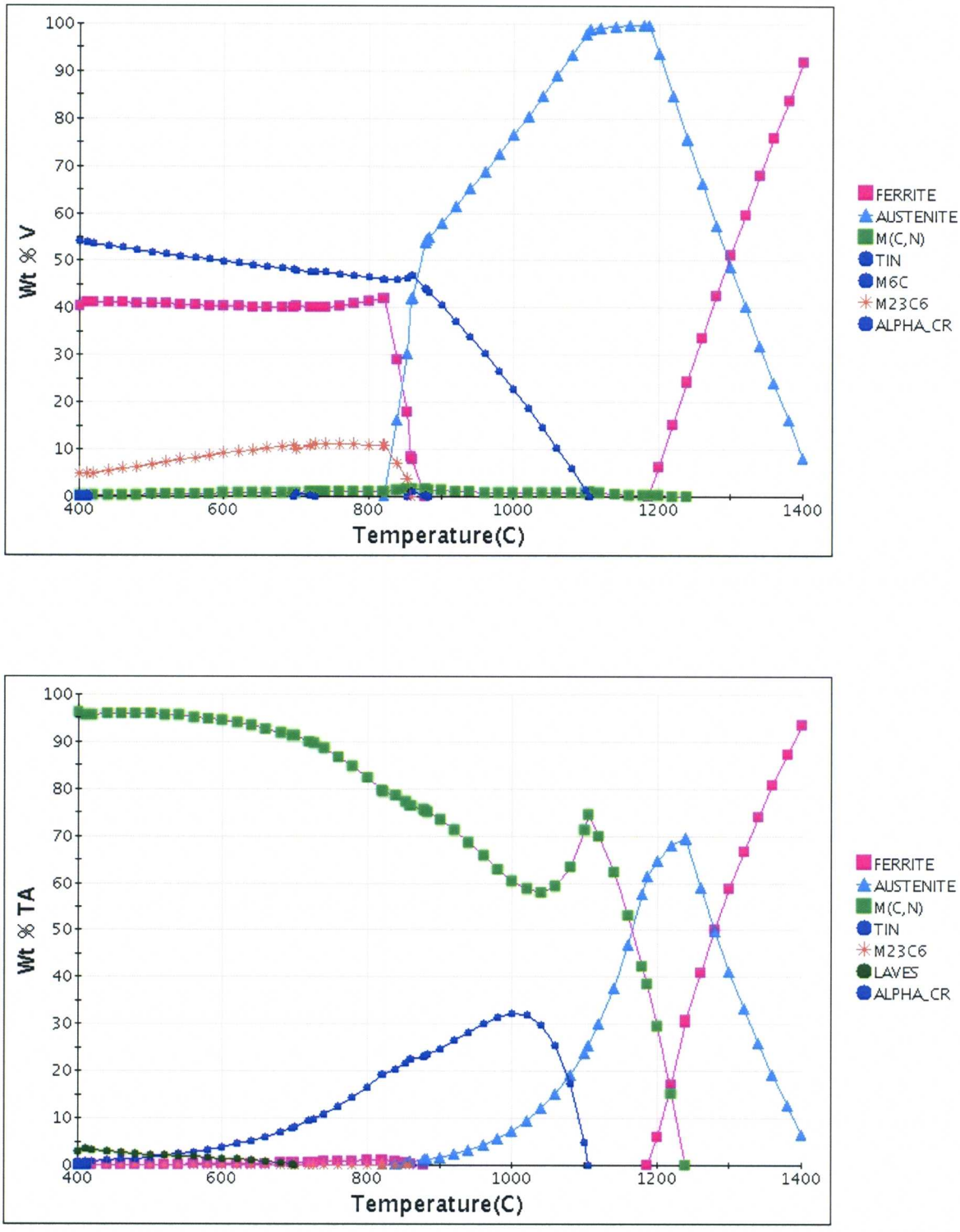

Figure 53. Calculated equilibrium distributions of (a) vanadium and (b) tantalum in different phases in 9Cr-2WVTa steel over the range 400-1400°C.

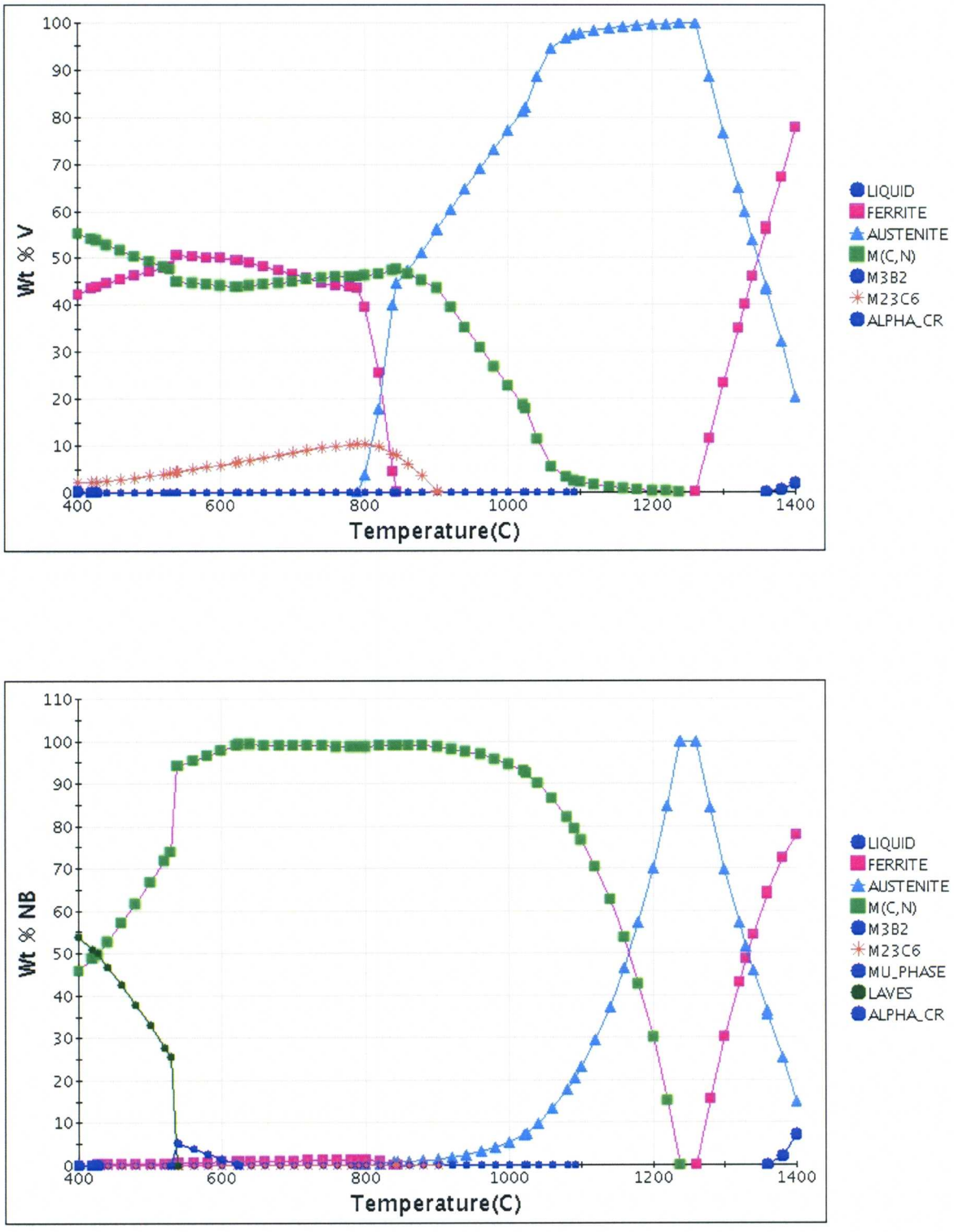

Figure 54. Calculated equilibrium distributions of (a) vanadium and (b) niobium in different phases in COST CB2 steel over the range 400-1400°C.

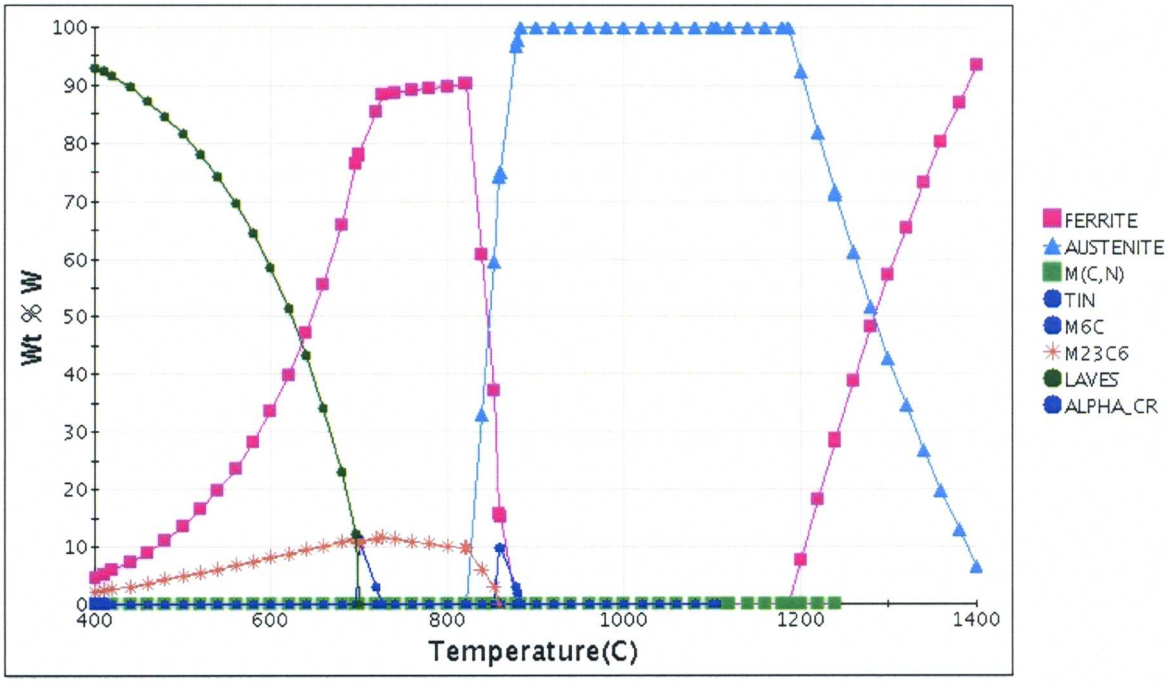

Figure 55. Calculated equilibrium tungsten distribution in different phases in 9Cr-2WVTa steel over the range 400-1400°C.

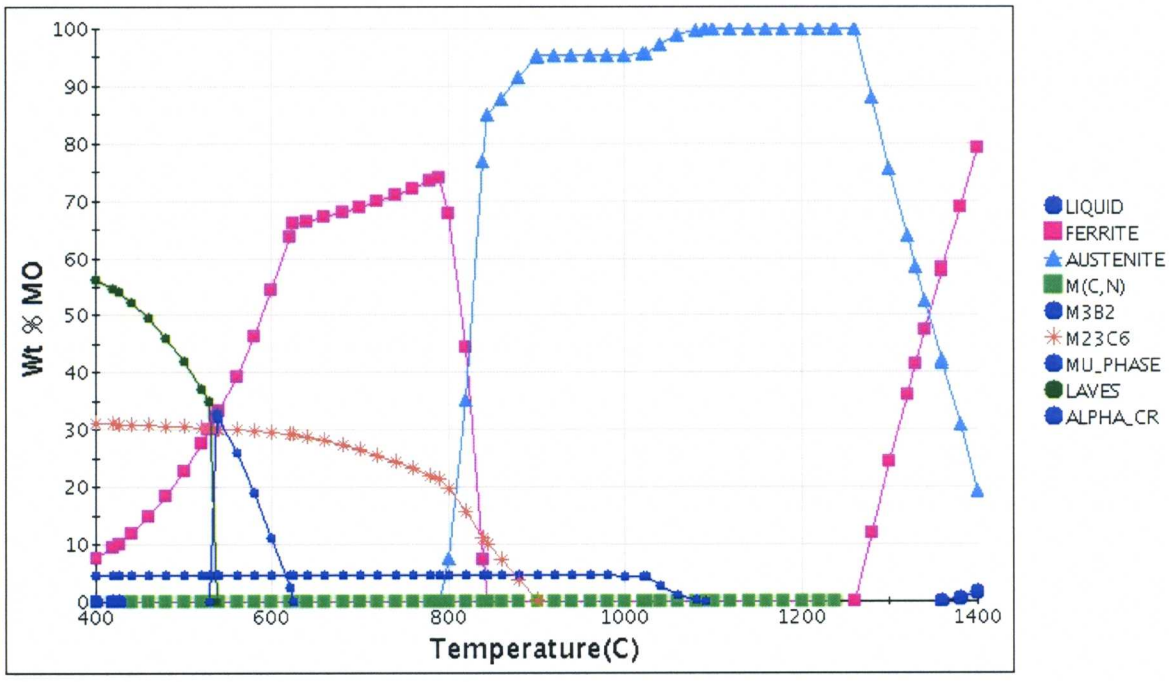

Figure 56. Calculated equilibrium molybdenum distribution in different phases in COST CB2 steel over the range 400-1400°C.

Discussion: High-Chromium Steels

The tensile and creep results combined with the computational thermodynamic calculations allow for speculation on the causes of the differences in the steels, which can then be used to propose improved compositions. For this discussion, a service temperature of 600°C will be assumed. A recent review of the 9-12Cr steels discussed the effect of various alloying elements on the properties of the steels [6].

A major difference in 9Cr-2WVTa and COST CB2 steels is the composition of the N-rich MX precipitates—TiN (MN) for 9Cr-2WVTa versus M(C,N) for COST CB2. The JMatPro program does not distinguish the difference in the crystal structures, if any, of these two versions of MX. These precipitates are expected to form as fine particles (at least relative to $M_{23}C_6$) to provide dispersion strengthening [6]. The M(C,N) in COST CB2 is basically (VNb)N, whereas the TiN in 9Cr-2WVTa is essentially VN. Also, 0.16% TiN is calculated to be present in 9Cr-2WVTa at 600°C compared to 0.19% M(C,N) in the COST CB2, although the total MX present in the 9Cr-2WVTa is greater (0.26%) when the M(C,N) (TaC) in that steel is considered.. Note that a total of 0.09% of TiN and M(C,N) in 9Cr-2WVTa are stable at 1100°C compared to 0.06% M(C,N) in COST CB2 (Table 9). Precipitates formed or undissolved at 1100°C would presumably be present as large particles of relatively low number density relative to precipitates formed during tempering at 750°C. Thus, these undissolved particles are not expected to be as effective for dispersion strengthening as those developed during tempering—a more negative effect in the 9Cr-2WVTa. Also, the presence of the M(C,N) undissolved at 1100°C might affect precipitation at 750°C by acting as precipitate nuclei, further coarsening the precipitate distribution. The unknown here is the size and distribution of these phases, but if, as expected, they are important to the elevated-temperature strength, then the M(C,N) of the COST CB2 must develop the favored size and distribution. Detailed analytical TEM would be required to elucidate these possibilities.

The loss of considerably more tungsten from the ferrite solid solution at 600°C to form Laves phase in 9Cr-2WVTa compared to the loss of molybdenum to Laves phase formation in COST CB2 as discussed above is another difference that could negatively affect the 9Cr-2WVTa relative to COST CB2. The higher relative amount of molybdenum remaining in the ferrite projects to higher solid-solution strengthening in the COST CB2. Therefore, if tungsten and molybdenum were equally effective in solid-solution hardening, the molybdenum would have an advantage, which is opposite the present thinking in much of the literature for these types of steels [6].

Cobalt in solid solution is not thought to contribute significantly to elevated-temperature strength [7], and it may affect it negatively [8].

Finally, the role of boron needs to be considered. Note that calculation of the presence of M_3B_2 disagrees somewhat with experimental work (TEM and atom probe) that indicates boron is associated with $M_{23}C_6$ (no M_3B_2 has been reported in the literature for these steels). Boron is concluded to stabilize $M_{23}C_6$ into a finer distribution by the formation of $M_{23}(CB)_6$, which, in turn, is concluded to stabilize the subgrain structure against recovery [5,10-14], thus improving creep strength. Calculations discussed above indicate that only 0.005% of the total boron is in $M_{23}C_6$ at 600°C. Alternatively, perhaps the presence of M_3B_2 on subgrain boundaries might, if present, stabilize the subgrain structure (analytical TEM would be required to determine whether boron-rich precipitates are present). Regardless, as stated above, boron did not seem to make a significant difference in the creep behavior of the tests on the 3Cr and 11Cr steels.

New High-Chromium Cast Steels

The question is: What high-chromium steel compositions will have higher elevated-temperature strength than COST CB2? If the common wisdom is accurate that elevated-temperature strength of these high-temperature steels depends on dispersion strengthening by MX and solid-solution strengthening by the Mo and W, then the objective should be to maximize the amount and stability of MX phase and the amount of Mo and W in solution [5,9-17].

Based on computational thermodynamics calculations, it appears a favorable MX will be a vanadium-rich nitride, which also agrees with the consensus in the literature based on experimental studies on such wrought steels [5,9-13]. From a comparison of the 9Cr-2WVTa and COST CB2 mechanical properties, a single MX phase may be preferable to the duplex MX phases of 9Cr-2WVTa. This assumes that JMatPro is correct, and there are two distinct phases, and it is not an artifact of the calculation. Furthermore, based on the above discussion, the amount of undissolved MX at 1100°C should be eliminated or minimized as much as possible.

Therefore, one way to produce more nitride during tempering with less undissolved nitride at the 1100°C austenitization temperature would be to eliminate the Ta and Nb from the 9Cr-2WVTa and COST CB2 compositions, respectively, although this is contrary to common belief on the strengthening mechanisms of these steels. Further improvement should come with more nitrogen (≈0.04-0.05%) to more closely approach a stoichiometric VN for 0.2% V. For the basic COST CB2 composition (a choice of the molybdenum-containing steel) minus the niobium, an increase in nitrogen to 0.04% is calculated to increase the amount of M(C,N) to 0.21% at 750 and 600°C, and austenitization at 1100°C would dissolve all the M(C,N) (Fig. 57).

One difficulty with the above composition is that there may be a problem adding nitrogen to the casting. A somewhat higher equilibrium nitrogen concentration occurs with the 11Cr steels (0.034 for the 11Cr steels versus 0.028 for the 9Cr steels, based on the compositions of the present castings, see Table 1). Therefore, 11Cr steels patterned after the COST CB2 with (Fig. 58) and without (Fig. 59) niobium are a possibility, although this would not provide the amount of nitrogen for the maximum effect of nitrides on strength.

Calculations of the amounts of molybdenum and tungsten remaining in solution at 600°C discussed above indicated that molybdenum should be chosen over tungsten, since only about 30% of the tungsten remains in solution at 600°C, compared to about 60% of the molybdenum.

Based on this discussion, five 11Cr compositions are suggested (Table 10): (1) high-Cr (11% Cr) COST CB2 composition (11Cr-1.5MoCoMnNbVB, Cast A), (2) this composition without niobium (11Cr-1.5MoCoMnVB, Cast B), (3) this composition without niobium and boron (11Cr-1.5MoCoMnV, Cast C), (4) Cast C with molybdenum replaced by tungsten (Cast D), and (5) Cast A with molybdenum replaced by tungsten (Cast E). By comparing the new compositions with each other and with previous results, these compositions will provide information on the effect of Cr, W, Nb, Ta, and B on microstructure and mechanical properties.

The amounts of calculated M(C,N) precipitates present at 1100, 750, and 600°C for these five 11% Cr modified COST CB2 compositions with and without niobium are summarized in Table 11. Results indicate that the amount of MX precipitate formed at the tempering temperature will be greater for the steels without niobium, although the total amount will be greater for the niobium-containing steel, because of the precipitate that remained undissolved at 1100°C in the niobium-containing steel. As stated above, it is doubtful that the undissolved precipitate, which is usually large compared to that formed at lower temperatures, will contribute significantly to elevated-temperature strength.

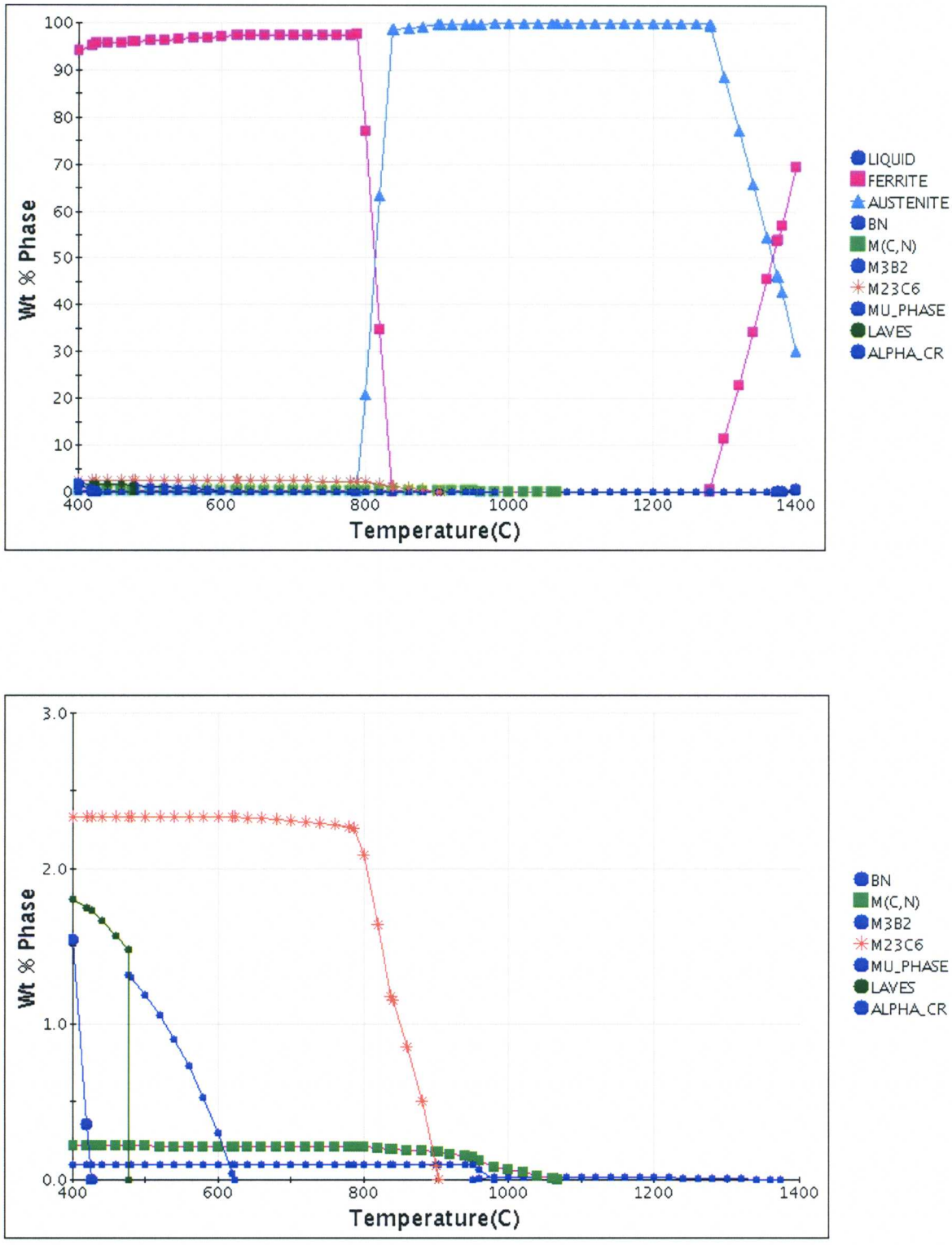

Figure 57. Calculated equilibrium (a) phases and (b) precipitates in modified COST CB2 (9Cr-1.5MoVB) steel over the range 400-1400°C.

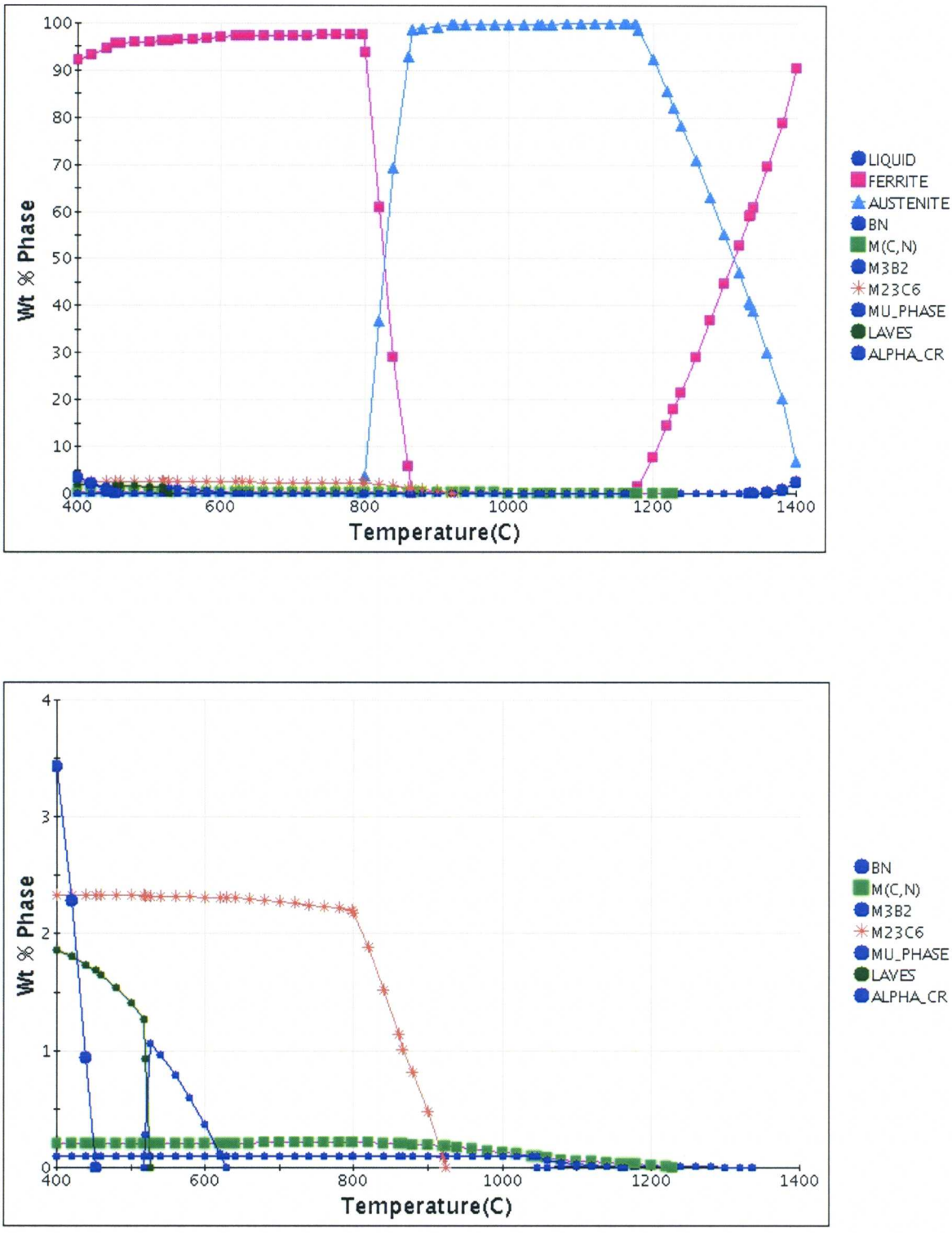

Figure 58. Calculated equilibrium (a) phases and (b) precipitates in an 11Cr steel with the COST CB2 composition (except for the chromium) over the range 400-1400°C.

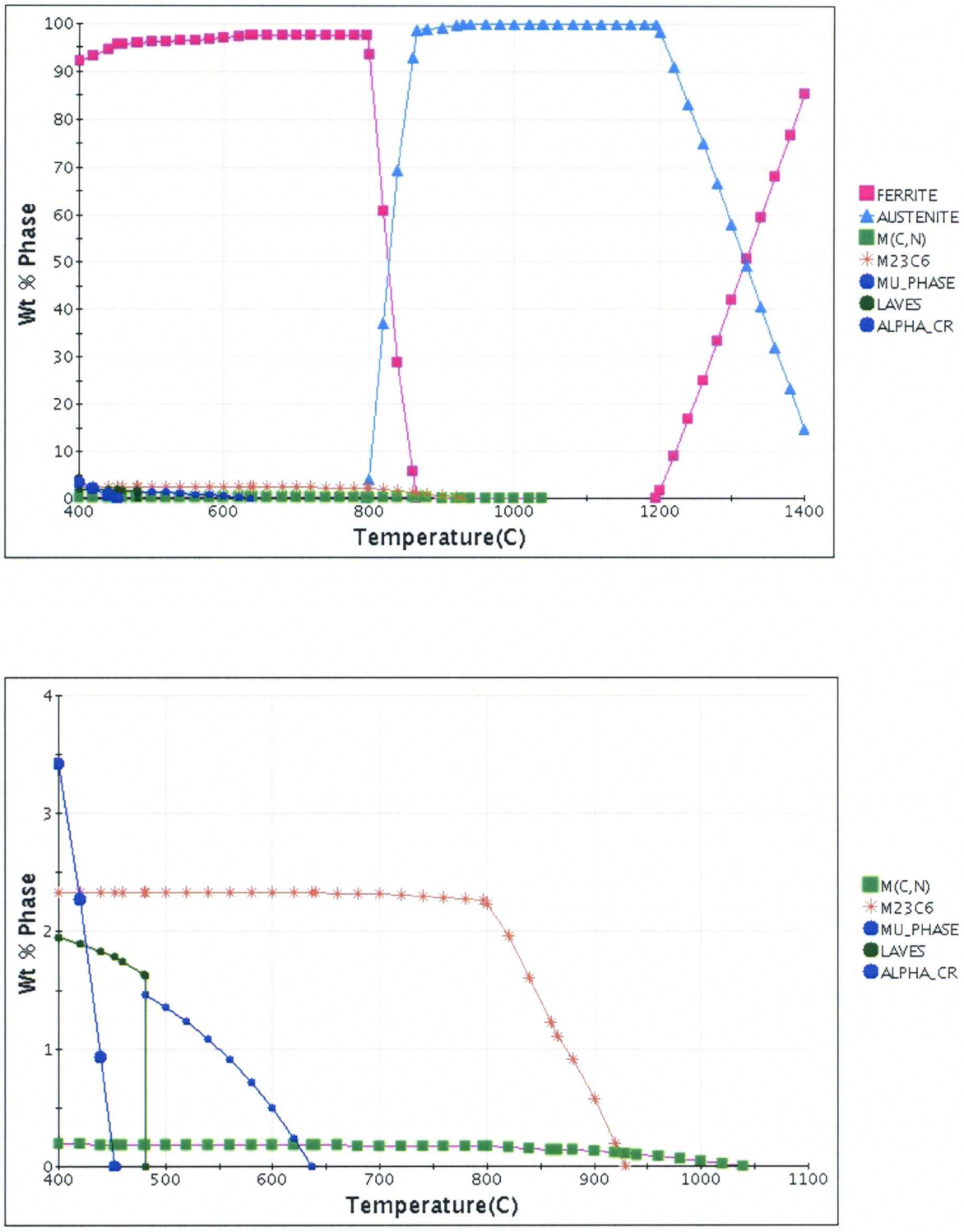

Figure 59. Calculated equilibrium (a) phases and (b) precipitates in an 11Cr-1.5MoCoMnV steel over the range 400-1400°C.

Table 10. Proposed Compositions for Future Steel Castings*

Element	Cast A	Cast B	Cast C	Cast D	Cast E
C	0.12	0.12	0.12	0.12	0.12
Mn	0.8	0.8	0.8	0.8	0.8
Ni	0.2	0.2	0.2	0.2	0.2
Cr	11.0	11.0	11.0	11.0	11.0
Mo	1.5	1.5	1.5		
W				2.0	2.0
V	0.20	0.20	0.20	0.20	0.20
Co	0.8	0.8	0.8	0.8	0.8
Nb	0.06				0.06
B	0.008	0.008			
N	0.034	0.034	0.034	0.034	0.034

*Designation of Steels

Cast A: 11Cr-1.5MoCoMnNbVB
Cast B: 11Cr-1.5MoCoMnVB
Cast C: 11Cr-1.5MoCoMnV
Cast D: 11Cr-2WCoMnV
Cast E: 11Cr-2WCoMnNbV

Table 11. Calculated M(C,N) Precipitates in Proposed Cast Steels

Temperature	Cast A	Cast B	Cast C	Cast D	Cast E
1100°C	0.059	0	0	0	0.067
750°C	0.22	0.18	0.18	0.18	0.23
600°C	0.21	0.18	0.18	0.18	0.22

Computational Thermodynamics Analysis: 3Cr Steels

The compositions of the four 3Cr steels, 3Cr-3WV, 3Cr-3WVTa, 3Cr-3WVTaB, and 3Cr-2W-0.5MoV, were analyzed with JMatPro, and there are again interesting observations concerning the replacement of Mo and Nb by W and Ta, respectively. In this case, there was no 3Cr COST steel for comparison. However, based on implications from the comparison of 9 and 11Cr steels with COST CB2, a comparison of 3Cr compositions containing W and Ta with compositions containing Mo and Nb was made to determine what differences are indicated by computational thermodynamics. For the JMatPro calculations, all compositions were assumed to contain 0.25Si, 0.50Mn, 0.1C, and 0.008N. Unless otherwise stated, other compositions used were 3Cr, 3W, 1.5Mo, 0.25V, 0.1Ta, 0.05Nb, and 0.005B. Compositions are in wt%.

3Cr-3WV vs. 3Cr-1.5MoV steels

There were significant differences in the precipitate phases predicted for 3Cr-3WV (Fig. 60) and 3Cr-1.5MoV (Fig.61), where Mo was substituted on an approximate atom-for-atom basis. The major difference is that only three precipitate phases appear in the calculations for the Mo-containing steel compared to five in the W-containing steel: M_7C_3 and Laves phases form in the 3Cr-3WV steel and not in 3Cr-1.5MoV. Considerably more M_6C forms in the 3Cr-3WV over a wider temperature range. The amount of $M_{23}C_6$ is different in the steels, there being more of it present in the Mo-containing steel over a wider temperature range. In the 3Cr-3WV steel, $M_{23}C_6$ begins to form at around 600°C, and only below 500°C does the amount increase substantially (up to about 1.25% at 400°C), compared to beginning to form at 800°C in the 3Cr-1.5MoV and there being about 1.2% present over the range 800-400°C. The chromium-rich M_7C_3 forms in a temperature range (about 600-690°C) above that where $M_{23}C_6$ ceases. The amount of M(C,N) in the two steels is similar at the 750°C tempering temperature (0.16% for 3Cr-3WV and 0.17% for 3Cr-1.5MoV), but at a service temperature of 600°C, the 3Cr-3WV contains the most (0.13% vs. 0.09%).

3Cr-2W-0.5MoV vs. 3Cr-3WV and 3Cr-1.5MoV Steels

The substitution of 0.5% Mo for 1% W (Fig. 62) simplifies the precipitation relative to 3Cr-3WV in that the 3Cr-2WMoV contains no M_7C_3. At the lower temperatures, it contains less M_6C and Laves than the 3Cr-3WV but more M_6C and more Laves than the 3Cr-1.5MoV. The latter steel contains no Laves. It also contains more $M_{23}C_6$ than either 3Cr-3WV or 3Cr-1.5MoV. It contains ≈0.17% M(C,N) at 750°C compared to 0.16% in the 3Cr-3WV and 0.17% in the 3Cr-1.5MoV. In the 3Cr-2W-0.5MoV at 600°C, ≈0.09% M(C,N) forms, compared to 0.08% for the 3Cr-1.5MoV and 0.13% for 3Cr-3WV.

3Cr-3WVTa and 3Cr-3WVNb vs. 3Cr-1.5MoVTa and 3Cr-1.5MoVNb steels

When tantalum is added to the 3Cr-3WV composition, two more precipitates appear, labeled "TiN" and "Cu"* by JMatPro (Fig. 63). Precipitate curves show interesting behavior between ≈700 and 800°C. The M_7C_3 is stable over only part of that range, and the Cu becomes stable at ≈700°C and remains stable to 400°C. The Cu is basically a (Ta,V)C phase (Fig. 64, top); at 600°C, it is about 25 at % Ta, 25 at % V and 50 at % C. The TiN is basically a chromium-rich (CVTa)(CN) and is stable from1400 down to ≈800°C, below which there is a gap between ≈800 and 710°C where it is not stable (this gap is possibly a calculation anomaly in the program). It then becomes stable at 710°C, but only at that temperature and not below that temperature (Fig. 63).

* JMatPro uses one symbol throughout its calculations for different systems to label a phase with a given crystal structure, which means that in cases such as "TiN" and "Cu" in the present case where no Ti or Cu are present, the actual compositon of the phase must be calculated.

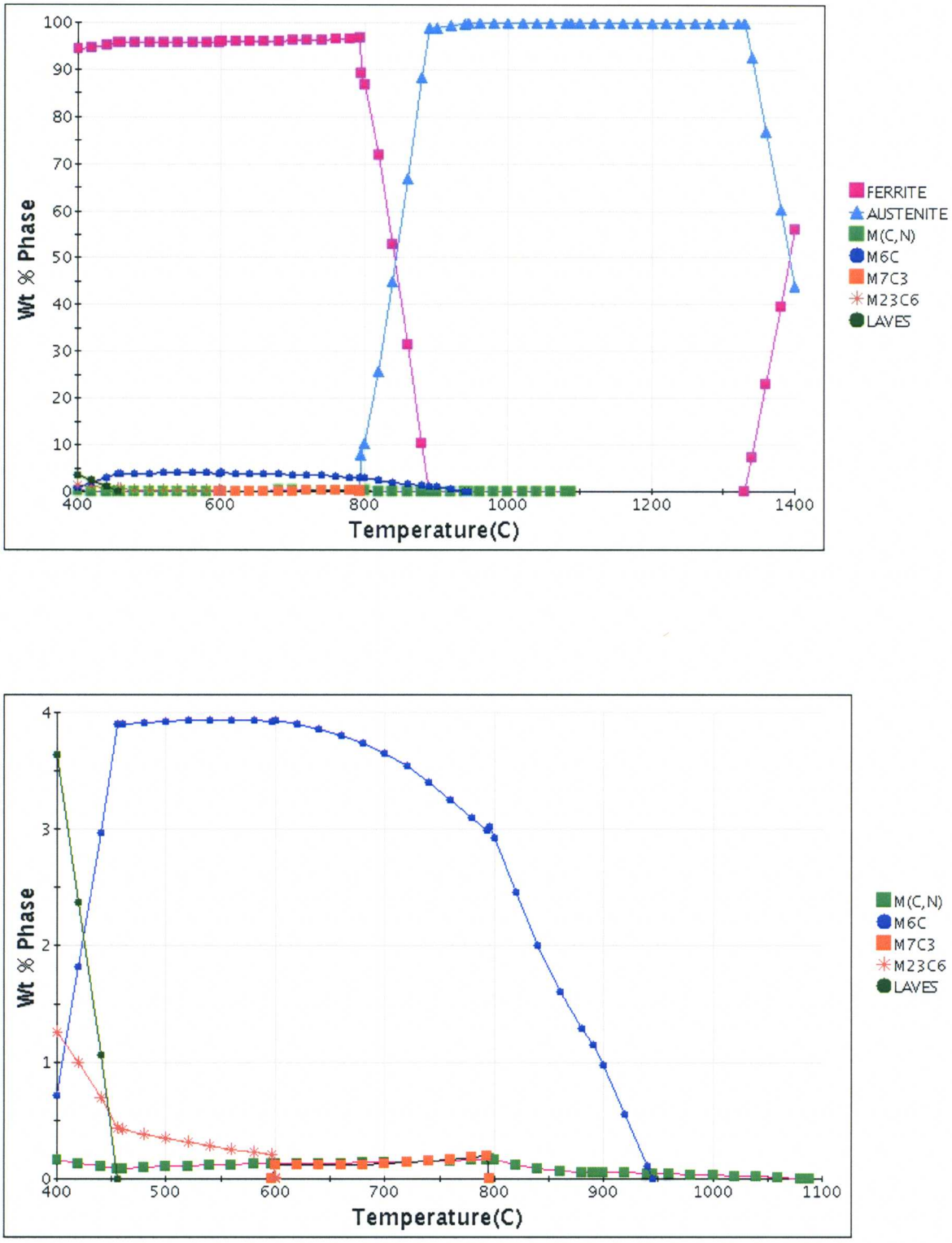

Figure 60. Calculated phases for 3Cr-3WV steel over the range 400-1400°C: (top) all phases and (bottom) precipitate phases.

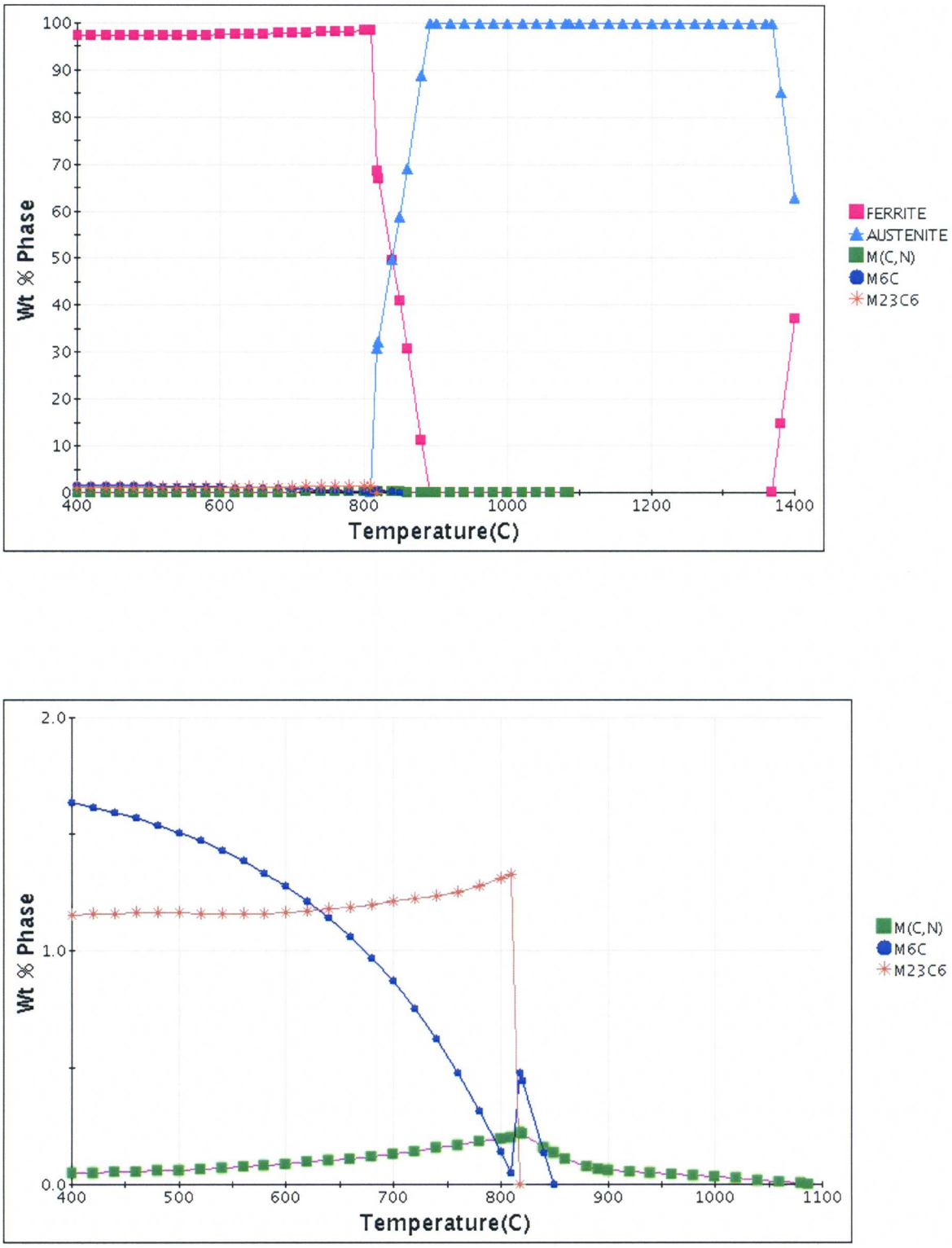

Figure 61. Calculated phases for 3Cr-1.5MoV steel over the range 400-1400°C: (top) all phases and (bottom) precipitate phases.

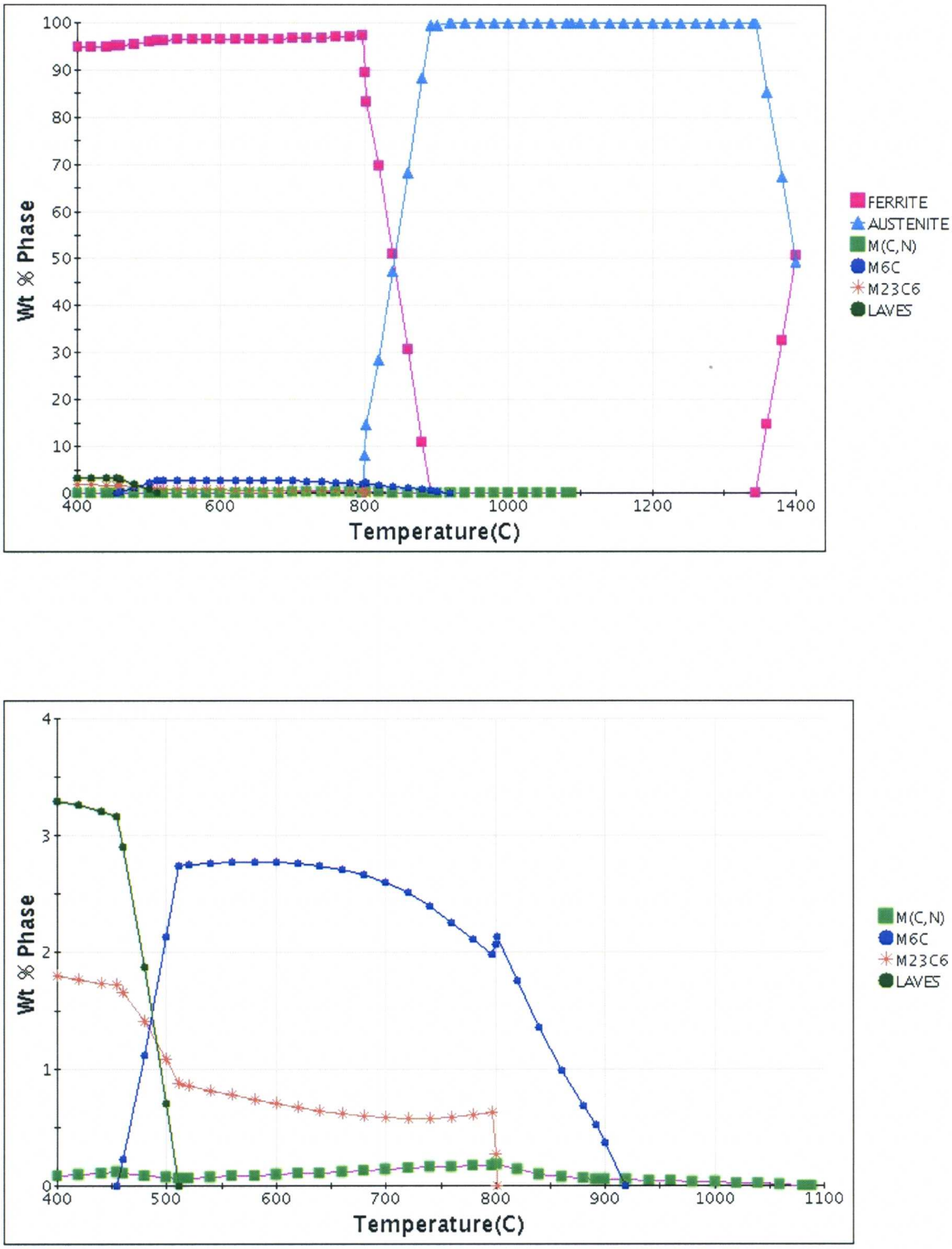

Figure 62. Calculated phases for 3Cr-2WMoV steel over the range 400-1400°C: (top) all phases and (bottom) precipitate phases.

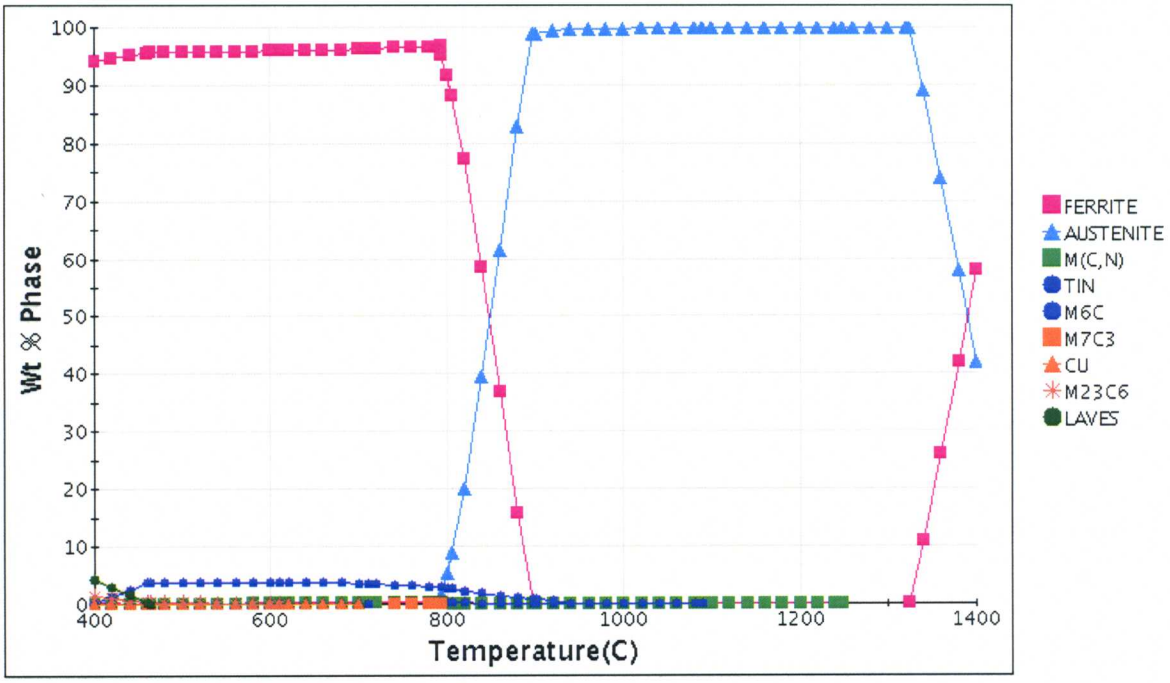

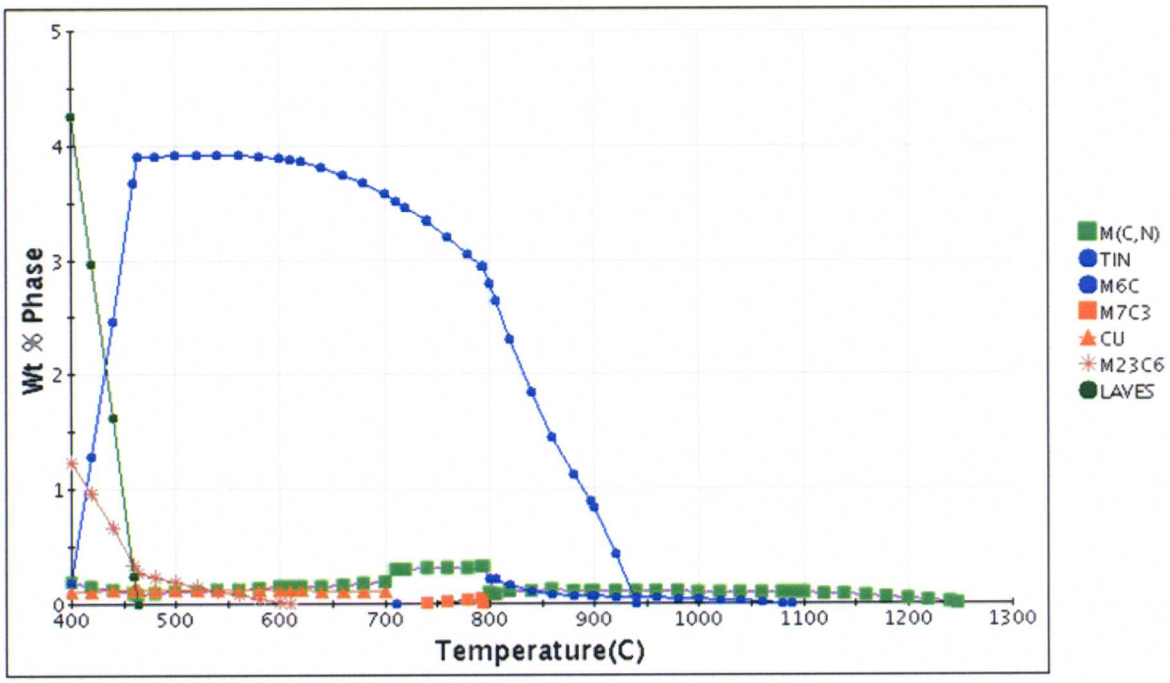

Figure 63. Calculated phases for 3Cr-3WVTa steel over the range 400-1400°C: (top) all phases and (bottom) precipitate phases.

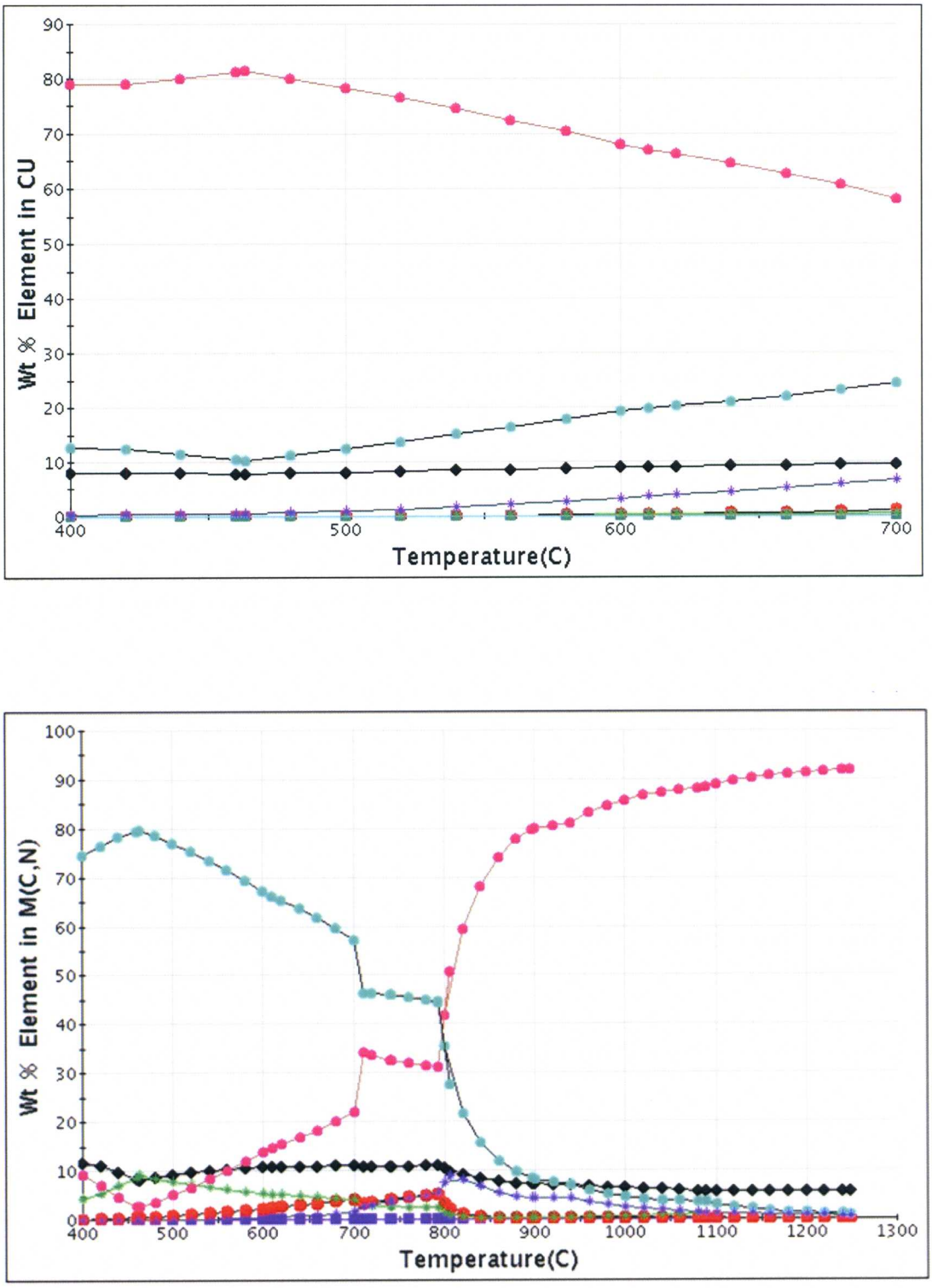

Figure 64. Calculated (top) Cu and (bottom) M(C,N) phases for 3Cr-3WVTa steel over the range 400-1400°C.

The M(C,N) is also quite complicated (Fig. 64, bottom), being basically tantalum-rich carbide above ≈800°C and transforming to vanadium-rich carbide below ≈700°C. There is about 0.3% present at 750°C, but at 600°C, there is only 0.14% M(C,N), the rest having been replaced by 0.12% of the Cu phase.

If tungsten is replaced by molybdenum (3Cr-1.5MoVTa) in the calculations, only four precipitates appear; Cu and M_7C_3 are no longer present (Fig. 65). At the tempering temperature of 750°C, ≈0.3 % M(C,N) is present, but this decreases to about 0.12% at 600°C, it having been replaced by 0.1% TiN. The TiN is not stable between about 854 to 764°C, but is stable from 764°C to 400°C, in contrast to the behavior in the 3Cr-3WVTa, where there was a gap in the stability, and below the gap it was stable at 710°C and not at lower temperatures (again, this could be due to a calculation anomaly). The $M_{23}C_6$ and the M_6C in the 3Cr-1.5MoVTa relative to 3Cr-3WVTa is similar to the relative behavior of the W- and Mo-containing steels without Ta, as discussed above (compare Figs. 63 and 64 with Figs. 60 and 61).

The addition of Nb instead of Ta to 3Cr-3WV to give 3Cr-3WVNb results in a somewhat simpler diagram than for 3Cr-3WVTa (Fig. 66), in that the Cu phase does not appear. There is again a gap in the precipitation diagram (Fig. 66, bottom), this time for Cr-rich precipitates: M_7C_3 is stable from ≈790 down to ≈710°C, and after a gap, $M_{23}C_6$ becomes stable at ≈592°C and remains stable to 400°C. About 0.25% M(C,N) is present at 750°C and 0.22% at 600°C. TiN is only stable from 549 to 544°C, but the stability occurs at the expense of the M(C,N).

Finally, the replacement of W and Ta by Mo and Nb to give 3Cr-1.5MoVNb (Fig. 67) produces a still simpler diagram in that there are only four phases (no Laves or M_7C_6). About 0.28% M(C,N) appears at 750°C, with the composition basically (VNb)C. The amount of M(C,N) is subsequently reduced by the appearance of TiN below about 640°C. At 600°C there is about 0.09% M(C,N) and 0.1% TiN. Below 600°C, M(C,N) is basically V(NC) and TiN is (NbV)C.

It needs to be noted that this discussion applies only to the calculated phases. In the end, it may be the precipitation kinetics that will determine the size and distribution of the phases and how effective they will be in strengthening the steels.

Boron Additions

When boron is added to 3Cr-3WV (Fig. 68), it does not seem to significantly affect any of the precipitates that form without boron (compare Figs. 60 and 68). The only difference is that BN forms between about 1290 down to 517°C. However, addition of 0.005B to 3Cr-3WVTa does have an effect (Fig. 69). In this case, the Cu phase does not form as in 3Cr-3WVTa, the M_7C_3 is only stable between 737 and 794°C, BN forms between 1290 and 516°C, and Cr_2B forms between 525 and 483°C. The other precipitates remain essentially unchanged from the 3Cr-3WVTa (compare Figs. 63 and 69). A similar observation applies to 3Cr-1.5MoVNbB (Fig. 70) in that the original phases of 3Cr-1.5MoVNb (Fig. 67) are relatively unchanged. The BN phase again forms and is stable from about 1280 down to 999°C. Instead of the Cr_2B phase that formed in 3Cr-3WVTaB, M_3B_2 forms between about 1130 down to 400°C.

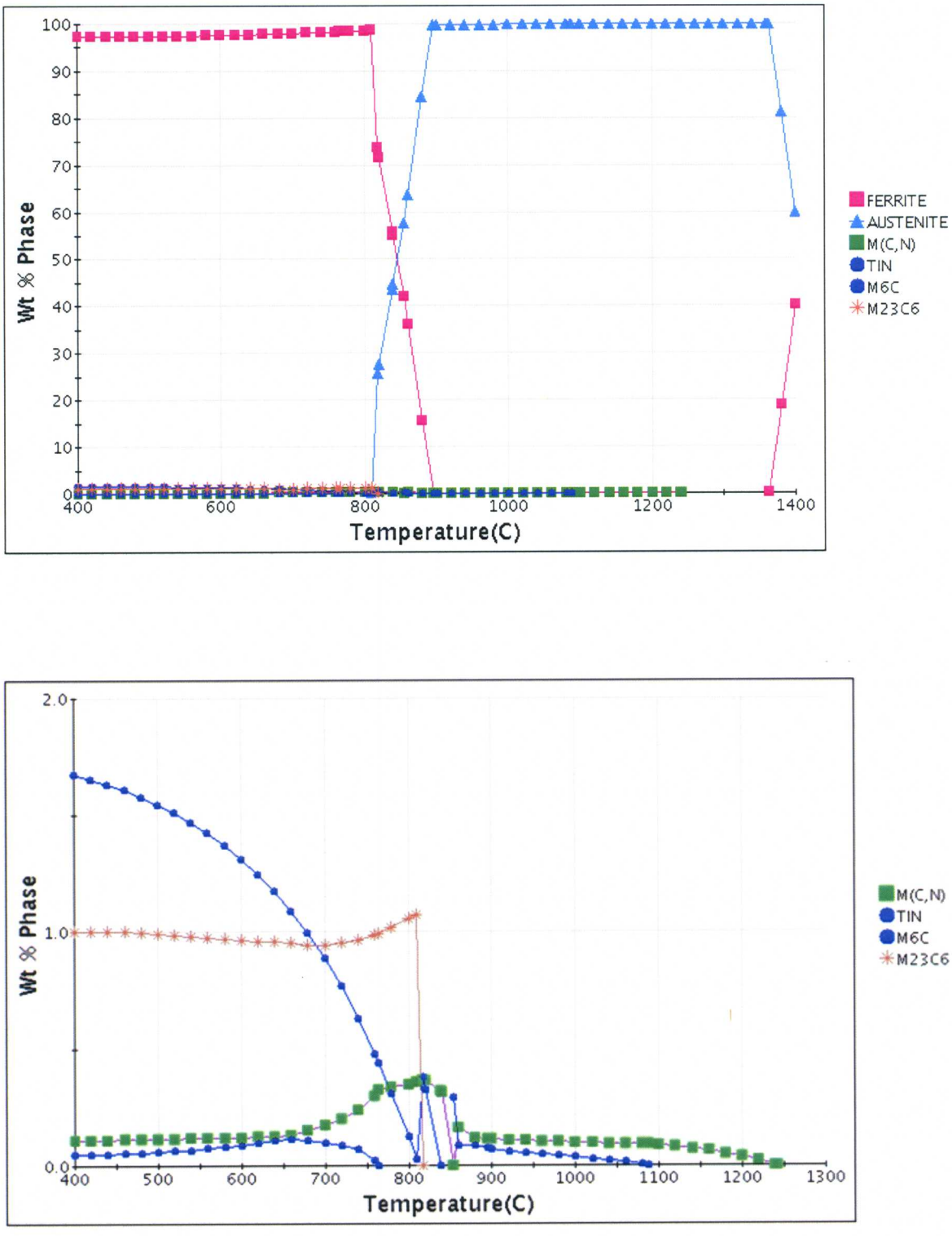

Figure 65. Calculated phases for 3Cr-1.5MoVTa steel over the range 400-1400°C: (top) all phases and (bottom) precipitate phases.

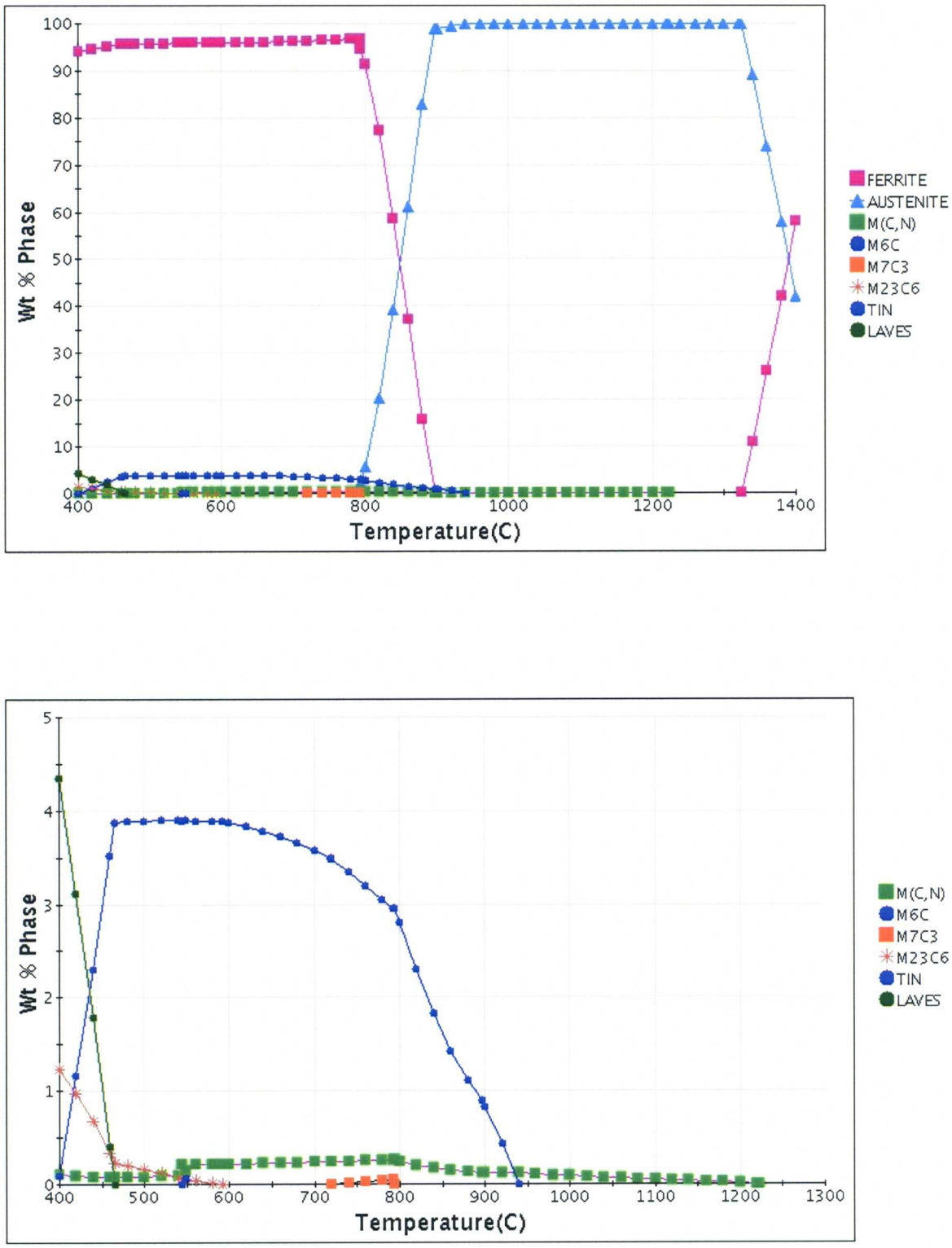

Figure 66. Calculated phases for 3Cr-3WVNb steel over the range 400-1400°C: (top) all phases and (bottom) precipitate phases.

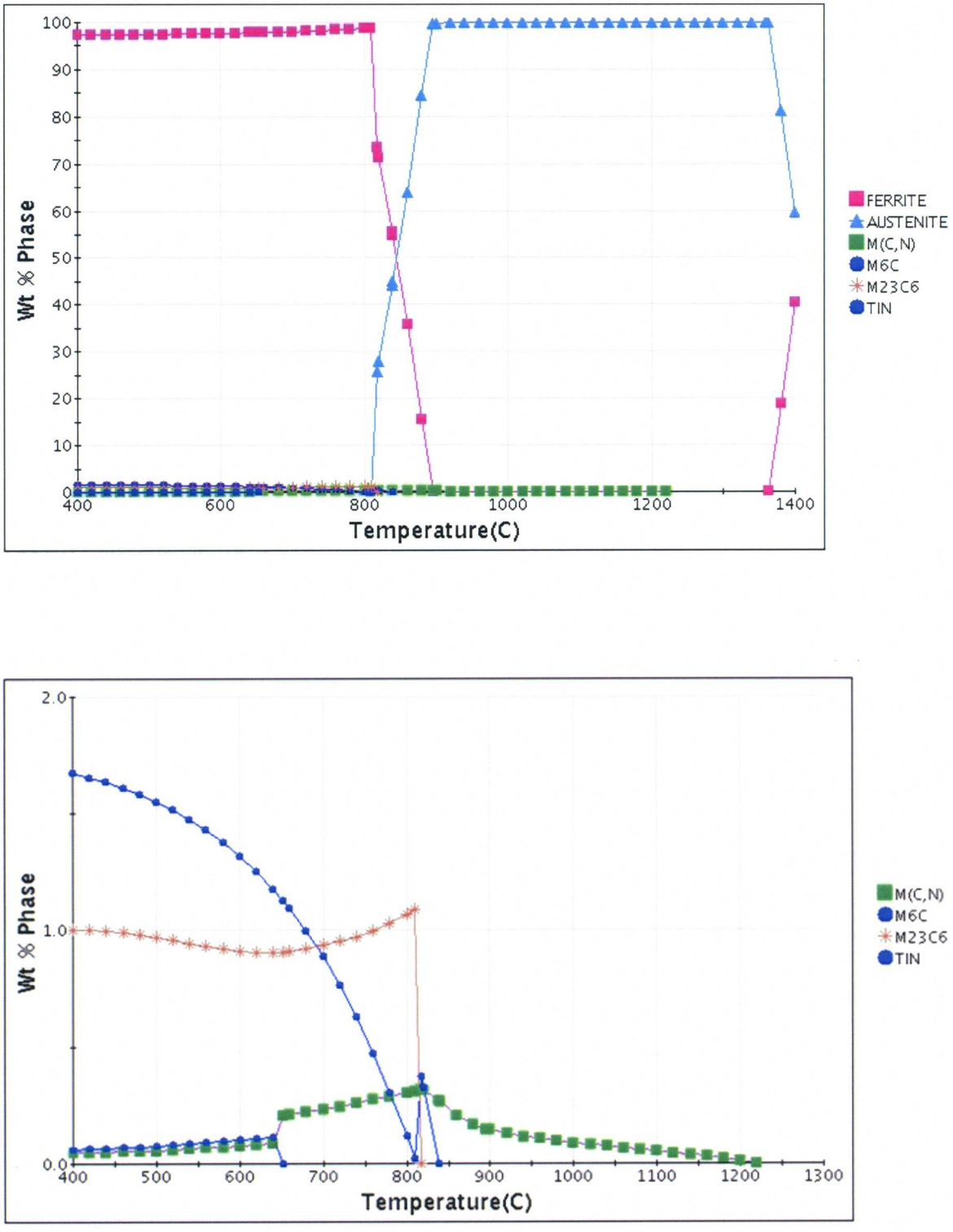

Figure 67. Calculated phases for 3Cr-1.5MoVNb steel over the range 400-1400°C: (top) all phases and (bottom) precipitate phases.

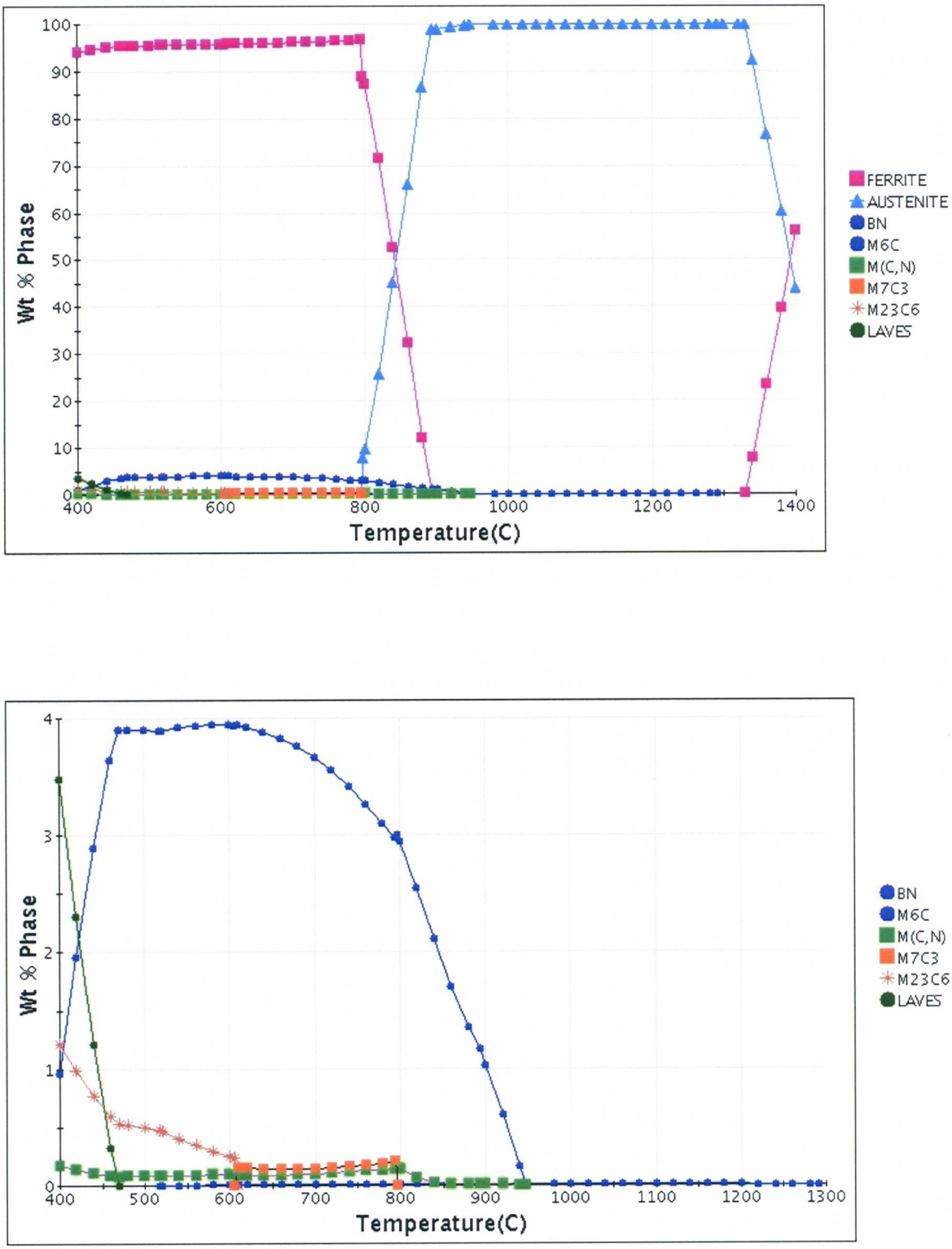

Figure 68. Calculated phases for 3Cr-3WVB steel over the range 400-1400°C: (top) all phases and (bottom) precipitate phases.

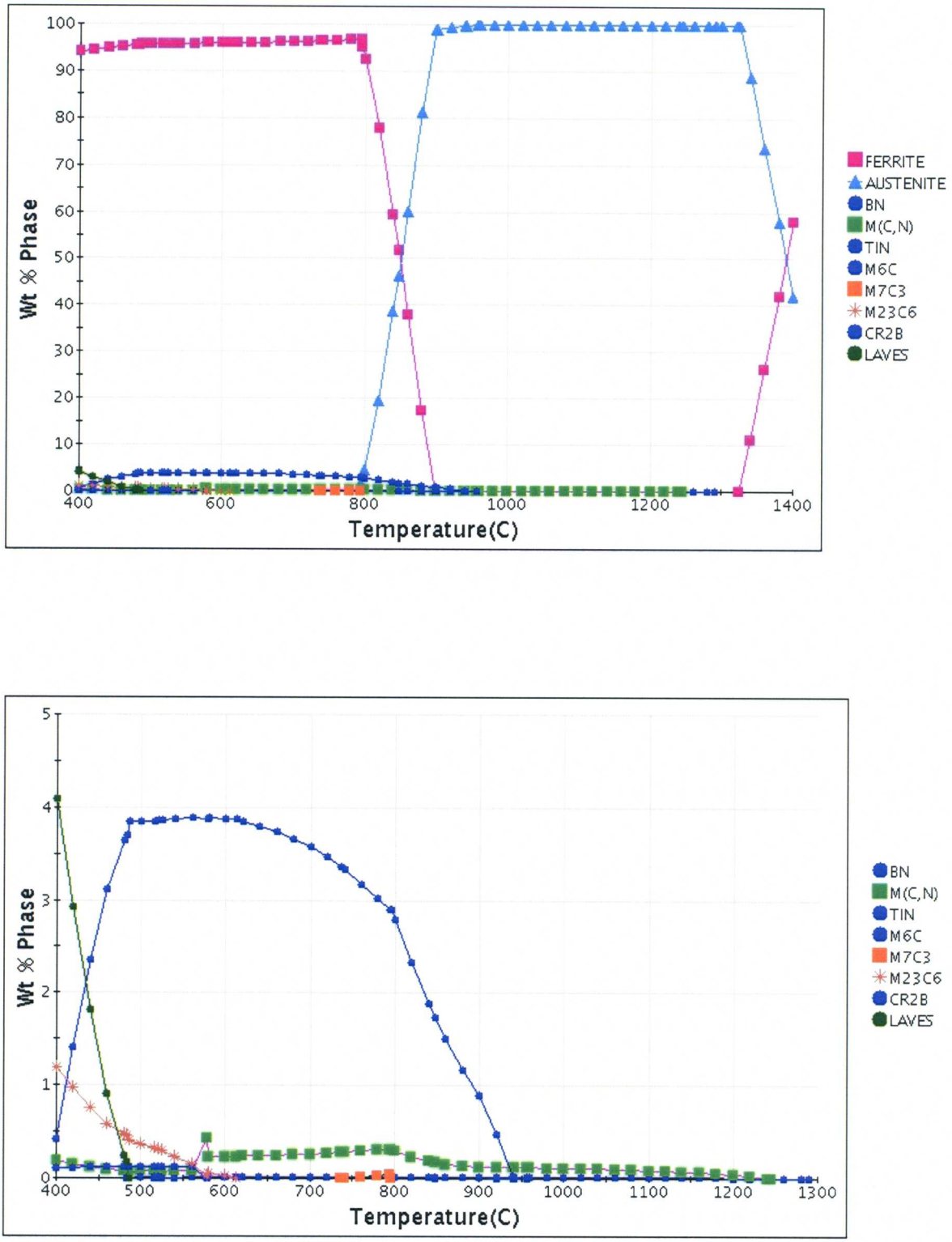

Figure 69. Calculated phases for 3Cr-3WVTaB steel over the range 400-1400°C: (top) all phases and (bottom) precipitate phases.

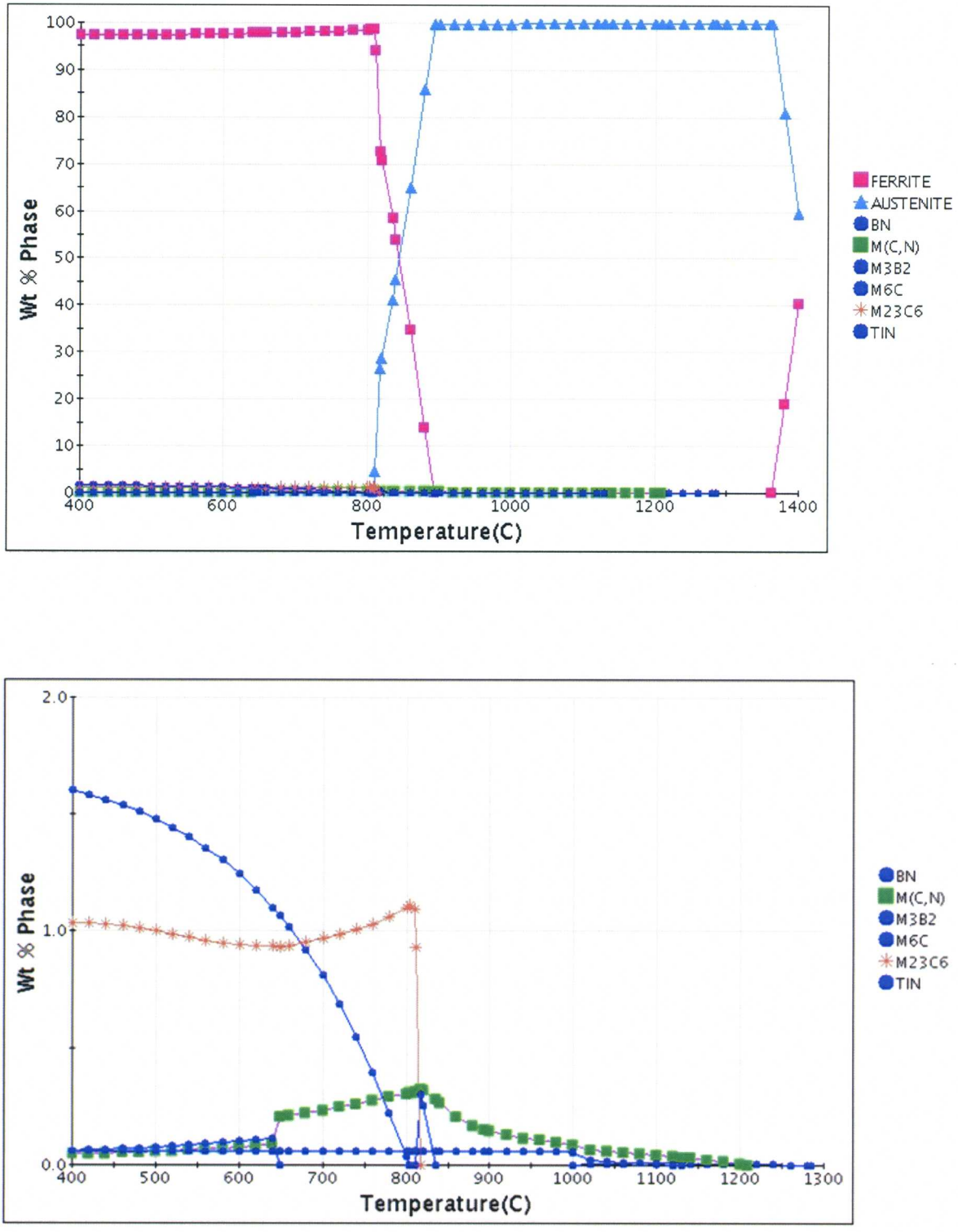

Figure 70. Calculated phases for 3Cr-1.5MoVNbB steel over the range 400-1400°C: (top) all phases and (bottom) precipitate phases.

Discussion: 3Cr Steels

It appears from JMatPro calculations that changing from a 3Cr-3WV base to a 3Cr-1.5MoV reduces the number of precipitate phases, regardless of whether Ta or Nb are added to those base compositions . A similar observation applies with boron additions to 3Cr-3WV or 3Cr-1.5MoV base alloys; the only change is precipitation of boron compounds. With the 3Cr-3WV base, there is also more M_6C and Laves phase. More importantly, for the 3Cr-1.5MoV base, Laves is never predicted by the calculations. There is also more M(C,N) in 3Cr-1.5MoV-base steels at the tempering temperature, but not necessarily at a 600°C service temperature.

It appears that the 3Cr-3WV-base steels, the ones we made our first choice because of their superior properties in the wrought condition, may have deficiencies for casting applications. This could be related to the larger number of phases appearing in these compositions and the tendency for segregation in castings, even after the heat treatment. Segregation can inhibit the formation of strengthening precipitates in the most effective size and distribution; it can also change the formation kinetics and subsequent distribution of some of the other phases. This effect of segregation in castings must play a large role in the properties of these steels, since the wrought 3Cr-3WVTa steel had elevated-temperature strength similar to that of modified 9Cr-1Mo and superior to that new commercial 2.5 Cr steels [3,4]. This must be the result of the minimization of segregation that comes about during the processing of the wrought material.

New 3Cr Cast Steels

The above discussion leads to the conclusion that 3Cr-1.5MoV, 3Cr-1.5MoVNb, 3Cr-1.5MoVB cast steels might be of interest (Table 12). The latter steel might be of interest because without Ta or Nb, all the MX-type precipitates could be dissolved at an 1100°C austenitization temperature. In addition, the presence of BN at this temperature, if present, may help control austenite grain size. Niobium and tantalum play that role when present in the steel composition.

Table 12. Proposed Compositions for Future Steel Castings

Element	3Cr-1.5MoV	3Cr-1.5MoVNb	3Cr-1.5MoVB	3Cr-3WVNb
C	0.1	0.1	0.1	0.1
Mn	0.5	0.5	0.5	0.5
Ni				
Cr	3.0	3.0	3.0	3.0
Mo	1.5	1.5	1.5	
W				3.0
V	0.25	0.25	0.25	0.25
Nb		0.065		0.065
B			0.005	

Summary of Experimental I and II

Heat treatment studies and information on the heat treatment used for COST CB2 led to a first normalizing treatment of 1100°C/1h/AC for all nine of the casting test blocks. Tempering was at 700°C/1h for the 3Cr steels and 750°C/1h for the 9 and 11Cr steels with the objective to produce similar hardnesses (strengths) for all the steels.

Optical metallography indicated that the castings contained defects (porosity). The 3Cr steels had 100% bainitic microstructures. The martensitic 9 and 11Cr steels contained δ-ferrite with the 11Cr-1WMoV and the COST CB2 having the least (estimated at <1%) and the 9Cr-2WVTa (≈14%), 11Cr-2WVTa (≈7%), and 11Cr-2WVTaB (≈3%) having the most.

The TEM of the 3Cr steels indicated they contained a high number density of precipitates in a range of precipitate sizes. Preliminary conclusions on the 3Cr steels was that microstructures of the 3Cr-3WV, 3Cr-3WVTa, 3Cr-2WMoV were tempered granular bainite, and the microstructure of 3Cr-3WVTaB was tempered carbide-free acicular bainite. If this interpretation proves correct, it implies that the boron increased the hardenability to cause the difference.

The TEM of 9Cr-2WVTa, 11Cr-1WMoVTa, 11Cr-2WVTa, and 11Cr-2WVTaB steels showed substructures indicative of tempered martensite, with the 11Cr-1WMoVTa showing more recovery and less precipitate than the others. The COST CB2 did not show the obvious lath structure of tempered martensite comparable to the other high-chromium steels, although optical microscopy indicated that this steel had a tempered martensite structure.

Extraction replicas and precipitate extractions of the steels were examined. Both the 3Cr and the 9 and 11Cr steels contained large Cr-rich precipitates identified as $M_{23}C_6$ in the high-chromium steels and as M_7C_3 and/or $M_{23}C_6$ in the 3Cr steels. The steels also contained V-rich, Ta-rich, and Nb-rich MX precipitates, depending on the steel composition.

Tensile tests indicated the 3Cr-3WVTaB was the strongest of all nine steels between room temperature and 650°C. All 3Cr steels were as strong as or stronger than COST CB2. However, the COST CB2 strength exceeded that of 9 and 11Cr steels.

Charpy impact results reflected the strengths with the weakest materials having the best impact properties. The 9Cr-2WVTa and 11Cr-2WVTa steels, which had strengths approaching the COST CB2 strength, had impact properties comparable to those of COST CB2.

Creep-rupture tests were conducted at 600 and 650°C, and the COST CB2 had better properties than any of the other steels. The steels with creep-rupture properties closest to the COST CB2 were the 9Cr-2WVTa, 11Cr-2WVTa, and 11Cr-2WVTaB steels.

Further heat treatment studies were conducted on the strongest 9 and 11Cr steels—9Cr-2WVTa, 11Cr-2WVTa, and 11Cr-2WVTaB—and it was determined that an austenitization treatment of 5 h at 1100°C would remove more of the δ-ferrite than the original 1 h at 1100°C did. After the three steels were normalized 1100°C/5h/AC and tempered 750°C/1h, tensile and creep tests were conducted. Although removing δ-ferrite improved the tensile and creep-rupture strengths, they were still not as good as those of COST CB2.

Computational thermodynamics analyses using the JMatPro program were carried out on the casting compositions to determine expected phases and how they might be used to explain the experimental observations, and finally, how this understanding of the phases could be used to determine compositions with improved properties. Some interesting observations were made concerning calculated precipitate-phase differences in the Cr-WVTa steels, which includes all the ORNL compositions, compared to Cr-MoVNb steels, the latter composition being represented in the castings by COST CB2.

Results from the calculations can be used to make a case for the superiority of the Mo-Nb-containing cast steels *vis-à-vis* W-Ta-containing steels. However, these calculations assume the results are correct for the equilibrium structure. Equilibrium at the 1100°C austenitization temperature and the 750°C tempering temperature is probably not a bad assumption for wrought materials. However, for castings, it is not so clear, even for the 1100°C heat treatments.

Based on the experimental studies and thermodynamics analyses, five high-chromium and four 3Cr steel compositions were proposed as the second iteration for these studies.

Experimental—Part III

Composition and Heat Treatment

Based on the results of Parts I and II of this project, nine new heats were purchased by ORNL from Voestalpine for the second iteration of the study (Table 13). The five 11Cr steels were designated as follows: 11Cr-1.5MoCoMnNbVB (Cast A), 11Cr-1.5MoCoMnVB (Cast B), 11Cr-1.5MoCoMnV (Cast C), 11Cr-2WCoMnV (Cast D), and 11Cr-2WCoMnNbV (Cast E).

Table 13. Composition of Steel Casting Test Blocks for Second Iteration*

Element	Cast A	Cast B	Cast C	Cast D	Cast E	Cast F	Cast G	Cast H	Cast I
C	0.10	0.11	0.12	0.10	0.11	0.086	0.10	0.090	0.095
Mn	0.84	0.75	0.74	0.86	0.83	0.50	0.51	0.53	0.53
P	0.010	0.010	0.011	0.009	0.008	0.010	0.011	0.011	0.010
S	0.006	0.007	0.008	0.005	0.005	0.008	0.007	0.006	0.006
Si	<0.01	<0.01	0.01	<0.01	<0.01	<0.01	<0.01	<0.01	<0.01
Ni	0.20	0.20	0.20	0.20	0.21	0.01	0.02	0.03	0.03
Cr	10.66	10.79	10.81	10.65	10.79	3.00	2.96	2.91	2.90
Mo	1.48	1.48	1.48	0.01	0.01	1.47	1.50	1.52	0.01
V	0.20	0.21	0.21	0.20	0.18	0.26	0.22	0.20	0.21
Nb	0.04	<0.01	<0.01	<0.01	0.05	<0.01	0.05	0.002	0.045
Ti	0.002	0.002	0.002	0.002	0.002	0.002	0.002	0.002	0.002
Co	0.62	0.62	0.62	0.63	0.64	<0.001	0.006	0.005	0.009
Cu	0.03	0.03	0.03	0.03	0.02	0.03	0.03	0.03	0.043
Al	0.009	0.014	0.014	0.014	0.014	0.011	0.012	0.004	0.012
B	0.002	<0.001	0.004	<0.001	0.001	<0.001	<0.001	0.002	0.001
Ta				<0.01	0.01		<0.01	<0.01	<0.01
W	0.001	0.01	0.01	1.78	1.80	0.01	<0.01	<0.01	2.24
As	0.014	0.013	0.012	0.024	0.003	0.013	0.002	0.002	0.003
Sn	0.002	0.002	0.002	0.003	0.004	0.001	0.001	0.001	0.004
N	0.014	0.013	0.014	0.011	0.012	0.007	0.008	0.008	0.009
O	0.007	0.005	0.006	0.005	0.005	0.006	0.005	0.007	0.005

*Steel Designations:

Cast A: 11Cr-1.5MoCoMnNbVB
Cast B: 11Cr-1.5MoCoMnVB
Cast C: 11Cr-1.5MoCoMnV
Cast D: 11Cr-2WCoMnV
Cast E: 11Cr-2WCoMnNbV
Cast F: 3Cr-1.5MoV
Cast G: 3Cr-1.5MoVNb
Cast H: 3Cr-1.5MoVB
Cast I: 3Cr-3WVNb

Designations for the four 3Cr steels were: 3Cr-1.5MoV (Cast F), 3Cr-1.5MoVNb (Cast G), 3Cr-1.5MoVB (Cast H), and 3Cr-3WVNb (Cast I).

One difference between the chemistries of the steels from the second batch (Table 14) and the first batch (Table 1) was the nitrogen concentration. It appears from Table 1 that the amount of nitrogen in the steels depended on the chromium concentration; the 3Cr steels contained 0.007-0.018%, the two 9Cr steels contained 0.027 and 0.028%, and the three 11Cr steels contained 0.031, 0.034, and 0.033% N. Because of the consistency of these observations on the first batch of steels, it was assumed similar nitrogen concentrations would be obtained in the second batch. The five 3Cr steels again had nitrogen concentrations consistent with the earlier batch, the concentrations all in the range 0.007-0.009% N. However, the nitrogen concentration of the 11Cr steels in the second batch ranged between 0.011 to 0.014% N, which was 2-3 times less than in the first batch of castings. As discussed below, this probably had some bearing on the performance of these steels.

To determine the normalization heat treatment to use on the new steels to produce a homogenous microstructure, 51-mm-thick blocks were annealed 1 and 5 hours at 1100°C followed by an air cool. Based on the observations of the optical microstructures, the 11Cr steels were also given a 7 h anneal. Hardness values for the 11Cr steels were fairly consistent in that they did not show much change for the different annealing times, given the type of scatter inherent in hardness measurements (Table 14). On average, the hardness values after 1 h at 1100°C were somewhat less than those of the previous 11Cr steels (Table 2). The hardnesses were similar to those of the 9Cr COST CB2, with the exception of 11Cr-1.5MoCoMnVNbB (Cast A) and 11Cr-2WCoMnNbV (Cast E) (Table 14), although the hardness of both these steels increased with longer annealing time.

The hardness of the 3Cr steels decreased between the 1 and 5 h austenitization treatments. After the latter treatment, all four steels had similar hardnesses.

Table 14. Vickers Hardness for Different Austenitization Treatments (HV)*

Cast—Designation	1100°C/1h	1100°C/5h	1100°C/7h
Cast A—11Cr-1.5MoCoMnNbVB	368	394	374
Cast B-11Cr-1.5MoCoMnVB	391	385	398
Cast C-11Cr-1.5MoCoMnV	404	416	426
Cast D-11Cr-2WCoMnV	394	373	380
Cast E-11Cr-2WCoMnNbV	353	396	390
Cast F-3Cr-1.5MoV	399	344	
Cast G-3Cr-1.5MoVNb	356	345	
Cast H-3Cr-1.5MoVB	340	335	
Cast I-3Cr-3WVNb	359	335	

*The steels were air cooled following the austenitization treatment.

Based on the hardness changes and the metallography (discussed in the next section), austenitization times of 7 and 2 h at 1100°C were chosen for the 11 and 3Cr steels, respectively.

In accordance with the procedures used previously and those generally used in industry, a tempering treatment of 1 h at 750°C was chosen for the 11Cr steels and 1h at 700°C for the 3Cr steels. The hardnesses after these treatments (Table 15) indicated that the 11 Cr steels were

somewhat softer than the 3Cr steels and the high-chromium (9 and 11%) steels in the first batch (Table 3).

Table 15. Vickers Hardness for Normalized-and-Tempered Steels (HV)

Cast—Designation	1100°C/7h + 750°C/1h	1100°C/2h +700°C/1h
Cast A—11Cr-1.5MoCoMnNbV	267	
Cast B—11Cr-1.5MoCoMnVB	246	
Cast C—11Cr-1.5MoCoMnV	254	
Cast D—11Cr-2WCoMnV	244	
Cast E—11Cr-2WCoMnNbV	272	
Cast F—3Cr-1.5MoV		299
Cast G—3Cr-1.5MoVNb		324
Cast H—3Cr-1.5MoVB		295
Cast I—3Cr-3WVNb		327

Metallography

The normalized microstructures of the five 11Cr steels after 1 h at 1100°C contained martensite with varying amounts of δ-ferrite (Figs. 71-74) which, for all of the steels, decreased with increased time at 1100°C, although all the steels still showed evidence of the phase after 7 h at 1100°C. The 11Cr-1.5MoCoMnNbV (Fig. 73) and 11Cr-1.5MoCoMnVB (Fig. 71) contained the most after the 7 h anneal, with much less present in the other steels (Figs. 72-74).

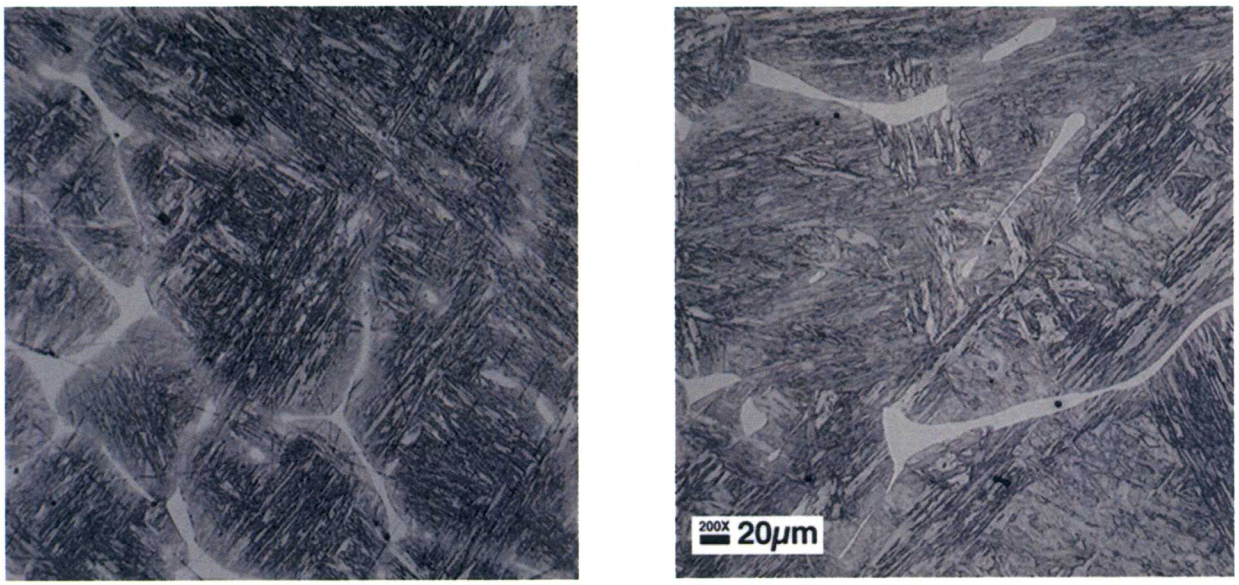

Figure 71. Optical microstructure of 11Cr-1.5MoCoMnNbVB steel (Cast A) austenitized 1 h at 1100°C (left) and 7 h at 1100°C (right).

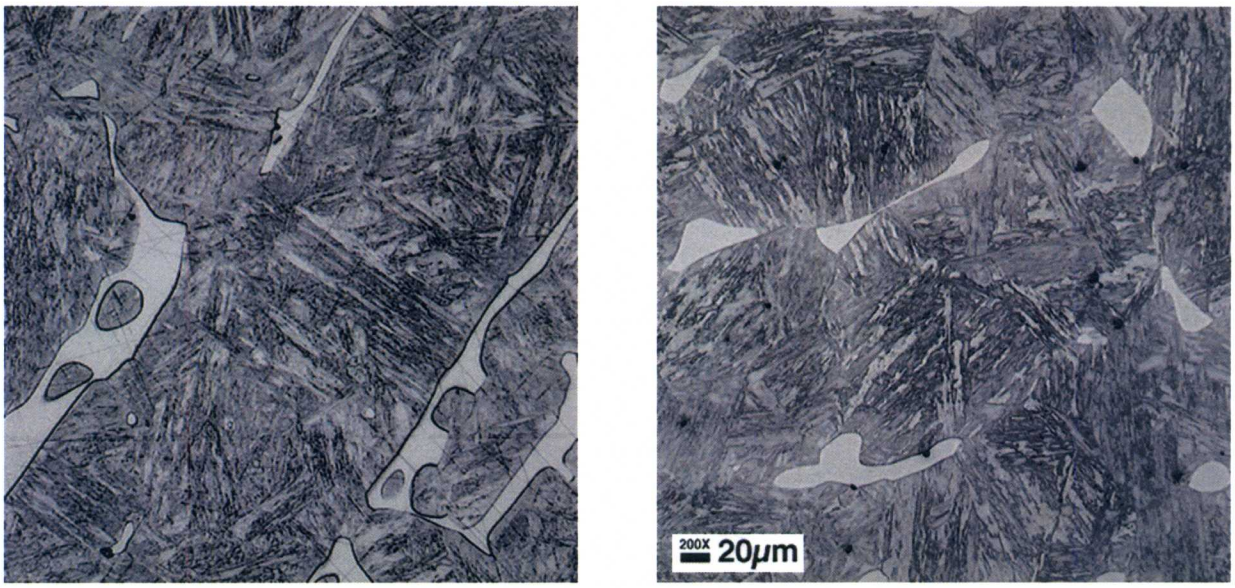

Figure 72. Optical microstructure of 11Cr-1.5MoCoMnVB steel (Cast B) austenitized 1 h at 1100°C (left) and 7 h at 1100°C (right).

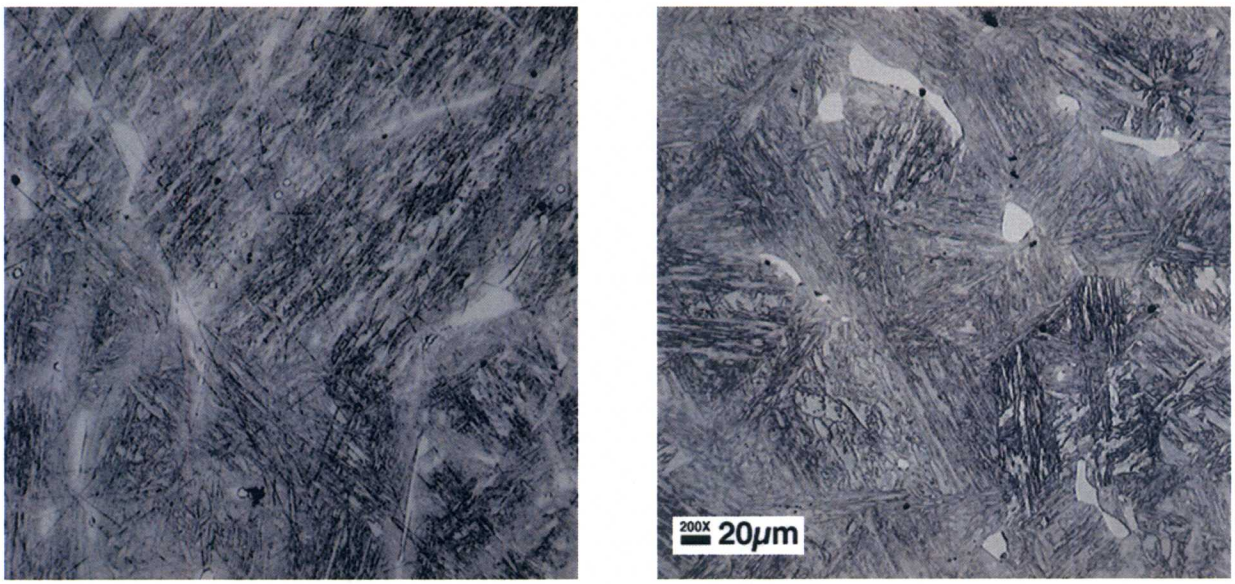

Figure 73. Optical microstructure of 11Cr-1.5MoCoMnV steel (Cast C) austenitized 1 h at 1100°C (left) and 7 h at 1100°C (right).

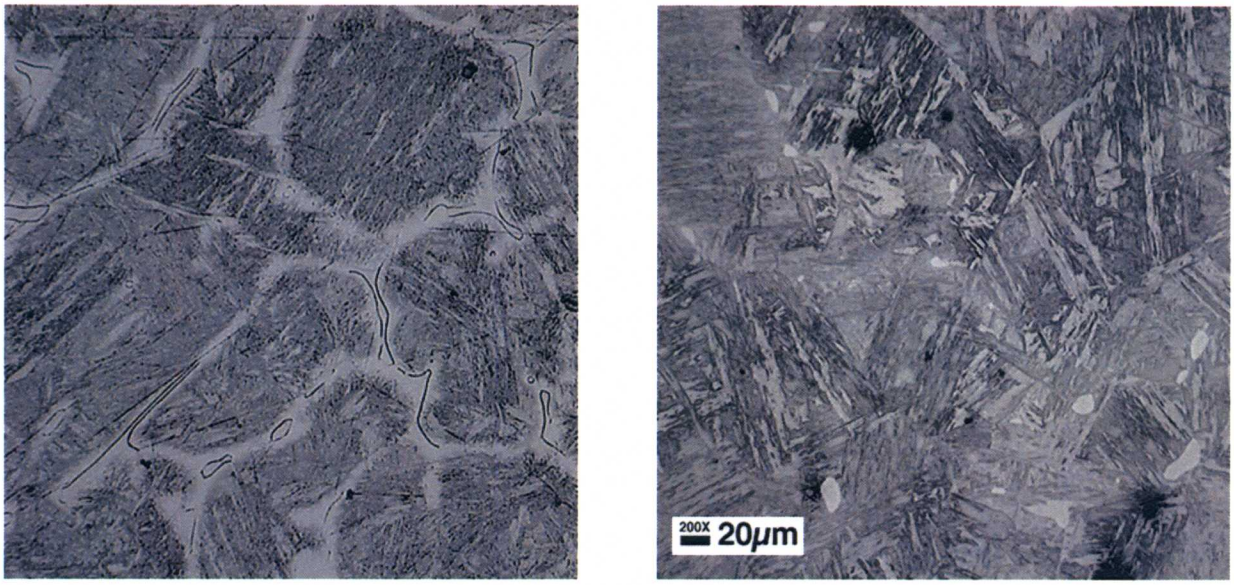

Figure 74. Optical microstructure of 11Cr-1.5MoCoMnV steel (Cast D) austenitized 1 h at 1100°C (left) and 7 h at 1100°C (right).

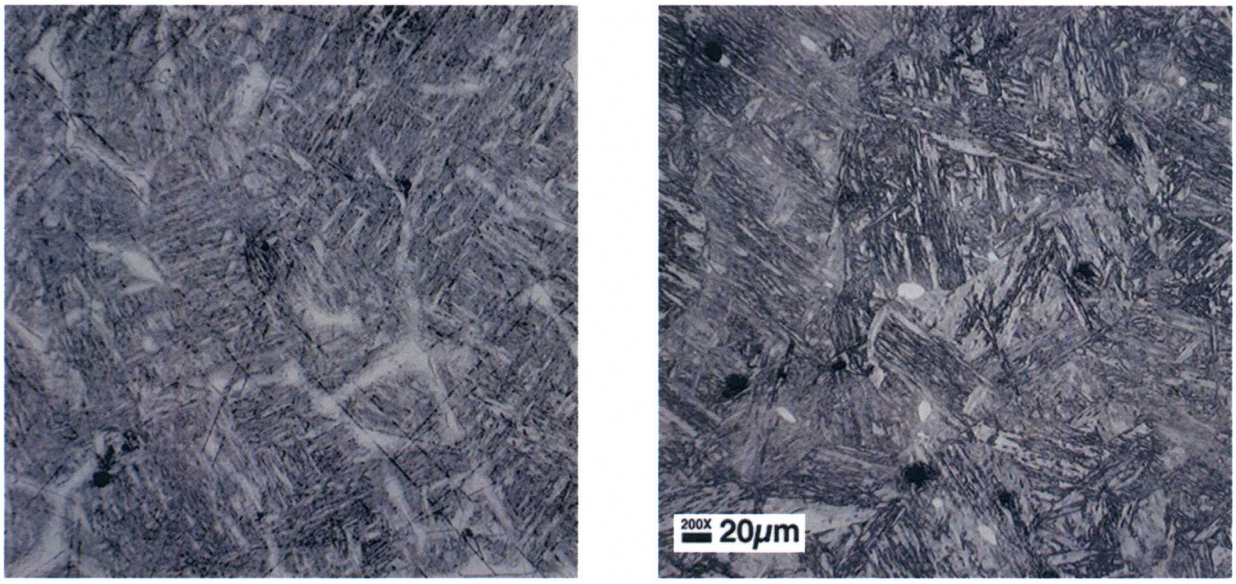

Figure 75. Optical microstructure of 11Cr-2WCoMnNbV steel (Cast E) austenitized 1 h at 1100°C (left) and 7 h at 1100°C (right).

All four 3Cr steels appeared to be 100% bainite after the 1 h at 1100°C anneal followed by an air cool (Fig. 76). There was no change in microstructure when the steels were annealed for 5 h at 1100°C.

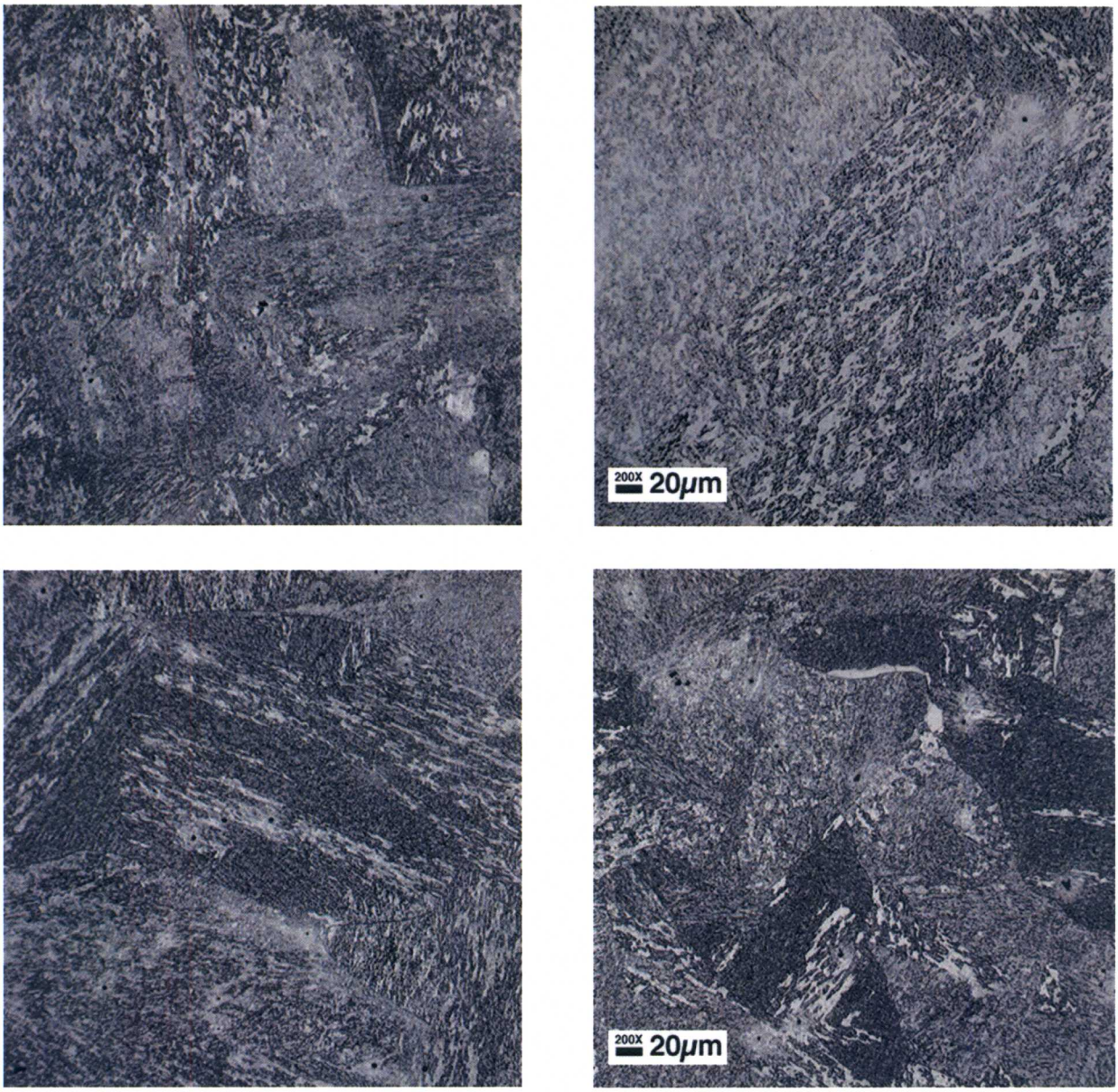

Figure 76. Optical microstructures of 3Cr-1.5MoV (Cast F) (top left), 3Cr-1.5MoVNb (Cast G) (top right), 3Cr-1.5MoVB (Cast H) (bottom left), and 3Cr-3WVNb (Cast I) (bottom right) steels austenitized 1 h at 1100°C (left) and 7 h at 1100°C (right).

After tempering, the appearance of the microstructures was little changed from those shown in Figs. 71-76, since tempering does not change the amount of δ-ferrite nor does it change significantly the appearance of this phase or the martensite and bainite.

Examination of the optical microstructures of the 11Cr or 3Cr steels of this batch indicated the test blocks contained porosity of the type present in the first batch of castings.

Electron Microscopy—Foil Specimens

Based on the mechanical properties results (discussed below) which showed that the 11Cr-1.5MoCoMnVNbB (Cast A), 11Cr-1.5MoCoMnV (Cast C), 11Cr-2WCoMnV (Cast D), 11Cr-2WCoMnNbV (Cast E), 3Cr-1.5MoVNb (Cast G), and 3Cr-3WVNb (Cast I) had the best properties, only these steels were examined by TEM (Figs. 77-80).

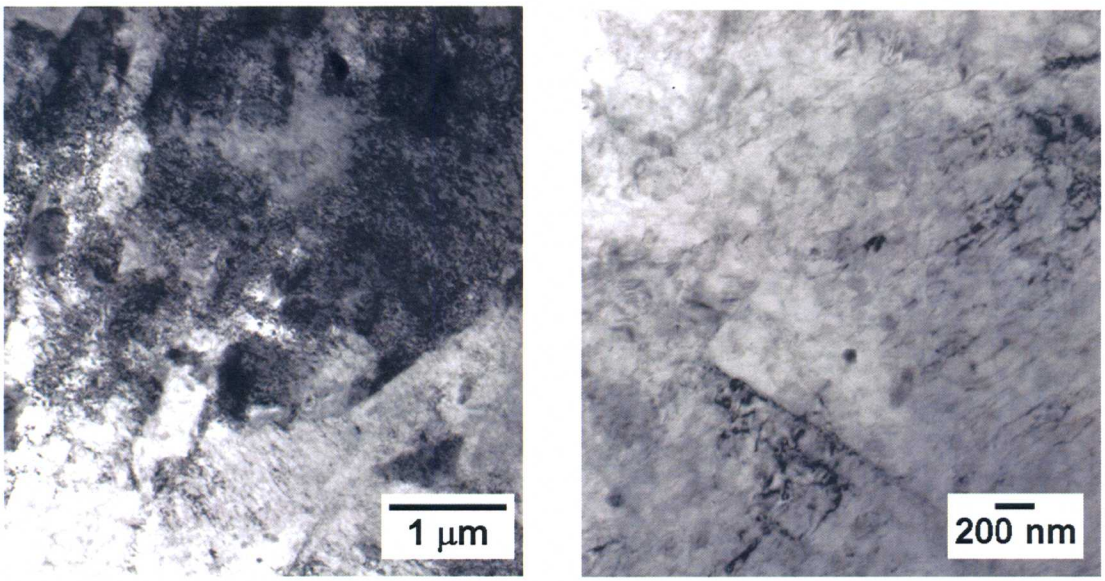

Figure 77. TEM photomicrographs of 11Cr-1.5MoCoMnVNbB (Cast A).

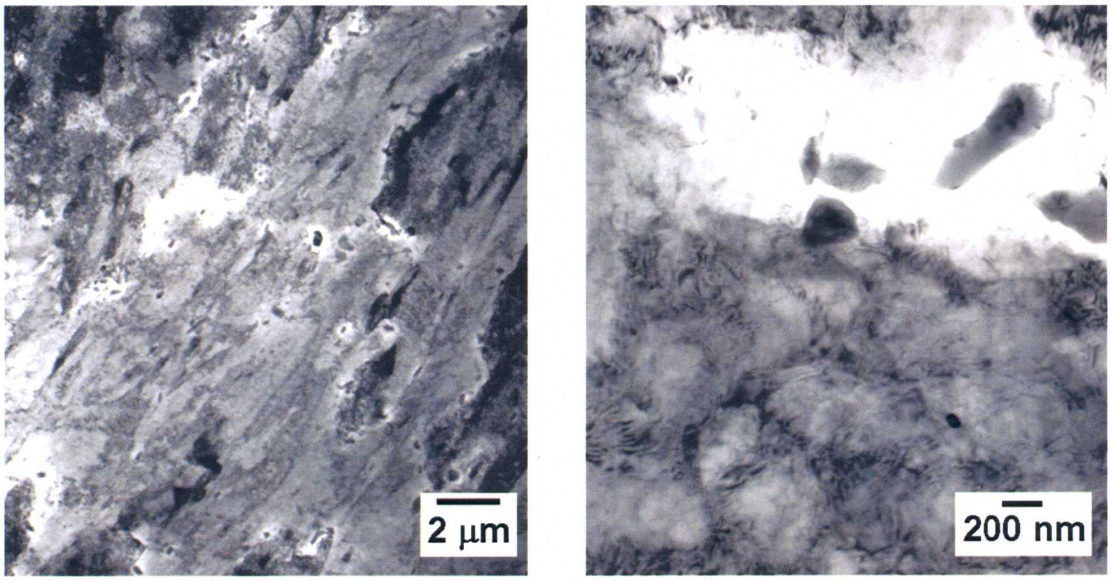

Figure 78. TEM photomicrographs of 11Cr-1.5MoCoMnV (Cast C).

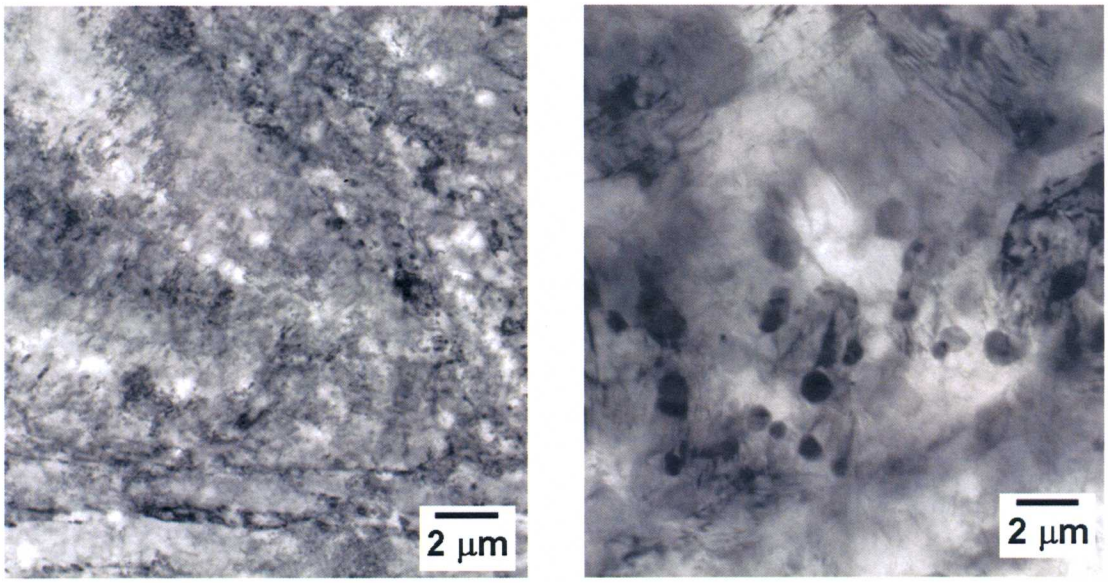

Figure 79. TEM photomicrographs of 11Cr-2WCoMnV (Cast D).

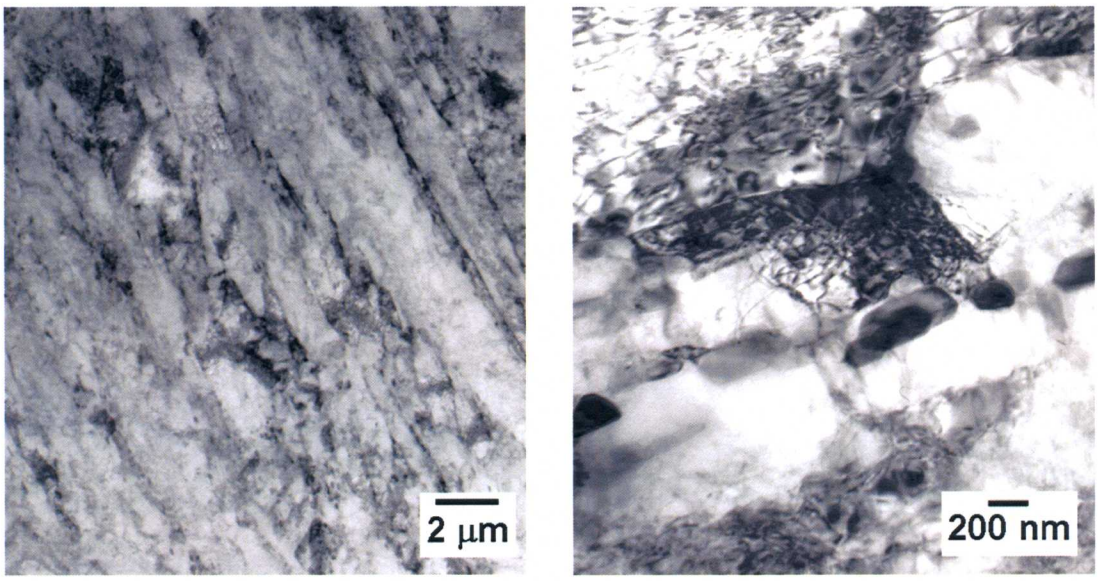

Figure 80. TEM photomicrographs of 11Cr-2WCoMnVNb (Cast E).

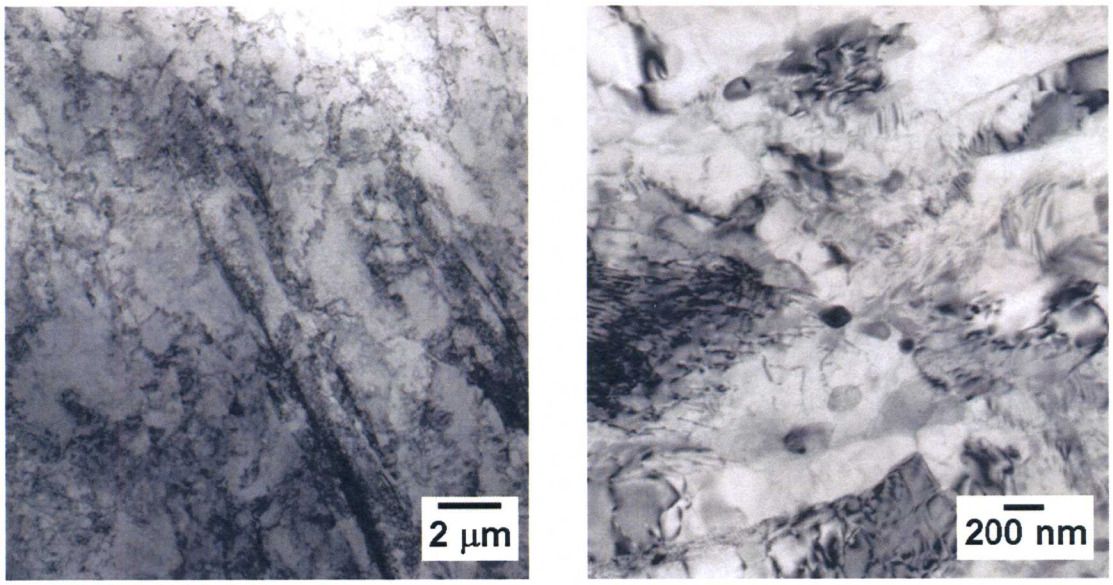

Figure 81. TEM photomicrographs of 3Cr-1.5MoVNb (Cast G).

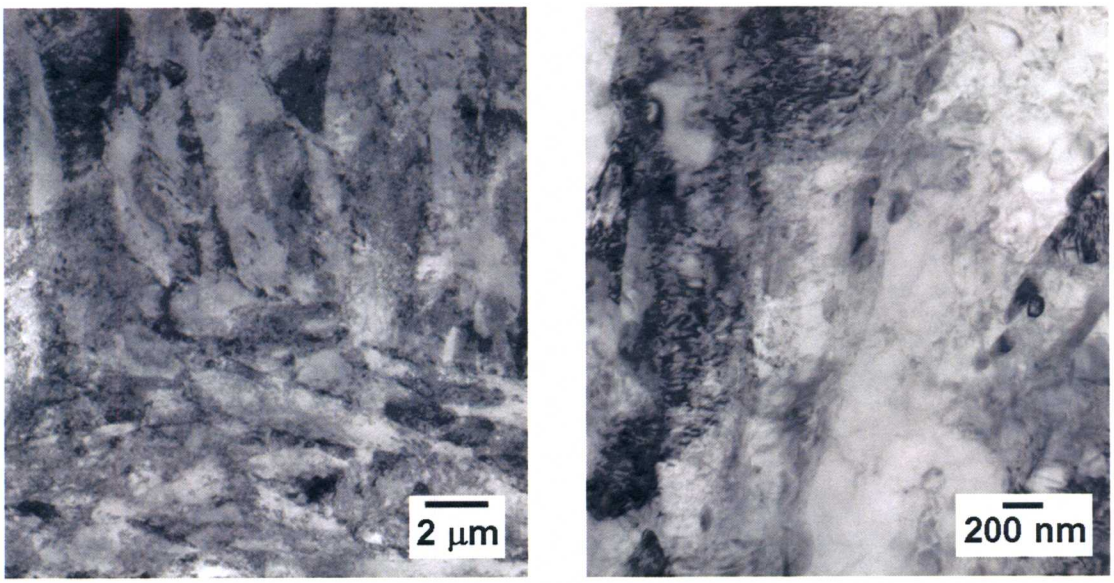

Figure 82. TEM photomicrographs of 3Cr-3WVNb (Cast I).

The microstructures appeared similar to those observed for the first batch of castings, as expected, with the obvious presence of the large precipitates (presumed to be $M_{23}C_6$ in the 11Cr steels and M_7C_3 and/or $M_{23}C_6$ in the 3Cr steels). Likewise there is also a distribution of smaller precipitates (MX).

Because of limited time caused by an earlier than planned cut off date to finish and the accompanying reduced funding for the final year of this project, no extraction replicas were examined to identify the precipitates in the second batch of steels.

Precipitate Extraction

Precipitates from the second batch of steels were extracted (Table 16). There was less precipitate extracted from the 11Cr steels for this batch of castings than for the 11Cr and COST CB2 steels from the extractions from the first batch (Table 4). Amounts extracted from the 3Cr steels for the second batch were similar to those of the first batch, with the exception of the large amount extracted from the 3Cr-3WVTaB from the previous batch.

Table 16. Amount of Precipitate in Steels

Steel	Extracted Precipitate (wt %)
Cast A—11Cr-1.5MoCoMnVNbB	1.14
Cast B—11Cr-1.5MoCoMnVB	2.54
Cast C—11Cr-1.5MoCoMnV	2.60
Cast D—11Cr-2WCoMnV	1.38
Cast E—11Cr-2WCoMnNbV	1.89
Cast F—3Cr-1.5MoV	0.97
Cast G—3Cr-1.5MoVNb	1.61
Cast H—3Cr-1.5MoVB	1.73
Cast I—3Cr-3WVNb	1.47

Mechanical Properties

Tensile Properties

Tensile properties of the 11Cr steels from the second batch of test blocks (Table 17) indicated that the 11Cr-2WCoMnVNb was the strongest of the five steels [Fig 83(a)], and it had a slight advantage over the 11Cr-1.5MoCoMnVNbB. The other three steels, which do not contain niobium, were not as strong. The ductility generally reflected the strength properties [Fig. 83(b)] in that the stronger steels had the lowest ductility.

One objective of the second batch of steels was to determine the effect of molybdenum and niobium in COST CB2 relative to tungsten and tantalum in the first batch of steels. The 11Cr-1.5MoCoMnVNbB steel was patterned after COST CB2, with the main difference involving the 11% Cr with the addition of extra manganese as an austenite stabilizer. When yield stresses for the second batch of steels are compared with the yield stress for COST CB2, the latter steel is again the strongest up to 650°C—the highest test temperature (Fig. 84). At 650°C, COST CB2 and 11Cr-2WCoMnNbV have similar strengths.

The 11Cr steels of the second batch are stronger than those of the previous batch, as shown in the yield strength comparison in Fig. 85, where the 11Cr-2WVTa, the strongest of the

Table 17. Tensile Properties of the Second Batch of Castings

Steel	Cast	Temp C	YS (ksi)	YS (MPa)	UTS (ksi)	UTS (MPa)	Elgn (%)	RA (%)
11Cr-1.5MoCoMnVNbB	A	21	103.0	709.7	124.0	854.4	12.0	50.0
11Cr-1.5MoCoMnVNbB	A	400	86.0	592.5	98.5	678.7	13.0	47.0
11Cr-1.5MoCoMnVNbB	A	500	77.0	530.5	87.0	599.4	19.0	66.0
11Cr-1.5MoCoMnVNbB	A	600	57.5	396.2	64.5	444.4	32.0	82.0
11Cr-1.5MoCoMnVNbB	A	650	45.4	312.8	53.0	365.2	27.0	82.0
11Cr-1.5MoCoMnVB	B	21	90.5	623.5	111.0	764.8	23.0	61.0
11Cr-1.5MoCoMnVB	B	400	79.0	544.3	91.5	630.4	17.0	62.0
11Cr-1.5MoCoMnVB	B	500	70.5	485.7	79.5	547.8	21.0	74.0
11Cr-1.5MoCoMnVB	B	600	49.5	341.1	56.5	389.3	36.0	85.0
11Cr-1.5MoCoMnVB	B	650	36.6	252.2	45.3	312.1	39.0	87.0
11Cr-1.5MoCoMnV	C	21	96.5	664.9	117.0	806.1	19.0	58.0
11Cr-1.5MoCoMnV	C	400	81.5	561.5	94.5	651.1	17.0	58.0
11Cr-1.5MoCoMnV	C	500	74.5	513.3	84.5	582.2	21.0	69.0
11Cr-1.5MoCoMnV	C	600	54.5	375.5	61.5	423.7	27.0	78.0
11Cr-1.5MoCoMnV	C	650	41.5	285.9	49.7	342.4	42.0	88.0
11Cr-2WCoMnV	D	21	98.0	675.2	118.0	813.0	20.0	58.0
11Cr-2WCoMnV	D	400	80.0	551.2	90.0	620.1	17.0	61.0
11Cr-2WCoMnV	D	500	70.0	482.3	77.0	530.5	21.0	74.0
11Cr-2WCoMnV	D	600	49.6	341.7	56.5	389.3	33.0	87.0
11Cr-2WCoMnV	D	650	38.0	261.8	46.2	318.3	38.0	88.0
11Cr-2WCoMnVNb	E	21	107.0	737.2	127.0	875.0	18.0	54.0
11Cr-2WCoMnVNb	E	400	90.5	623.5	102.0	702.8	14.0	58.0
11Cr-2WCoMnVNb	E	500	80.0	551.2	88.5	609.8	18.0	68.0
11Cr-2WCoMnVNb	E	600	62.5	430.6	68.5	472.0	26.0	81.0
11Cr-2WCoMnVNb	E	650	51.5	354.8	58.0	399.6	24.0	81.0
3Cr-1.5MoV	F	21	143.0	985.3	164.0	1130.0	15.0	44.0
3Cr-1.5MoV	F	400	123.0	847.5	146.0	1005.9	11.0	39.0
3Cr-1.5MoV	F	500	111.0	764.8	129.0	888.8	13.0	45.0
3Cr-1.5MoV	F	600	89.5	616.7	104.0	716.6	13.0	41.0
3Cr-1.5MoV	F	650	79.5	547.8	91.0	627.0	8.0	15.0
3Cr-1.5MoVNb	G	RT	136.0	937.0	153.0	1054.2	9.0	23.0
3Cr-1.5MoVNb	G	400	117.0	806.1	135.0	930.2	11.0	39.0
3Cr-1.5MoVNb	G	500	106.0	730.3	121.0	833.7	13.0	46.0
3Cr-1.5MoVNb	G	600	85.0	585.7	95.5	658.0	12.0	34.0
3Cr-1.5MoVNb	G	650	73.5	506.4	81.5	561.5	10.0	25.0
3Cr-1.5MoVB	H	21	137.0	943.9	159.0	1095.5	12.0	29.0
3Cr-1.5MoVB	H	400	120.0	826.8	141.0	971.5	12.0	47.0
3Cr-1.5MoVB	H	500	110.0	757.9	128.0	881.9	14.0	57.0
3Cr-1.5MoVB	H	600	88.0	606.3	102.0	702.8	12.0	35.0
3Cr-1.5MoVB	H	650	76.0	523.6	87.0	599.4	8.0	17.0
3Cr-3WVNb	I	21	133.0	916.4	150.0	1033.5	15.0	44.0
3Cr-3WVNb	I	400	121.0	833.7	142.0	978.4	11.0	40.0
3Cr-3WVNb	I	500	111.0	764.8	128.0	881.9	15.0	55.0
3Cr-3WVNb	I	600	88.0	606.3	103.0	709.7	11.0	32.0
3Cr-3WVNb	I	650	77.0	530.5	88.5	609.8	6.0	14.0

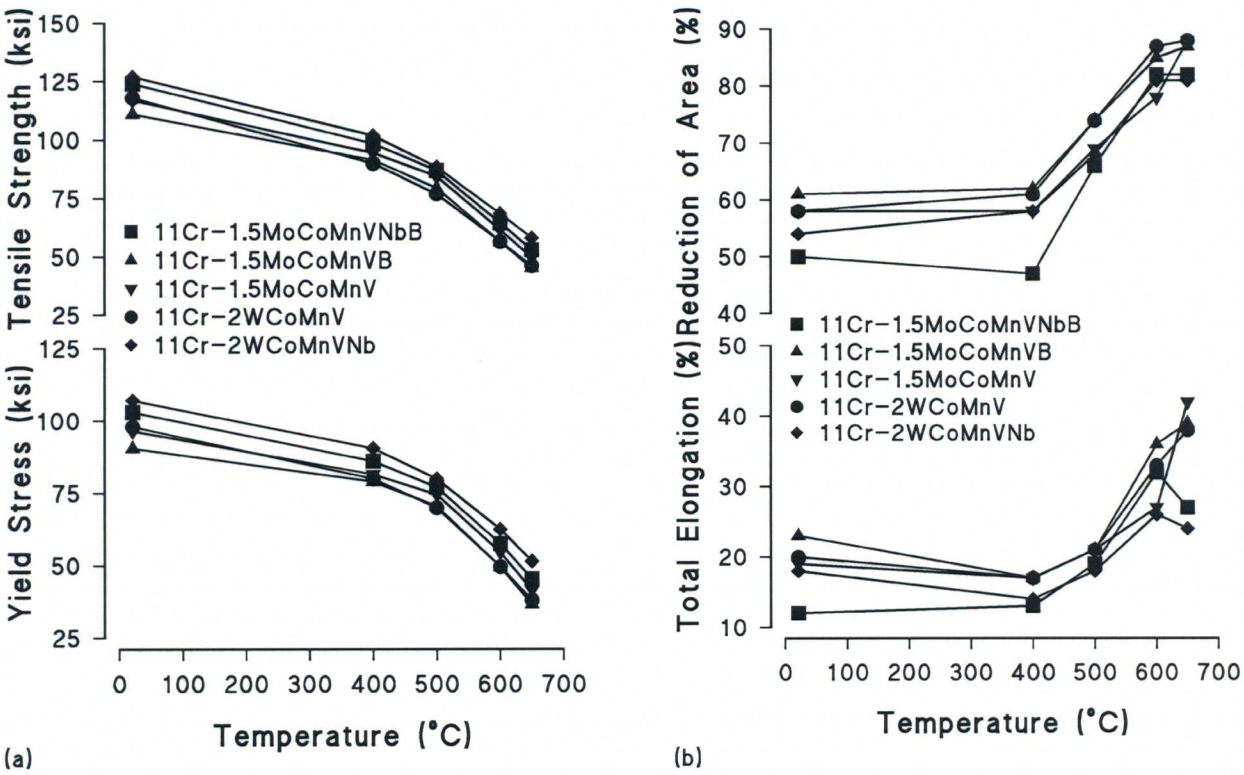

Figure 83. (a) Yield stress and ultimate tensile strength and (b) total elongation and reduction of area as a function of temperature for second batch of 11Cr steels.

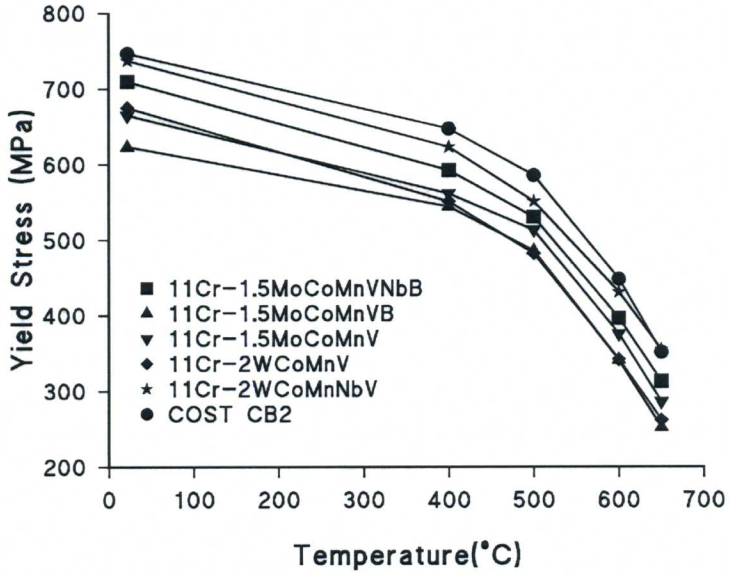

Figure 84. Yield stress for steels as a function of temperature from second batch of castings compared with the yield stress of COST CB2.

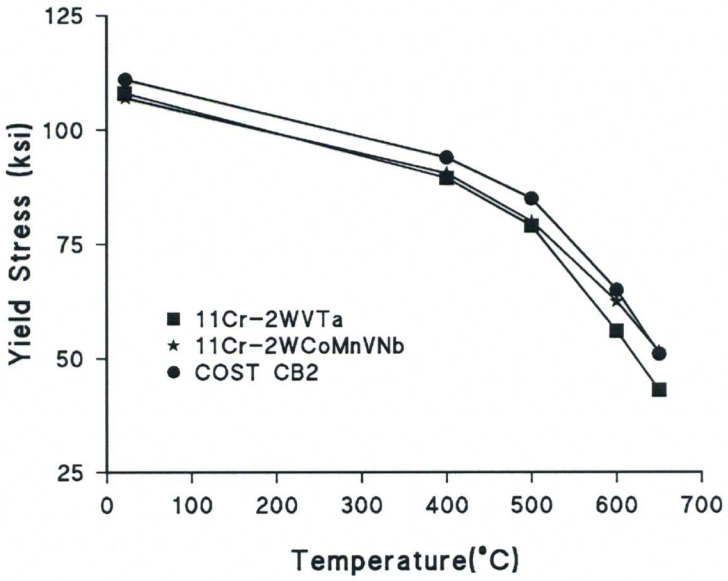

Figure 85. Yield stress as a function of temperature for the strongest steel from the second batch of castings compared with the yield stresses of the strongest steel from the first batch and with COST CB2.

previous 9 and 11Cr steels, is compared with 11Cr-2WCoMnNbV and COST CB2. Although the 11Cr-2WCoMnNbV and 11Cr-2WVTa have similar strengths at the lowest test temperatures, the strength of the 11Cr-2WVTa decreases much more with temperature than does the 11Cr-2WCoMnNbV, which has properties similar to COST CB2 at the highest test temperature.

The 3Cr steels show a different behavior from the 11Cr steels, in that the steels with niobium are the weakest [Fig. 86(a)] at room temperature, and the 3Cr-1.5MoVNb remains the weakest at all test temperatures. As the test temperature is increased, the difference between the other three steels becomes quite small. The ductility data show considerable scatter [Fig. 86(b)], and there are differences with the 11Cr steels. Whereas the 11Cr steels show an increase in ductility with increasing test temperature, the 3Cr steels show a decrease. The 3Cr steels are also less ductile than the 11Cr steels.

As observed for the first batch of 3Cr steels, they generally have higher strengths than the 11 Cr steels (Fig. 44), which is the result of the lower tempering temperature. A comparison of the strongest steels from the two batches indicates an advantage for the steels containing molybdenum and niobium compared to tungsten and tantalum (Fig. 87). An interesting and unexpected observation was that the yield stress values of the 3Cr-3WV and 3Cr-1.5MoV [Fig. 87(a)] are slightly greater than those of 3Cr-3WVTa and 3Cr-1.5MoVNb [Fig. 87(b)], respectively.

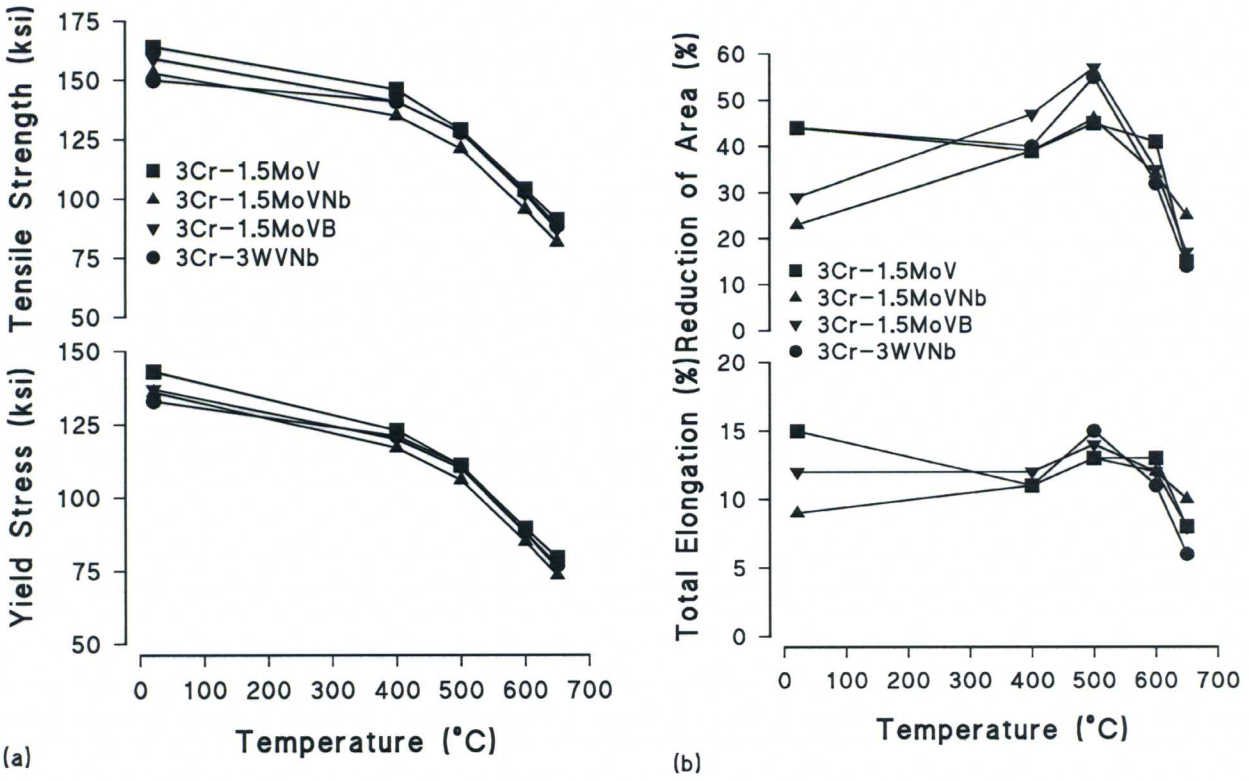

Figure 86. (a) Yield stress and ultimate tensile strength and (b) total elongation and reduction of area as a function of temperature for 3Cr steels from the second batch of casting test blocks.

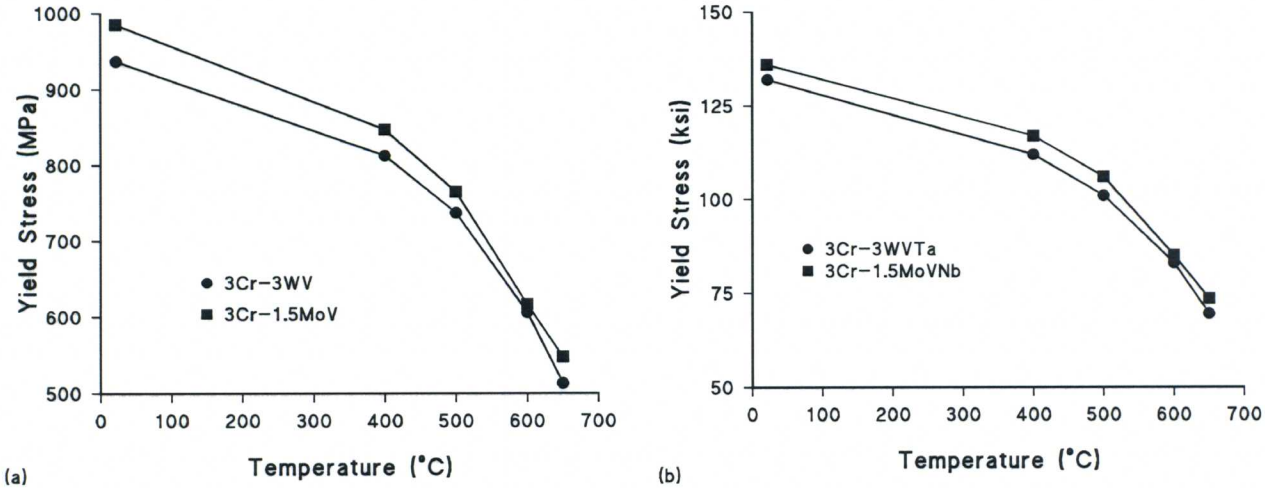

Figure 87. Yield stress behavior for 3Cr steels comparing the effect of (a) Mo with W and (b) Mo and Nb with W and Ta.

Creep-Rupture Properties

Because of the funding reduction and because the program was cut short in time, fewer creep tests were completed to rupture on the second batch of castings (Table 18). For the 11Cr steels, the 11Cr-1.5MoCoMnVNbB and the 11Cr-2WCoMnVNb were much stronger than the other three 11Cr steels. For tests at 30 ksi at 650°C, rupture times for these steels exceeded those for COST CB2 (Fig. 88); because of their low strength in the tensile tests, the other three steels were not tested at 30 ksi. The best times for 30 ksi at 650°C for the first batch of steels were for 11Cr-2WVTa and 11Cr-2WVTaB, estimated as 20-30 h.

Table 18. Creep-Rupture Properties of the Second Batch of Casting Test Blocks

Steel	Cast	Temp °C	Stress ksi	Time-0.5% h	Time-1% H	Rup Time h	Elong %	RA %
11Cr-1.5MoCoMnNbVB	A	600	30	2370	2411	2489.2	16.9	56.0
11Cr-1.5MoCoMnNbVB	A	650	20	624	1477	1975.7	16.4	56.4
11Cr-1.5MoCoMnNbVB	A	600	40	59.8	117	182.3	22.6	71.0
11Cr-1.5MoCoMnNbVB	A	650	30	38.1	55.9	64.9	12.2	47.9
11Cr-1.5MoCoMnVB	B	600	30	15.9	50	146.2	23.3	79.5
11Cr-1.5MoCoMnVB	B	650	20	30.3	55	98.6	31.3	84.1
11Cr-1.5MoCoMnV	C	600	30	90.9	269	612.4	23.3	67.5
11Cr-1.5MoCoMnV	C	650	20	44.2	72.6	123.5	41.9	80.2
11Cr-1.5MoCoMnV	C	600	35	9.7	26.4	73.4	27.2	78.7
11Cr-2WCoMnV	D	600	30	235	782	1421.3	23.7	67.5
11Cr-2WCoMnV	D	650	20	53.2	96.6	167.6	31.0	82.9
11Cr-2WCoMnV	D	600	35	14.1	50.5	154.8	24.5	75.9
11Cr-2WCoMnNbV	E	600	30	1259		2683.4[a]		
11Cr-2WCoMnNbV	E	650	20	1527		2538.9[a]		
11Cr-2WCoMnNbV	E	600	35	1259		1531.3[a]		
11Cr-2WCoMnNbV	E	650	30	75.7	114	133.4	17.1	65.0
3Cr-1.5MoV	F	600	30	344	347	368.5	20.8	46.3
3Cr-1.5MoV	F	650	20			23.8		
3Cr-1.5MoV	F	650	10	242	321	1359	13.0	49.8
3Cr-1.5MoVNb	G	600	30	1143	1659	1783.2	7.6	21.7
3Cr-1.5MoVNb	G	650	20	203	276	344.5	17.3	53.7
3Cr-1.5MoVNb	G	600	35	650	863	903.4	8.0	25.0
3Cr-1.5MoVB	H	600	30			268.6	4.2	5.6
3Cr-1.5MoVB	H	650	20	53.6	87.6	106.4	6.0	9.8
3Cr-1.5MoVB	H	600	25	396	618	643.6	3.9	4.8
3Cr-3WVNb	I	600	30	282	390	421.4	7.0	11.6
3Cr-3WVNb	I	650	20	298	273	325.3	21.1	54.1
3Cr-3WVNb	I	600	25			1124.2[a]	0.9	

[a] Test discontinued before rupture.

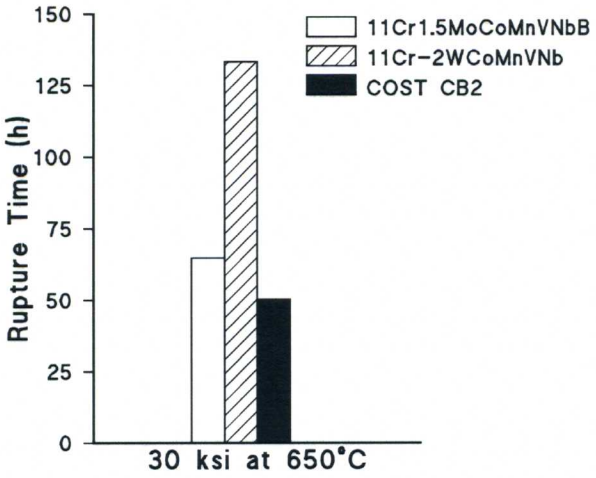

Figure 88. Comparison of creep-rupture properties of 11Cr-1.5MoCoMnVNbB and 11Cr-2WCoMnVNb steels from the second batch of castings with COST CB2 from the first batch.

Creep-rupture tests were also conducted on the 11Cr-1.5MoCoMnVNbB and the 11Cr-2WCoMnVNb at 30 ksi at 600°C, but neither was tested to failure because of the early cessation of the project. The 11Cr-2WCoMnVNb gave the best time to 0.5% strain (Table 18), but the COST CB2 had a slight advantage: 1382 h to 0.5% strain for COST CB2 compared to 1259 h for the 11Cr-1.5MoCoMnVNbB.

In agreement with results from the first batch of castings, the creep-rupture properties of the 3Cr steels were inferior to the high-chromium steels. When rupture times for tests at 30 ksi at 600°C [Fig. 89(a)] and 20 ksi at 650°C [Fig. 89(b)] are compared for the four 3Cr-MoNb steels

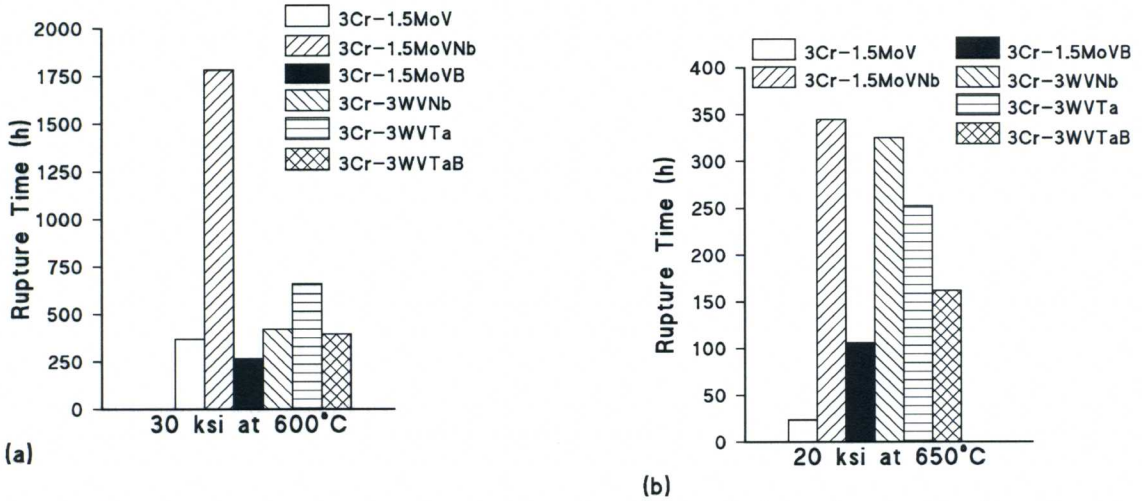

Figure 89. Comparison of the rupture times for 3Cr steels from the two batches of casting test blocks tested at (a) 30 ksi at 600°C and (b) 20 ksi at 650°C.

of the second batch and the two best 3Cr-WTa steels of the first batch, the results indicate the effectiveness of the Mo-Nb combination over W-Ta combination. The creep-rupture data also indicated the importance of the presence of tantalum and niobium to creep strength, which was not obvious in the tensile results (Fig. 87). That contradicts the conclusion reached above that

the absence of Ta and Nb should allow all the MX precipitate to dissolve during austenitization, which should aid precipitation strengthening.

It should be noted that the 1783 h rupture time for the 3Cr-1.5MoVNb in the 600°C test at 30 ksi compares favorably with some of the high-chromium steel tests at these conditions, even the 11Cr-1.5MoCoMnVNbB, which for these conditions failed in 2489 h. However, it was much less than for the 11Cr-2WCoMnVNb and COST CB2 steels. This rupture time exceeds the rupture life of the wrought 3Cr-3WV steel, but not that of the wrought 3Cr-3WVTa steel [3]. The rupture times at 650°C and 30 ksi for 3Cr-1.5MoVNb, 3Cr-3WVNb, and 3Cr-3WVTa (Fig. 89) also exceeded those for the wrought 3Cr-3WV, and the values approached those for 3Cr-3WVTa (469 h).

Discussion: Experimental Part III

The results on the 11% Cr steels of the second batch of casting are promising for two reasons. First, they indicate high-chromium steels with enhanced properties similar to those of the 9Cr COST CB2 are possible. This is important if future power-generation applications for the steels are to be pushed to temperatures beyond 600°C. Under such conditions, higher chromium would be required for oxidation and corrosion resistance. This might be the reason that 11Cr-1.5MoCoMnVNbB and the 11Cr-2WCoMnVNb steels had longer rupture times than COST CB2 (Fig. 88) in the 650°C tests.

Second, the results provided some insight on the relative merits of the elements tungsten and tantalum *vis-à-vis* molybdenum and niobium as alloy-strengthening agents. Based on the first batch that showed the superiority of COST CB2 and on the second batch that indicated that 11Cr-1.5MoCoMnVNbB steel had properties approaching those of COST CB2, the molybdenum-niobium combination is superior to the 11Cr-WVTa steels of the first batch. However, for some tensile and creep-rupture tests, the 11Cr-2WCoMnVNb steel had properties as good or better than those of COST CB2, indicating that a tungsten-niobium alloying combination may be a better than the other two combinations.

One important difference between the two batches of castings was the much larger amount of δ-ferrite in the second batch. The δ-ferrite can have a negative effect on mechanical properties. A reason for the δ-ferrite is the much lower nitrogen in the second batch. Based on the first batch, it was expected that the 11Cr steels would contain ≈0.033% N, since the first batch of 11Cr steels all contained this amount. The second batch contained less-than half as much. The reason for this difference is unclear, since based on the consistency of the nitrogen concentrations in the first batch (Table 1), it was assumed this was an equilibrium concentration for the casting process used. Therefore, since nitrogen is an austenite stabilizer, the presence of over two times more nitrogen would be expected to significantly reduce the amount of δ-ferrite, and thus lead to improved properties. This was verified with computational thermodynamics calculations, which indicated for an 1100°C austenitization temperature, no δ-ferrite should be present.

It is now well established that nitrogen is a prime reason for the enhanced creep strength of wrought modified 9Cr-1Mo over the steels that preceded its development [5,10,16-18]. The presence of nitrogen promotes the formation of stable vanadium-rich nitrides and/or carbonitrides (MX). When niobium is present in the composition, niobium-rich carbonitrides also form to further enhance creep strength.

To examine the effect of nitrogen on the 11Cr-1.5MoCoMnVNbB, an attempt was made to produce this composition with no nitrogen added—a repeat of the composition of Cast A (designated 11Cr-1.5MoCoMnVNbBR, 11CrMoR in Table 19)—and one with 0.034% N—a composition with nitrogen concentration similar to the steels in the first batch (designated 11Cr-1.5MoCoMnVNbBN, 11CrMoN in Table 19). Small air-induction melts (4 x 6 x 1 in ingots, ≈15 lb) were produced, one without a nitrogen added, the other with 0.034% N added (Table 19).

Table 19. Concentration of Small Air-Induction Casts of 11Cr-1.5MoCoMnVNbB Steels

Steel	C	Mn	Ni	Cr	Mo	V	Nb	Co	B	N	O
11CrMoR	0.094	0.88	0.21	10.77	1.56	0.20	0.07	0.90	0.008	0.028	0.042
11CrMoN	0.076	0.87	0.53	10.51	1.52	0.02	0.07	0.89	0.007	0.061	0.038

The heat with no nitrogen added had a nitrogen concentration similar to the 11 Cr steels in the first batch—0.028% N (Table 19). The second heat contained much more than the desired nitrogen, 0.061% (0.034% N was added to the melt, and another 0.027% N was picked up from the atmosphere). In addition to more nitrogen than desired, the oxygen concentration was up to ten times that obtained in the casting test blocks (Tables 1 and 13). The presence of nitrogen reduced δ-ferrite. In 11CrMoR with 0.028% N, δ-ferrite was detected, but it was estimated at <1% [Fig. 90(a)]. No δ-ferrite was detected in 11CrMoN with 0.061% N [Fig. 90(b)].

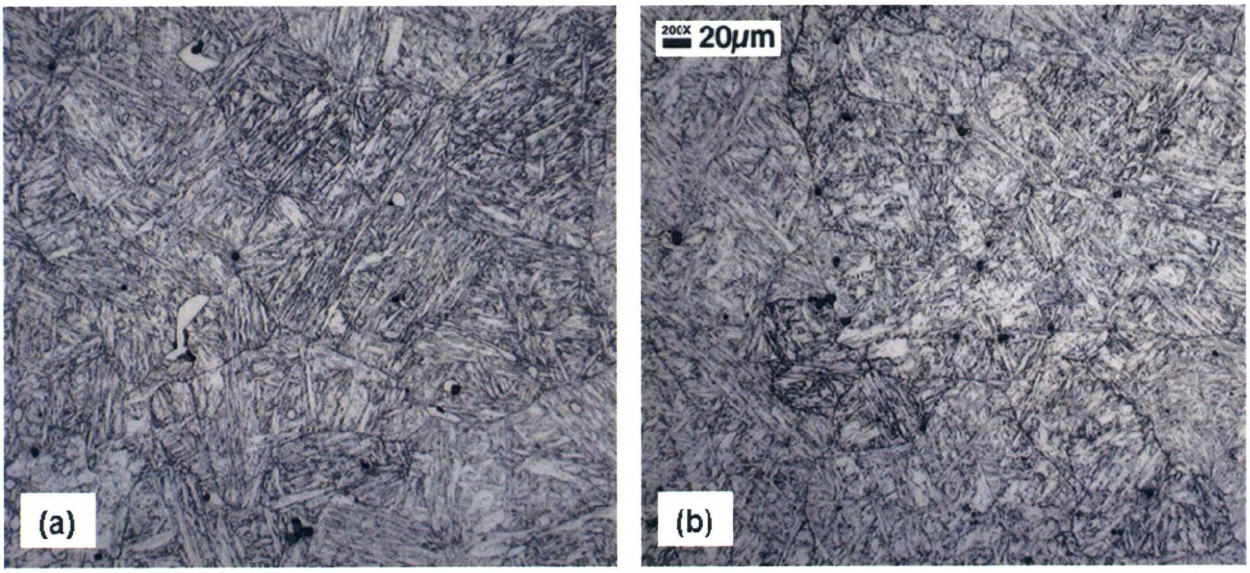

Figure 90. Optical micrograph of small air-induction castings of an 11Cr-1.5MoCoMnVNbB steel composition (Cast A) that contained (a) 0.028% N and (b) 0.061% N.

The ultimate objective in making these castings was to compare the tensile and creep properties of the steels with and without nitrogen and with Cast A. Because of the high gas content—nitrogen and oxygen—the steels had extensive porosity, and it was not possible to machine sound tensile and creep specimens. Therefore, no tensile or creep properties are reported.

In the commercial wrought NF616 steel, the presence of 0.005-0.008% B is credited with promoting enhanced creep strength [5,14,17]. The NF616 is a modification of modified 9Cr-

1Mo with some molybdenum replaced by tungsten and the addition of ≈0.005 B. As discussed above, some of the boron is incorporated in the $M_{23}C_6$ to produce $M_{23}(CB)_6$. This has the effect of refining and stabilizing these precipitates compared to $M_{23}C_6$ in the absence of boron. The finer distribution of the $M_{23}(CB)_6$ particles that form on prior-austenite grain boundaries and former lath (subgrain) boundaries during tempering stabilize the subgrain structure for a longer time relative to the larger $M_{23}C_6$ particles formed in the absence of boron. The eventual loss of long-time creep strength of these wrought steels is attributed to coarsening of precipitates, which allows the growth of the subgrain structure to proceed at an accelerated rate.

Although several of the 11Cr steels from the two batches contained boron, there were no indications that boron affected the properties, either positively or negatively. This is probably because no long-term creep tests (>10,000 h) were conducted. Based on the experience with elevated-temperature 9-12% Cr wrought steels, any high-chromium cast steel compositions should probably contain 0.005-0.008% B for enhanced creep strength.

Although Laves and μ-phase probably did not play a role in the failure of the relatively short-time creep-rupture tests performed in the present experiments, they could be important in future tests. Laves is Fe_2Mo or Fe_2W; μ appears at higher temperatures in the molybdenum-containing steels and contains more molybdenum than Laves phase. According to calculations with JMatPro for these steels, Laves phase is indicated to contain ≈45 wt % Mo compared with ≈51 wt % for μ. For long-time (low-stress) creep strength, tungsten and/or molybdenum provide solid-solution strengthening [5]. The formation of Laves or μ removes these elements from solution and, in turn, lowers creep strength.

Based on computational thermodynamics calculations (Table 20), it is found that even though on an atomic fraction basis where 1.5 wt % Mo is ≈50% more than 2 wt % W, much less Laves and μ form in the molybdenum-containing steels; thus, more of the molybdenum remains in solution at service temperatures of 600 and 650°C. If tungsten is reduced from 2 to 1.5%, there is a significant increase in the amount in solution. On the other hand, reducing the molybdenum from 1.5 to 1% causes a 7% increase at 600°C, but it causes a decrease at 650°C. At the latter temperature, more molybdenum is absorbed by the $M_{23}C_6$ (Table 2), thus lowering the amount relative to the 1.5% Mo. Also, in the molybdenum-containing steels, M_3B_2, and this compound contains 2.9% Mo for the 1% Mo steel. These calculation need to be considered in the development of these steels for long-term creep strength.

Table. 20. Calculation of Effect of Laves and μ Phases on W and Mo in Solution*

Amount, %	Amount Laves/μ, %		Conc. W/Mo in Ferrite, %		Conc. W/Mo in $M_{23}C_6$, %	
	600°C	650°C	600°C	650°C	600°C	650°C
1.5W	1.24	0.62	43.6	67.4	5.0	7.1
1.8W	1.73	1.10	36.1	55.9	4.2	5.9
2W	2.05	1.44	32.4	50.1	3.74	5.3
1Mo	0	0	59.5	61.9	36.2	33.7
1.5Mo	0.58	0	52.7	73.0	24.7	24.1

* Calculations based on a nominal 11Cr-xMo/W-0.80Co-0.80Mn-0.20Ni-0.20V-0.06Nb-0.005B-0.030N-0.10C.

It is interesting to observe that the present-day elevated temperature steels, such as NF616, HCM12A, and E911, were developed by modifying modified 9Cr-1Mo by replacing some or all of the molybdenum by tungsten, primarily with the argument that tungsten diffuses

more slowly than molybdenum, which slows recovery and Laves precipitation processes [20-26]. These calculations contradict that argument for the long-term creep properties, and as discussed above, the improved creep properties of these steels over modified 9Cr-1Mo is now attributed mainly to nitrogen and boron present in the steels.* Boron was not present in modified 9Cr-1Mo.

Summary and Conclusions

The objective of this project was to develop cast elevated-temperature ferritic/martensitic steels as-good-or better than commercial steels now being used or contemplated for use. To accomplish that objective, 18 (two iterations of nine each) casting test blocks were purchased and tested. With the aid of optical microscopy and microhardness measurements, heat-treatment studies were conducted to determine normalizing-and-tempering treatments for the test blocks. After a heat treatment was selected and applied, specimens were examined by transmission electron microscopy. Evaluation of the test blocks involved tensile, impact and creep tests.

The new steel compositions were patterned after 3Cr-2WVTa and 9Cr-2WVTa wrought reduced-activation steels developed at ORNL in the DOE fusion reactor program. In the first iteration, test blocks of 3, 9, and 11% Cr compositions were evaluated. They included the following compositions: 3Cr-3WV, 3Cr-3WVTa, 3Cr-2WMoV, 3Cr-3WVTaB, 9Cr-2WVTa, 11Cr-1WMoV, 11Cr-2WVTa, 11Cr-2WVTaB, and COST CB2. COST CB2 is a 9Cr-1.5MoCoMnVNbB steel that was the best cast steel developed in Europe, and it was used as a baseline for the evaluation of the other compositions. The 11Cr compositions were chosen because future turbine designs will operate at temperatures as high as 650°C, where higher chromium will be required for oxidation and corrosion resistance.

The first iteration indicated that Cr-WVTa cast steels were not as strong as a Cr-MoVNb steel (COST CB2) and not as strong as the wrought the 3 and 9Cr compositions. Analysis of composition data by computational thermodynamics calculations with the JMatPro program led to purchase of nine new casting test blocks designed to elucidate the difference in the Cr-WVTa and Cr-MoVNb steels. Compositions of the second iteration were: 11Cr-1.5MoCoMnNbVB, 11Cr-1.5MoCoMnVB, 11Cr-1.5MoCoMnV, 11Cr-2WCoMnV, 11Cr-2WCoMnNbV, 3Cr-1.5MoV, 3Cr-1.5MoVNb, 3Cr-1.5MoVB, and 3Cr-3WVNb. Heat treatment and microstructural studies were again carried out, along with tensile and a limited number of creep tests.

Although the 3%Cr steels of the second iteration, indicated a favorable effect of the Mo-Nb alloying combination over the W-Ta combination, they were again generally inferior to the best 11% Cr and COST CB2 steels. However, from the limited testing, it appeared that the creep-rupture properties of 3Cr-1.5MoVNb may approach those of the wrought 3Cr-3WVTa. In that respect, these properties show some promise for future development. For completeness, the properties of the 3Cr steels should be compared to those of the present low-chromium steels being used for turbine applications. Because of time and funding considerations, neither the consideration of how these steels could be developed further nor a comparison of the 3% Cr steels and other low-chromium cast steels was carried out. Instead, at the end of the project, most of the remaining time and funds were devoted to the 11% Cr steels.

For the 11% Cr steels of the second iteration, the 11Cr-1.5MoCoMnVNbB—an 11% Cr version of the 9% Cr COST CB2—and the 11Cr-2WCoMnVNb were much stronger than the

* Note that in the case of the reduced-activation steels for nuclear fusion applications, molybdenum was replaced by tungsten for nuclear considerations.

other three 11Cr steels. In tensile tests over the range room temperature to 650°C, they were not as strong as COST CB2, with one exception. At 650°C, the 11Cr-2WCoMnVNb was as strong as COST CB2. In the limited creep tests at 650°C and 30 ksi, the rupture times for 11Cr-1.5MoCoMnVNbB and 11Cr-2WCoMnVNb steels exceeded that for COST CB2, with the 11Cr-2WCoMnVNb much stronger than either of the other two steels. For a test on 11Cr-2WCoMnVNb at 600°C at 30 ksi that was not carried out to rupture, the time to 0.5% creep strain for this steel approached that for COST CB2.

Results for the 11Cr steels in the second iteration showed the 11Cr-1.5MoCoMnVNbB to be superior to the 9 and 11Cr-2WVTa compositions of the first iteration, indicating that the Cr-MoVNb combination is superior to the Cr-WVTa combination (this assumes that the Co, Mn, and B do not contribute to the strength). However, the indication that the properties of the 11Cr-2WCoMnVNb exceed those of 11Cr-1.5MoCoMnVNbB steel and approached those of COST CB2 suggest that the Cr-WVNb combination may have favorable properties.

In developing the Cr-W steels, an atom-for-atom replacement of molybdenum by tungsten was attempted, which is not the case for the 11Cr-1.5MoCoMnVNbB and COST CB2 steels compared to the 11Cr-2WCoMnVNb. On an at % basis, 1.5 wt. % Mo is about 50% more than 2 wt. % W. This conclusion that the Cr-WVNb combination may be superior to the Cr-MoVNb is complicated by the calculations that show tungsten at these concentrations leads to a higher amount of Laves phase than molybdenum. Formation of Laves phase removes tungsten from solution, and thereby lowers the solid solution strength of the steel. Solid-solution strengthening is believed to enhance the long-time (low-stress) creep behavior of these steels.

The nitrogen concentrations in the 11% Cr steels of the second iteration were <50% of that in the 9 and 11% Cr steels of the first iteration. This led to the presence of considerable δ-ferrite, which is expected to be detrimental to the strength. If similar nitrogen concentrations were present in the 1.5MoCoMnVNbB and 11Cr-2WCoMnVNb, the δ-ferrite should be eliminated. Furthermore, based on the present understanding of the elevated-temperature strengthening mechanisms in the wrought steels, it is suggested that if the nitrogen is similar to that in the 11Cr steels of the first iteration, the elevated-temperature strength of the 11Cr-1.5MoCoMnVNbB and 11Cr-2WCoMnVNb steels should be better than that of COST CB2.

The results for the high-chromium steels lead to the conclusion that 11% Cr cast steels with properties exceeding those of COST CB2 (9Cr-1.5Mo-0.80Co-0.80Mn-0.20V-0.06Nb-0.008B-0.028N-0.12C) are possible. As the next iteration in the development of 11Cr steels, Fe-11Cr-2W-Co-Mn-Ni-V-Nb-N-B-C and Fe-11Cr-1.5Mo-Co-Mn-V-Nb-N-B-C compositions are suggested. In particular, the steels should contain 0.030-0.04% N (similar to that in the first iteration) and 0.005-0.008% B. Other elements should be similar to those of the second iteration and COST CB2: 0.80% Co, 0.80% Mn, 0.20% V, 0.20% Ni, 0.06% Nb, and 0.11% C.

Based on the results of the two iterations examined in this CRADA, these proposed steels should have properties as good as or better than the best steels in this study. It is important to determine long-term creep-rupture properties for the new compositions at 600 and 650°C, for which long-term (>10,000 h) tests are required. Tests of these steels should address the relative solid-solution strengthening effectiveness of tungsten and molybdenum. The COST CB2 should be used as a control for the tests. Such steels with the higher chromium concentrations than COST CB2 should, because of their better corrosion and oxidation resistance, have the capability of being used in turbine designs for temperatures of 600-650°C.